Seismic hazard in Norway due to large earthquakes

Martine Johnsen

Master of Science, Geodynamics

Department of Earth Science

UNIVERSITY OF BERGEN

01.06.2015

Abstract

There are many faults located in Norway, posing as potential earthquake sources. Even though the seismicity is characterized as low to moderate, earthquakes of magnitude 3.5 or lower occur regularly. The seismic hazard following such a small event is very low; however, the occurrence of small earthquakes may promote the possibility of larger events. This thesis is based on the potential seismic hazard in Norway due to large earthquakes, and this study performs simulations of three or four different earthquake scenarios on 13 faults located in Norway, in areas where cities and towns are situated nearby, and these magnitudes are: the highest possible magnitude for each fault based on the fault length (ranges from M_W 7.7 to M_W 6.9), M_W 7.0, M_W 6.5 and M_W 6.0.
The simulations show the expected ground motion in peak ground acceleration (PGA), and the PGA caused by the earthquake scenarios are quite high, with a maximum of 317.6 cm/s^2. This could correspond to shaking of intensity VIII on the Modified Mercalli Intensity Scale. The M_W 6.5 and M_W 6.0 scenarios would result in PGA between 191.4 and 91.11 cm/s^2, which may indicate intensity VI – VII. The area outside the 50 cm/s^2 contour line would be exposed to PGA below 50 cm/s^2 and the shaking in this area could correspond to intensity IV – VI.

A stochastic simulation code, EXSIM12, was used in performing these simulations.
The difference in maximum PGA for scenarios of similar magnitude shows that the distribution of the PGA and the maximum value are dependent on several factors, for example the length and width of the fault, as well as the number of iterations per site, and whether the simulations are performed with random or fixed hypocenter location. Both increasing the number of iterations per site and changing from random to fixed hypocenter location result in smoother distribution of the PGA and lower maximum value for the earthquake scenarios.

Acknowledgements

First, I would like to express my greatest appreciation to my supervisor, Mathilde Bøttger Sørensen, Associate Professor at the University of Bergen, for providing great guidance and helpful comments during the process. I am particularly thankful for her patience and support in regards to EXSIM12 and working with GMT plots.

Secondly, I would like to thank my co-supervisors Kuvvet Atakan and Haakon Fossen for guidance and discussion of my work. I would also like to give thanks to my fellow students and everyone who have provided the literature that my study builds on, especially Randi Karin Tveit who has provided the research that my thesis brings further.

Finally, I would like to thank Gro Helene Carlsen, Jens Harald Johnsen, Karen Johnsen and Arnstein Stangeland Waldeland for supporting me through the Master study, and helping me stay focused during the final stages of writing and editing the thesis.

Table of Contents

1 INTRODUCTION

Norway is a part of the Baltic Shield, located well within a continental plate and thus far away from any plate boundaries. The margins along the coast of Norway are passive margins, meaning that there is no ongoing subduction in this area. The Atlantic Ocean due west of Norway is a mature ocean, characterized by well-developed margins of sedimentary deposits such as the Norwegian continental shelf. Steep mountains and fjords cutting into the coastline dominate the topography, and these features were developed during the Quaternary period when Norway and large parts of the Northern hemisphere was subjected to several ice ages, occurring in cycles. During the last ice age, which ended approximately 12 000 years ago, Norway was covered by an ice sheet that lay over Fennoscandia. The ice reached the continental shelf. Glaciers are strong eroding agents, and the fjords were formed when valley glaciers eroded in zones that were already weakened by faults and joints.

Because of the long distance to plate boundaries, Norway is not prone to large, devastating earthquakes. One of the largest earthquakes to occur here happened in Oslofjorden in 1904 and the magnitude is estimated to have been $M_S = 5.4$ (Bungum et al., 2009). The timespan between such events is long and earthquakes over magnitude 5 are rare. There are, however, many earthquakes occurring with small magnitudes, mostly 3.5 or lower. These events are usually too small to be felt by people, although some shaking may occur. A study performed by Fejerskov and Lindholm (2000) concluded that the main stress mechanism acting in Norway is the ridge push force. The ridge push force is caused by the mid-ocean ridge that is elevated above the seafloor, and as the new basalt cools, the density will increase. This results in an outward compressional force generated by the gravity that is perpendicular to the crest. Additional stress mechanisms in the Norwegian crust are density contrasts and post-glacial rebound after the deglaciation after the last ice age.

The instrumental study of seismic activity is relatively new; the first seismograph was installed in 1905 in Bergen, and the first seismograph outside of Bergen was installed in 1958 on Svalbard. During the 1960s, more seismic stations were installed, including a station on Jan Mayen. The Norwegian National Seismic Network (NNSN) was established in 1992 when several seismic networks were merged into one (Department of Earth

Science, 2015). This means that the instrumental study of earthquakes goes back 100 years, which is short, considering the time it takes to accumulate the stress necessary to exceed the friction and strength on a fault. Bungum et al. (2005) has found that the seismicity in Norway will cause a magnitude 5 event every 10 year, and a magnitude 7 event every 1100 year on average. This conclusion is based on the rates of seismicity in Norway over the 20th century, without regard to uncertainties associated with data calculations.

The largest earthquake in Norway is the M_S 5.8 event that occurred in Lurøy, Nordland in 1819 (Bungum and Olesen, 2005), which indicates that it is possible to have earthquakes with magnitudes over 6 in Norway. Even though the stress accumulation rates are very low, the Oslofjorden earthquake and the Lurøy earthquake are proof of seismic activity that suddenly can cause higher ground motion.

There are many studies concerning the seismic activity in Norway, e.g. Hicks et al. (2000), and neotectonic activity, e.g. Fjeldskaar et al. (2000). These studies generally discuss the distribution of seismicity and the generating mechanisms, earthquake occurrence and locations of neotectonic fault, meaning faults that have been active after the deglaciation. Olesen et al. (2000) did a study of return times for earthquakes in the Rana area in Nordland, Northern Norway, and they concluded that the return period for a magnitude 5 event is 130 years and 1500 years for a magnitude 6 earthquake. Further, they discuss the 1819 M_S 5.8 earthquake on Lurøy, and state that landslides and rock avalanches following the event are the main hazard in Norway, and both of these phenomenon occurred after the earthquake on Lurøy. In addition, the earthquake risk increases with population and development of larger societies in areas that are prone to earthquakes.

Tveit (2013) performed a seismic hazard study in Norway, with focus on the Øygarden Fault Zone off the coast of Bergen and the consequences of a M_W 6.0 earthquake. The goal of this study was to simulate the earthquake scenario and calculate the peak ground acceleration and the hazard it could pose to Bergen.

In addition, there are performed probabilistic seismic hazard assessment in Norway, where the seismic hazard is calculated using the recurrence of earthquakes in an area to estimate a model that states the probability of exceeding given values of ground motion,

usually peak ground acceleration or peak ground velocity. One such study were performed by Wahlström and Grünthal (2001), who studied the seismic hazard in Fennoscandia, and Bungum et al. (2000) performed another study, looking at the seismic hazard in Norway, the North Sea and England. Both studies revealed that areas like Nordland in Northern Norway and Hordaland in Western Norway have 10 % probability of exceeding peak ground acceleration of 600 cm/s^2 within 50 years, which is equivalent to a return period of 475 years.

The main remaining question is when a new large earthquake (magnitude 5.5 or higher) will occur in Norway, where it will occur, and how the following ground motion will affect the area surrounding the fault. Both of the largest earthquakes recorded in Norway occurred when the population density was smaller and there were fewer pipelines, roads etc. Further work should be concerned with other possible earthquake scenarios and the probability of the occurrence of a magnitude 5.5 earthquake.

The purpose of my master thesis is to identify major fault structures that are located near cities and towns in Norway, and to simulate the potential peak ground acceleration following an earthquake on the faults. The study area in my thesis is divided into three parts of Norway: The Oslo rift Zone, Eastern Norway; the county of Hordaland, Western Norway; and the county of Nordland, Northern Norway. These areas were included because of the seismic activity associated with the locations. The peak ground acceleration has been simulated for 13 faults, and the earthquake scenarios are based on the highest potential magnitude possible for each fault, ranging from M_W 7.7 to M_W 6.9, depending on the fault length. The motivations for this study is to simulate and estimate the peak ground acceleration that could follow an earthquake located close to a city or town in Norway.

2 TECTONIC AND GEOLOGICAL BACKGROUND

2.1 TECTONIC BACKGROUND AND SEISMICITY IN NORWAY

2.1.1 The Caledonian Orogeny

The Caledonian Orogeny that occurred in Ordovician, Silurian and Early Devonian time, 485 – 405 Ma, strongly affected the geology of Norway. The Caledonian Orogenic Belt grew from the collision between the Laurentian plate (Greenland, Canada and North America) and the Baltic Shield (Norway, Sweden and the British Isles), Figure 2.1-1 shows that Norway collided with Greenland. The collision started when subduction began at both coasts of the pre-historic Iapetus Ocean that was located between the two plates. The Iapetus Ocean was opened during Precambrian time, and in the transition between Cambrian and Ordovician time the plate motion was reversed (Ramberg et al., 2013). Because of the active subduction zones on both sides of the Iapetus Ocean, the ocean did close up relatively fast. The collision started with island arcs colliding with the continent, and slowly turned into a heads on continent-continent collision where Greenland collided with Norway. The Caledonian Orogeny is therefore divided into four main faces: The Finnmarkian event occurred in Lower Cambrian time; The Trondheim event occurred in Lower Ordovician time; The Taconian event occurred in Mid to Late Ordovician time; and The Scandian event occurred in Mid Silurian to Early Devonian time (Roberts, 2003). The Scandian event is the main continental collision, while the two first events are collision with island arcs and micro continents and the Baltic plate. The Taconian event is also a collision with island arcs but it occurred on the Laurentian plate.

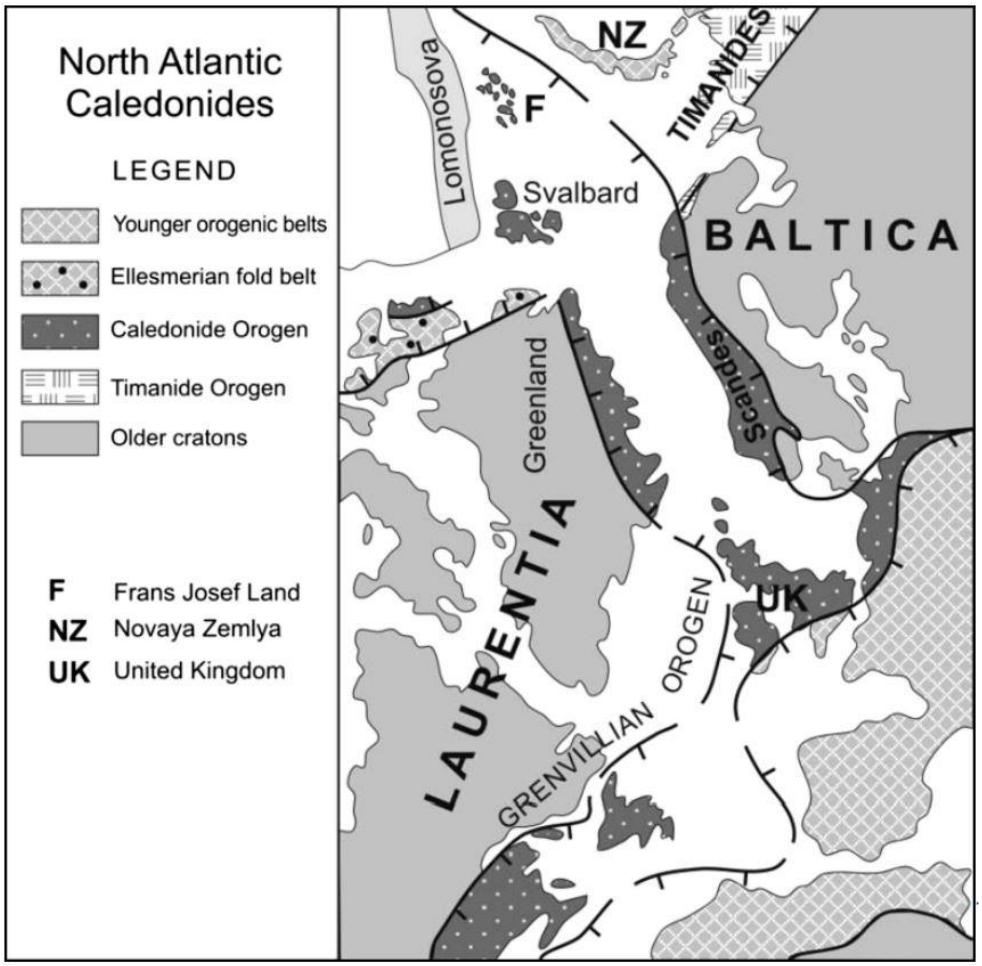

Figure 2.1-1 Map of the Caledonian Orogeny in Scandinavia (from Lorenz et al. (2011)).

The Scandinavian orogeny occurred between Greenland and Baltica, and lead to the formation of several thrust fronts in Norway. The thrusting and suturing of the continents lasted to approximately 408 Ma, when the plate motion was reversed to extension due to the first mode of orogenic collapse, which occurred at the same time as the thrusting. Thrusting and extension worked simultaneously until 395 Ma when the thrusting ceased and main crustal collapse stage started in the second mode of extension (Roberts, 2003). The collapse of the orogeny resulted in reversion of the thrust faults into normal faults and detachment faults, which may explain why most on the faults onshore Norway are normal faults.

The Caledonian orogeny resulted in the super-continent Pangea that lasted through Devonian and early Carboniferous time. In Permian time however, extension started with the opening of the Atlantic Ocean and the rift process in the Oslo region.

2.1.2 Seismicity in Norway

The seismicity in Fennoscandia as a whole is characterized as low to intermediate intensity, but it is higher than expected for an intraplate region. The magnitude of earthquakes occurring onshore in Norway is usually below 5.5, and earthquakes over magnitude 5.0 are very rare (Bungum et al., 2010). Figure 2.1-2 shows the seismicity of Fennoscandia, and it is clear that the seismicity is quite high in Norway compared to Sweden and Finland. Based on Figure 2.1-2, it appears as the highest concentrations of earthquakes are along the Norwegian coast, peaking in Western Norway. The size of the red dots representing the earthquakes are dependent on the size of the give event. All magnitudes are present in this figure, from 0.1 to the largest registered event, M_S 5.4 in Oslofjorden.

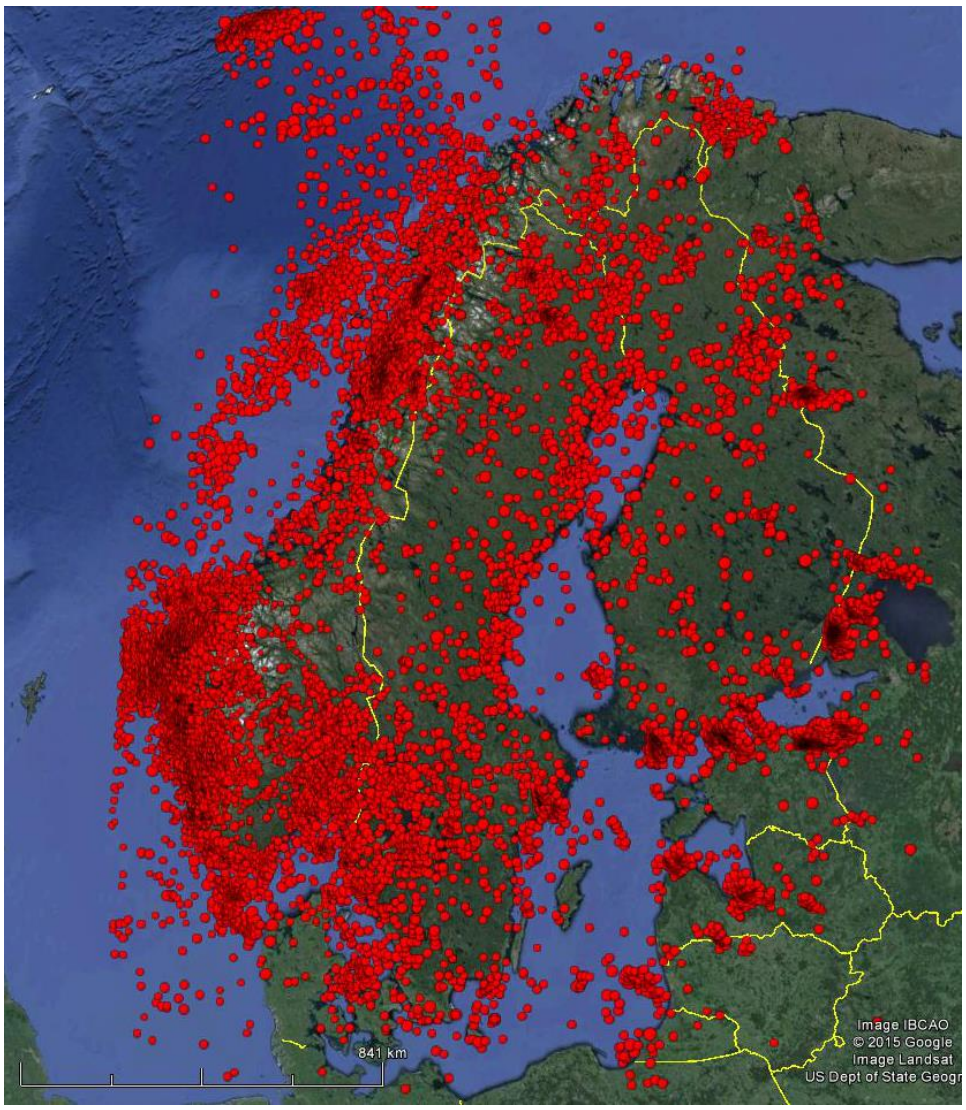

Figure 2.1-2 The seismicity in Fennoscandia. The earthquake catalog starts in 1497 and ends on January 1 2015. The red dots in the figure are earthquakes where the size of the dot illustrate the size of the event.

Earthquakes of smaller magnitude occur regularly in Norway. The driving forces behind the earthquakes have been discussed for a long time, and Fejerskov and Lindholm (2000) concluded that the main mechanism for generating stress in the Norwegian crust is the ridge-push force. The ridge-push force occurs because of the elevation of the ridge above the ocean floor. The new basaltic lava formed at the top of crest is hot with low density and as this basalt cools will the density increases and it moves away from the crest. As the cooling continues will the process cause a force perpendicular to the crest driven by gravity (Fejerskov & Lindholm, 2000). They also discussed other stress generating mechanisms: post-glacial rebound and loading/unloading of sediments. Stress caused by post-glacial rebound occurs because the land went through uplift after the deglaciation. When the weight of the ice sheet was lifted, the land that had been pressed down into the asthenosphere started to rise, causing stress changes in the upper crust. The rate of uplift was at its top right after the deglaciation, but there is still some residual stress left, making the post-glacial rebound a driving mechanism for earthquakes today. After the uplift follow erosion and deposition of sediments. Sediment loading leads to more pressure on the crust under basin, which then generates stress. However, the actual importance of sediment loading as a stress generating mechanism is difficult to assess. In addition, the continental margin along Norway generates extensional horizontal deviatoric stresses that is perpendicular to the margin in the continental crust. These deviatoric stresses, together with the force from the ridge-push, may cause rotation of the stress making the stress parallel with the continental margin instead of perpendicular to it (Fejerskov & Lindholm, 2000). Of the stress generating mechanisms discussed here is only the ridge-push force is on a tectonic scale, the others being regional or local and thus generating smaller amounts of stress. Nevertheless, these forces generate the stresses in the crust necessary to cause rupture on a fault.

2.2 THE OSLO RIFT, EASTERN NORWAY

After the collision and suturing of Norway and Greenland stopped followed the orogenic collapse of the Caledonian mountain belt. Following the collapse started tectonic rifting in the Oslo region, which lead to the formation of normal faults, Figure 2.2-1.

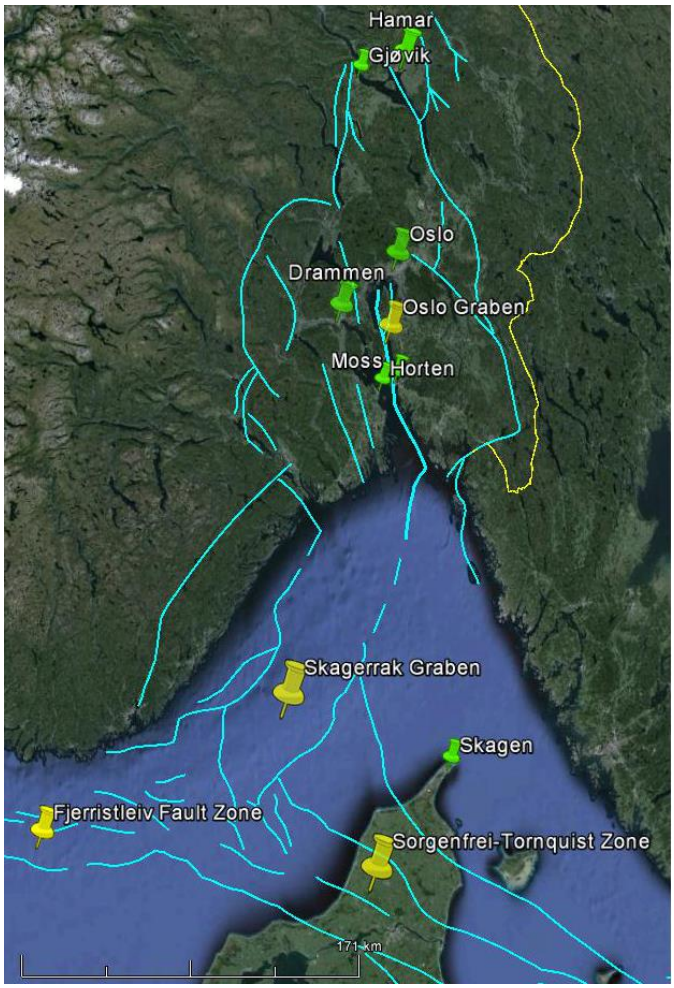

Figure 2.2-1 The Oslo Rift Zone with faults (turquoise lines) from Ro and Faleide (1992). The green pins are cities in the area and yellow pins are locations of grabens and rift zones in the system.

Oslo is the capital and largest city in Norway, and Oslofjorden and adjacent areas were exposed to stretching and rifting of the crust during Carboniferous and Permian time, between 359 and 252 Ma (Ramberg et al., 2013). During this time, the crust in Northwestern Europe was an active rift zone with magmatism, volcanism and earthquakes. This resulted in a graben system extending 400 km northeast from the Sorgenfrei-Totnquist Zone and Skagerrak Graben, located in Skagerrak, the sea between Denmark and Norway, Figure 2.2-1. The major part of this graben system is found under water, however, the northern part of the Oslo Rift, which is the Oslo Graben, is exposed on land (Neumann et al., 1992).

Rifting of the crust usually starts in three zones extending from a joint center. This triple junction occurs today in the East African Rift System, and according to Corti (2009) is this form of rifting archetypical. Triple junction also occurred in the Oslo Rift Zone; Skagerrak Graben and Oslo Graben, Fjerrsitselv Fault Zone, and Sorgenfrei-Tornquist Zone, Figure 2.2-1, are most likely the three arms where rifting occurred from a joint center. The rifting stopped in Cretaceous time (65 Ma) causing the rift to die out, leaving extensional structures like normal faults and grabens. The part of Oslo graben that is exposed onshore is oriented N-S, and the offshore graben, which is the Skagerrak Graben, is oriented NE-SW parallel to the Norwegian coast, Figure 2.2-1. The Fjerritselv Fault Zone and Sorgenfrei-Tornquist Zone run NW-SE, and are almost perpendicular to the Skagerrak Graben (Ro and Faleide, 1992).

Oslofjorden is located in Oslo Graben and continues north-northeast from Skagerrak. Before the rift it was basement rocks of Precambrian age that were deformed in the Caledonian Orogeny between Silurian and Devonian time, and later eroded to a peneplane (Neumann et al., 1992). The lithology in the Oslo rift consists of magmatic rocks like basalts and rhombus porphyry with sedimentary beds. This feature indicates tectonism with magmatic activity occurring contemporaneous (Ro and Faleide, 1992).

Rift structures in the Oslo Graben are divided into two segments, The Vestfold Graben Segment in the south and the Akershus Graben Segment in the north where the main boundary faults trend NNW-SSE to NNE-SSW (Ro and Faleide, 1992). The sedimentary rocks within the graben consist of a post-rift sequence of Lower-Paleozoic time and an early syn-rift sequence of Upper Paleozoic time. According to Ro and Faleide (1992) the rift zone was uplifted during the rift event causing the sediments in the rift to be exposed to erosion, and the rift remained above sea level after the rifting had ended. Sundvoll et al. (1990) estimate that at least 2-3 km of sediments and magmatic rocks are eroded in the Oslo Graben after the rifting ceased.

Even though the tectonic activity long since died out are there still earthquakes happening in the Oslo Rift region. The seismicity is moderate to low, and most earthquakes that occur is of M_W 3.5 or lower. This is true for Norway as a whole and not just the Oslo Rift Zone. Figure 2.2-2 shows the Oslo Rift Zone with the major faults and the seismicity in the region from the earliest event in 1612 to January 1 2015. It is evident that there has been some activity on the faults throughout the last centuries, but

there are however also many events that has occurred outside of these structures. There may be other geological structures located there that are not considered in this study, or it may be zones of weakness where the accumulated stress suddenly exceed the stress level of the structures.

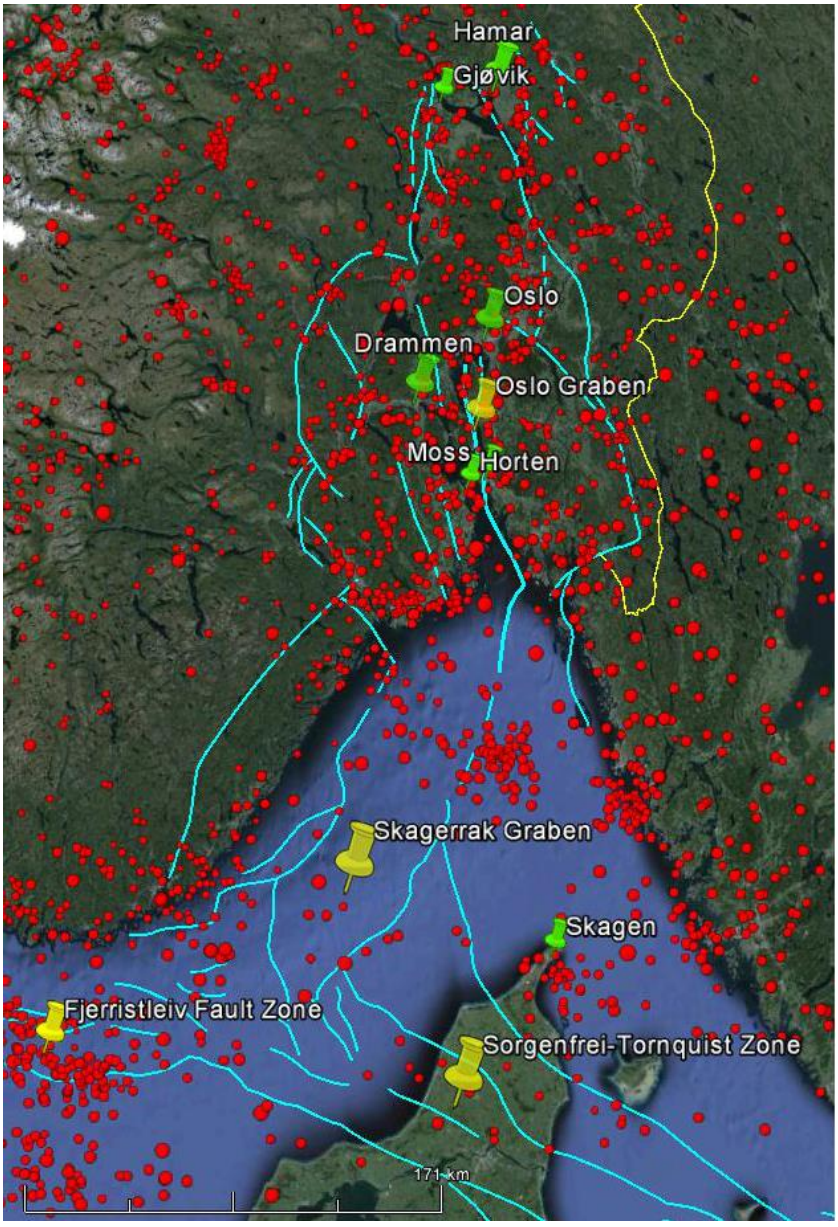

Figure 2.2-2 The Oslo Rift zone with faults drawn in light turquoise from Ro and Faleide (1992) and the seismicity illustrated as red dots. Each dot is an earthquake and the size of the red dots indicate the size of the earthquake. Green pins are cities in the area, yellow pins are structures related to the rift zone.

On October 23 1904 Oslofjorden was hit by an M_S 5.4 earthquake (Bungum et al., 2009). This earthquake is the largest event in Fennoscandia since the M_S 5.8 earthquake in 1819 in Nordland. The earthquake was felt in almost entire Northern Europe. The intensity of the earthquake was most likely VII closest to the rupture, and between II

and IV in Fennoscandia (Bungum et al., 2009). Fault plane solutions from the event show that the earthquake was a result of normal to strike slip movement on a fault in Oslo Graben, under Oslofjorden. This earthquake was one of the first events to be recorded on seismographs in Europe, and Bungum et al. (2009) have used the seismograms from the event to estimate the depth of the earthquake to approximately 24 km.

2.3 HORDALAND, WESTERN NORWAY

Different parts; the Sunnhordland Batholith and dikes; and the Bergen Arc System dominate the geology in Hordaland. The Sunnhordland Batholith occupies approximately 1000 km^2 and it is a complex of rocks ranging from granites to gabbros. It is comprised of several major granitoid plutons that post-date the gabbroic rocks (Andersen and Jansen, 1987). The actual boundary between the batholith and its envelope is preserved on Stord and Bømlo, two islands located at the outlet of Hardangerfjorden, Figure 2.3-1. However, a major tectonic boundary has developed along the present margin of the batholith. The tectonic boundary, which is the Northern Sunnhordland and Sunnhordland Fault Figure 2.3-1, changes orientation from NE-SW strike with moderate dip in the northern part of Sunnhordland, where it curves around Tysnesøy, to NW-SE strike with steep to vertical dip near Langevåg, the southern tip of Bømlo, Figure 2.3-1. This change in orientation of the two adjacent fault points to a two-fold division of the structure (Andersen and Jansen, 1987).

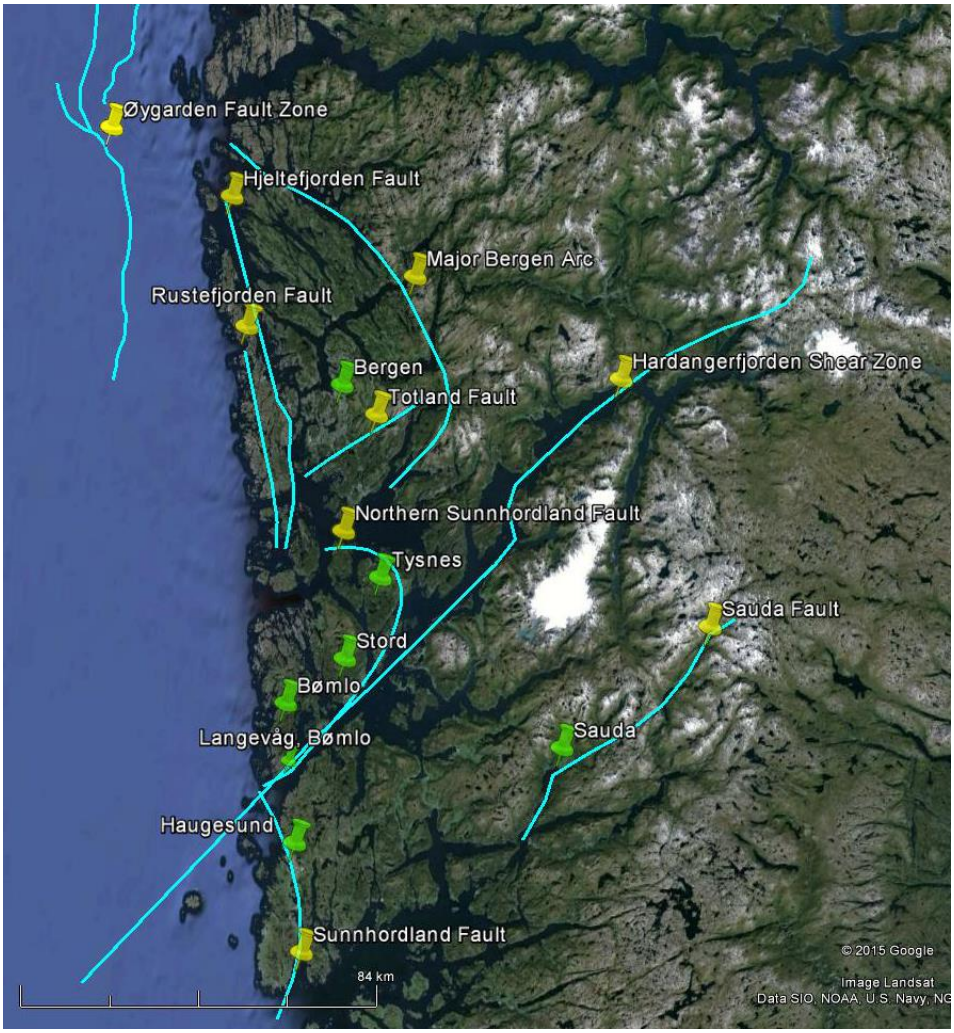

Figure 2.3-1 The main faults, drawn in turquoise, in Hordaland, drawn from Tveit (2013), Fossen (1998) and Fossen (2000). Yellow pins mark the fault and their names, red pins are cities and towns located near the faults.

In addition to the Sunnhordland Fault, the mouth of Hardangerfjorden is covered with tectonic lineaments with two main orientations – NW-SE and NE-SW, shown in Figure 2.3-2. On January 29 1989, an earthquake occurred on one of the lineaments close to Etne. The earthquake measured 4.25 ± 25 on the locale magnitude scale and occurred at 13.8 km depth, 9 km from the town of Etne (Karpuz et al., 1991). The lineaments around Etne are a part of the Etne Fault Zone, which is a continuous lineament passing through basement rocks from the Caledonian orogeny and Precambrian time. This zone is a part of a larger lineament system trending NW-SE in the Sunnhordland area. According to Karpuz et al. (1991) the NW-SE trending lineaments, which are green in Figure 2.3-2, are usually associated with tectonic elements from Precambrian time, and not a part of the Caledonian or Mesozoic structures.

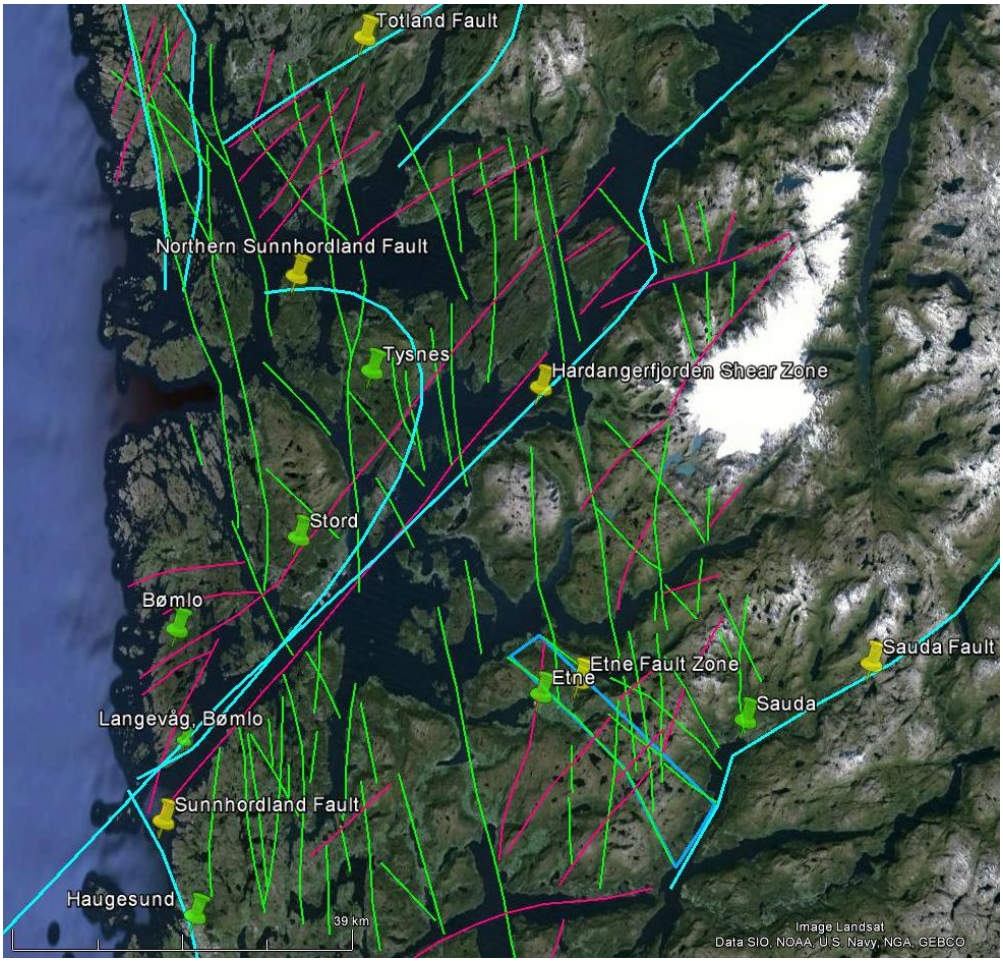

Figure 2.3-2 The lineaments (pink and green lines) in Sunnhordland drawn from Karpuz et al. (1991). The major faults crossing Sunnhordland are shown in turquoise. Yellow pins marks the faults and fault names, red pins are nearby cities and towns.

One of the largest tectonic structures in Norway is the Hardangerfjorden Shear Zone. Fjords tend to form in zones of weakness in the crust, and the weakness zone in Hardangerfjorden was the Hardangerfjord Shear Zone. This large shear zone is located in the crust under the Hardangerfjorden. The Hardangerfjorden Shear Zone is a low-angled extensional structure that stretches for more than 600 km, and it is ductile with a maximum displacement of 10-15 km (Fossen and Hurich, 2005). It was formed during continued extension of the crust that caused a shear zone that affects the orogenic wedge in addition to the basement. Deep seismic studies have shown that the shear zone goes as deep as the lower crust at approximately 220-250 km (Fossen and Hurich, 2005). The Hardangerfjorden Shear Zone is marked in Figure 2.3-1.

The seismicity of Hordaland is generally a little higher that for the Oslo Rift Zone, but the activity is still characterized to be low to moderate. This is because the majority of the events are of very small magnitude, 3.5 or lower here as well. Figure 2.3-3 shows

Hordaland with the earthquakes that have occurred since 1612. There are two clusters of earthquake located north of Bergen, Figure 2.3-3. These clusters may be previous events occurring on the Major Bergen Arc, or they could be related to local work on roads or tunnels.

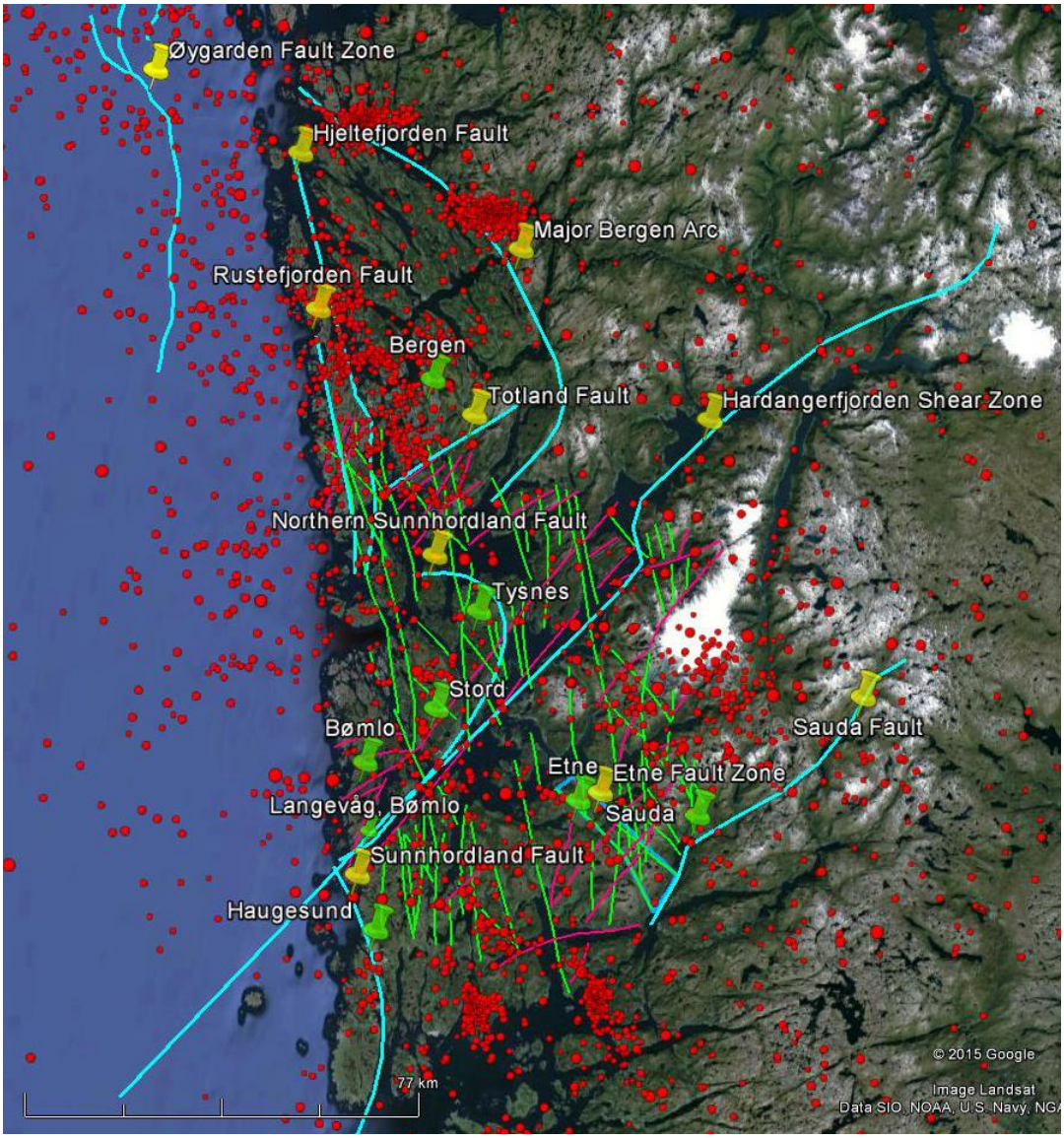

Figure 2.3-3 Major faults (turquoise lines) in Hordaland and lineaments (pink and green lines) in Sunnhordland showed with the seismicity in the area. The red dots are previous earthquakes, and the size of the dot reflects the size of the earthquake. Yellow pins mark the faults and fault names, green pins are nearby cities and towns.

2.4 NORDLAND, NORTHERN NORWAY

The geology of Nordland consists of rocks from the Caledonian orogeny, more accurately fragments broken off the nappes that were thrust over Norway during the collision. These rocks are dominantly around 400 Ma of age with exposed basement from Precambrian time (Hicks et al., 2000, Atakan et al., 1994). The nappes are metamorphic rocks, like mica shales with marble and large, granitic intrusions.

The faults in Nordland, shown in Figure 2.4-1, are mostly normal faults that were formed or reversed during the collapse of the Caledonian mountain belt when the plate motion switched to extension.

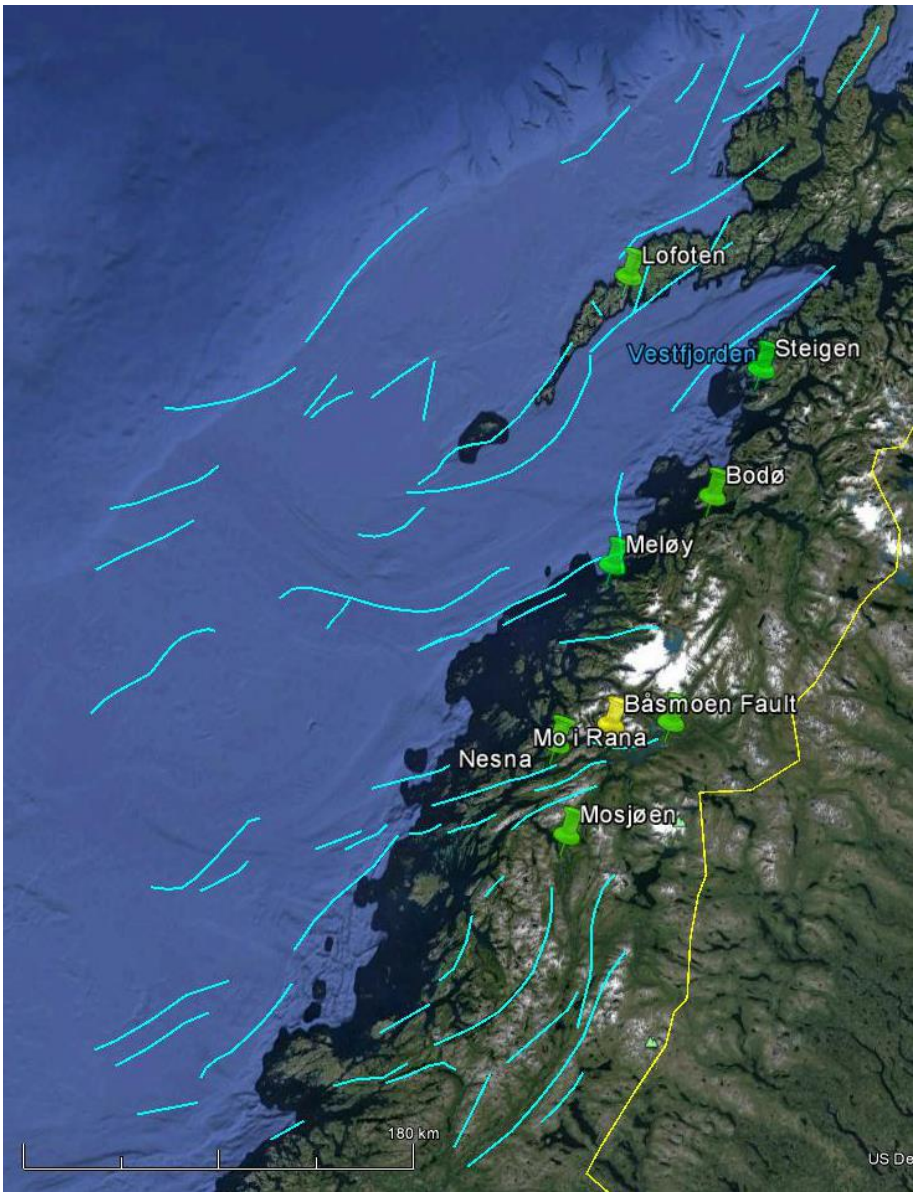

Figure 2.4-1 Faults (drawn in turquoise) in Nordland drawn from Olesen et al. (2010). Green pins mark cities and towns in Nordland, and the yellow pin marks the location of Båsmoen Fault (closer look in Figure 2.4-2).

Of the areas in Nordland, the area around Ranafjorden is probably studied the most. There was high interest in the early 1990s because of the many earthquakes associated with the area, and the fault that was of highest interest was the Båsmoen Fault, Figure 2.4-2. This area had had increased seismicity, and geologists therefore thought that it could be a site for post-glacial movement on the fault. Geological Survey of Norway performed fieldwork in Ranafjorden to localize the potential post-glacial faults, but found no indications that supported the theory. In addition, the fieldwork showed that the Båsmoen Fault was not the source of seismic activity, but smaller structures located around the main fault in Ranafjorden. Olesen (1994) concluded that aseismic sliding because of episodic movements along the faults was the motions in the crust that accumulated the stress.

Figure 2.4-2 The Båsmoen Fault (yellow) drawn from Olesen (1994). The red pin marks Båsmoen Fault, the green pin is in Mo i Rana, the nearest city, while the yellow pin marks Ranafjorden.

Ranafjorden is located between two nappe complexes, the Rødlingsfjell Nappe to the north and east and the Helgeland Nappe to the south and west. The most abundant lithologies in the area are gneiss, mica schist and marbles and they have been deformed and exposed to metamorphism during the Caledonian orogeny (Olesen, 1994).

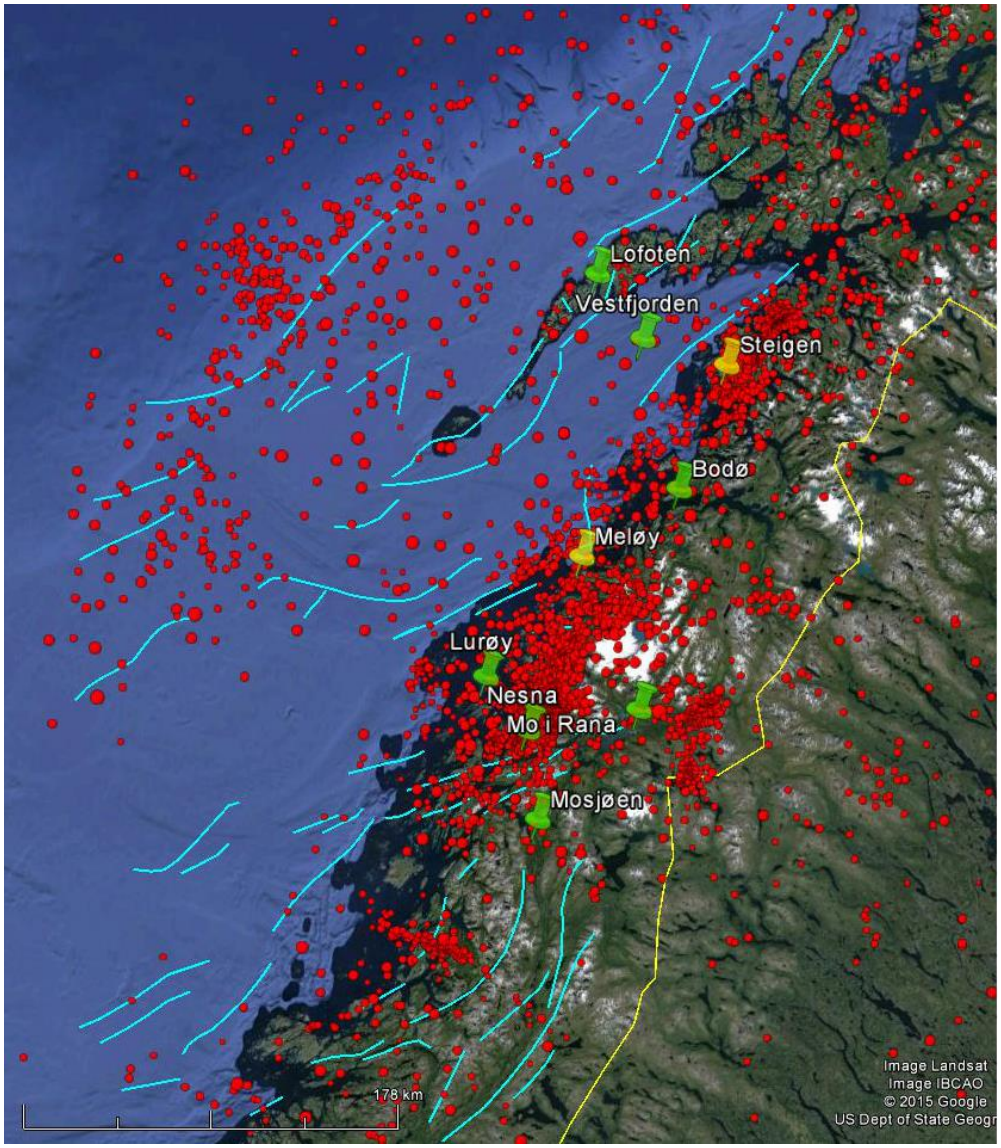

Figure 2.4-3 Faults drawn in turquoise with the seismic activity in Nordland. The seismicity is marked red dots representing previous earthquakes. Green pins are cities and towns near the faults, yellow pins marks the locations of the earthquake swarms, Meløy and Steigen.

Nordland has had an interesting occurrence of seismicity; the activity in Ranafjorden and two earthquake swarms on Steigen and Meløy, Figure 2.4-3, both in 1977/1978. 10 000 small events were recorded by sensitive stations in the field during the first 10 weeks in December 1978 in Steigen (Atakan et al., 1994). Despite this prominent activity was no main event recorded. The occurrence of earthquake swarms is not well understood. One theory says that the swarms occur due to several different forces like ridge-push from the mid-ocean ridge in the Atlantic, because of residual stress after the uplift event after the melting of the ice sheet and as a response to sediment loading due to high rates of sedimentation since Tertiary (Atakan et al., 1994). All of these forces are considered important in generating earthquakes in an intraplate setting. Nevertheless,

all of these forces are of larger scale and they will not explain the occurrence of the local earthquake swarms on Steigen. Atakan et al. (1994) found that the structures in the crust are more complex than first assumed, and new deep seismic data showed that there is clear low-angled reflectors in the upper mantle beneath the Lofoten Ridge. This can be because of a large-scale detachment zone that may cut across the Moho and comes near the surface parallel to Vestfjorden, Figure 2.4-3 (Atakan et al., 1994). In addition to the earthquake swarms on Steigen, another intraplate earthquake sequence occurred in Nordland in 1978, on Meløy, due south from Bodø, Figure 2.4-3. Here as well were 10 000 small events recorded during the first 10 weeks (Bungum et al., 1979). The generating mechanisms for this earthquake occurrence is not known, and as for the earthquake in Steigen is it unlikely that the ridge-push force and post-glacial rebound caused the activity. Bungum and Husebye (1979) accepted the phenomenon on Meløy as a unique example of intraplate seismicity. Both Steigen and Meløy are located in a distinct seismic zone, ranging from 65 to 70 degrees north. Unknown activity in this zone may be the cause of the seismic activity that occurred in November-December 1978.

One of the largest know earthquakes in Norway occurred on Lurøy, Figure 2.4-3, on August 31 1819. The magnitude of the event is based on witnesses and intensity of the ground motion, and it is estimated to be M_S = 5.8 (Bungum and Olesen, 2005).

Because there have been several large earthquakes in Norway, the M_S 5.4 earthquake in Oslofjorden in 1904 and the M_S 5.8 earthquake in 1819 in Lurøy, it is not wise to rule out that such events may occur in the future. The seismicity in Norway is moderate to low, but it is not aseismic. Because small earthquakes occurs regularly, the possibility of one of the many faults in Norway rupturing in a larger, perhaps damaging earthquake, cannot be excluded.

3 METHOD

3.1 LITERATURE SEARCH

The first part of the master thesis was to find information about geological structures, seismicity and tectonics, and to map faults and lineaments in Norway based on published literature. Searching for literature about Norway as a whole was too general because there were too many results in Google Scholar and Oria. I therefore decided, with my supervisor, that I should split the search into the highest seismic active areas and look for literature about those areas. The main areas chosen are therefore Nordland and Southern Norway with focus on Oslo Rift Zone and Hordaland.

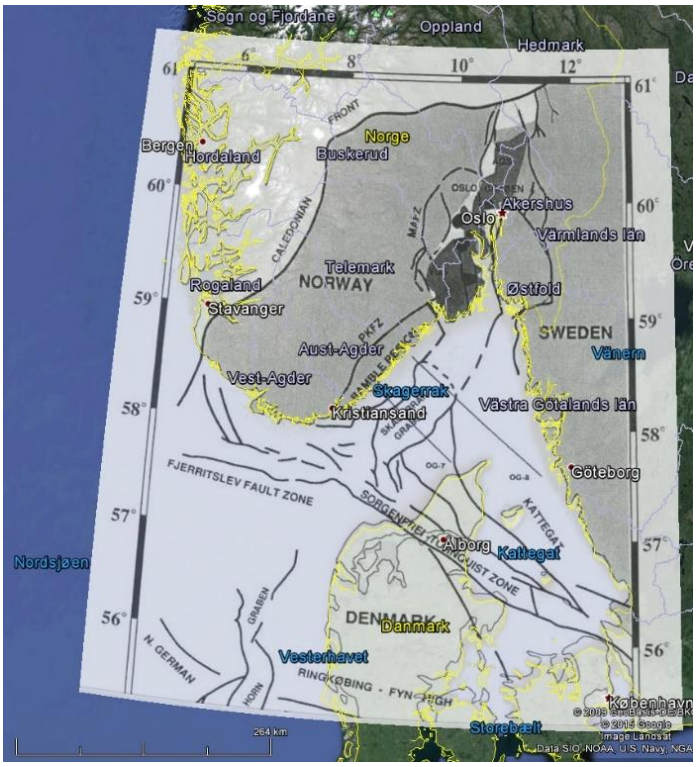

Figure 3.1-1 This figure shows the method for inserting a figure from literature into Google Earth. The coasts in the figure and in Google Earth are aligned as close as possible and then the faults are drawn in, using the figure as a template. This example is from Ro and Faleide (1992).

The next step was to map the geological structures by inserting figures from published literature into Google Earth to draw in the faults in the program using the inserted figure as a guide. The figures had to be adjusted so the coast in the figures matched with the coast in Google Earth, like the figure from Ro and Faleide (1992) in Figure 3.1-1. I used the line-tool to draw over the faults, and they will show in Google Earth when the

inserted figure is removed, as shown in Figure 3.1-2 on the next page. This process was repeated for several figures covering the study areas.

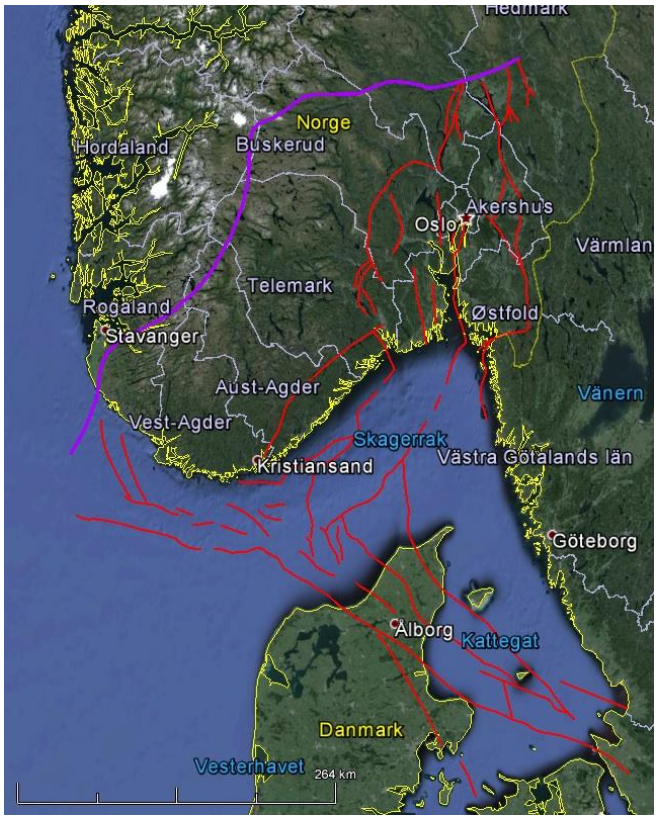

Figure 3.1-2 This figure shows the same area as Figure 3.1-1, but here are the faults drawn in and the inserted figure removed. The result showed here is the goal of this procedure, to map the faults in Google Earth and use them to correlate the seismicity.

The seismicity in Norway is from the NNSN (Norwegian National Seismic Network), and the earthquake database contains all earthquakes that have occurred in Norway up to January 1 2015. I used the gmap-tool in Seisan Explorer to plot the seismic activity in Google Earth.

3.2 STOCHASTIC FINITE FAULT MODELING

An earthquake releases energy in the form of heat and seismic waves, which propagates from the source. There are two main type of waves: Body Waves and Surface Waves. The body waves propagate through the Earth's interior and are divided into two categories, P-waves (primary) and S-waves (secondary). The P-waves are compressional waves and are the fastest ones, while the S-wave is a shear wave and arrives after the P-wave. In addition, the S-wave cannot move through liquids or gasses because it is dependent on the shear stresses in the medium through which they travel. The surface waves

propagate along the surface of the Earth are also divided into two categories, Rayleigh waves and Love waves. Rayleigh waves has a rolling movement, while Love waves propagates horizontally and are shear waves. The surface waves are often responsible for most of the ground motion and damage that occurs during an earthquake. The effect of the S-wave may be important in areas that are close to the fault.

There are several methods available to estimate the potential ground motion in an area: Deterministic seismic hazard analysis, probabilistic seismic hazard analysis and stochastic fault modeling, which is a branch of ground motion simulation. The deterministic hazard analysis simulate the earthquakes and their consequences numerically, using four basic steps (Reiter, 1991): The first step is to define the earthquake source or sources in the study area. The second step is to select a controlling earthquake, which describes the maximum potential of the source(s) in step 1. The third step is to define the effect of the earthquake at the site, usually some type of ground motion. The fourth and last step is to define the seismic hazard at the site, which is given as a simple statement with a specific value for the ground motion in the area. The probabilistic hazard analysis, on the other hand, simulates the expected ground motion based on the seismic activity in an area, or in other words: this method uses statistical analyzes of past seismicity to calculate a model using probability to describe the future (Orozova and Suhadolc, 1999). Reiter (1991) also described the elements of a probabilistic analysis in four basic steps: Step 1 is to define the earthquake sources in the desired area. Step 2 is to define the recurrence relationship indicating the probability of an earthquake with a specific magnitude occurring within a set time period anywhere in the area. Step 3 is to estimate the effect of the earthquake, usually in peak ground acceleration or peak ground velocity values. Step 4 is to determine the hazard at the site by adding the effect of all earthquakes of different sizes, locations, sources and probability in the area and presenting the hazard in a curve or model describing the probability of exceeding a given value for the selected ground motion.

The stochastic method is somewhat different from the deterministic and probabilistic analyzes. Boore (2003) defines the stochastic model as a method ‘to combine parametric or functional descriptions of the ground motion’s amplitude spectrum with a random phase spectrum modified such that the motion is distributed over a duration related to the earthquake magnitude and to the distance from the source’. This means that the

stochastic method uses data describing the source and crust in an area to simulate the potential ground motion that could occur after an earthquake of a given magnitude.

In the work with this thesis, I have used EXSIM, which is a stochastic simulation code, to simulate the potential ground motion at a number of sites. EXSIM is a further development of the programs SMSIM and FINSIM, and I will therefore explain them first.

3.2.1 SMSIM

Earthquake ground motion can be calculated several ways: the engineering society prefers to use a pure empirical method to calculate the possible ground motion of a site, while the scientific society prefers to do calculation using a physical method combined with empirical data from the seismogram or dimensions for a given fault. Boore (1983) wrote the first code for predicting ground motion based on the moment magnitude and a frequency-squared spectrum with a high-frequency cutoff f_m, as well as the anelastic attenuation path that is usually used in hazard modeling. In addition, a constant stress parameter ($\Delta\sigma$) was used. Assuming these applications made the hazard-model simple, because the scaling with source size is only dependent one parameter: the moment magnitude. The output from the simulation is the acceleration at a point at a given time. The first code became the program SMSIM (Boore, 1983). SMSIM considers the source a point, thus the energy that is released during rupture along the fault is concentrated at a point and not a plane. The end result of the SMSIM program is to give a transient time series with a stochastic character that agrees with the amplitude spectrum (Boore, 2009).

Tveit (2013) sorted the steps of the stochastic method of SMSIM from Boore (1983) and Atkinson et al. (2009), and these steps are illustrated in Figure 3.2-1:

1. A normally distributed random signal is generated, having 0 mean and unit variance (picture a in Figure 3.2-1)
2. The signal is then windowed using a window function (picture b in Figure 3.2-1)
3. Then the Fourier transform of the windowed signal is calculated (picture c in Figure 3.2-1)
4. The result is normalized, making the RMS amplitude spectrum one (picture d in Figure 3.2-1)

5. The theoretical, and thus deterministic, point-source spectrum is calculated by Equation 3.2.1-1
6. Equation 3.2.1-1 is then multiplied by the normalized random-signal complex spectrum. This is to obtain the Fourier spectrum of the ground motion at the site (picture e in Figure 3.2-1)
7. The final step is to calculate the inverse Fourier transform of the site spectrum. This is done to obtain the simulated accelerogram (picture f in Figure 3.2-1)

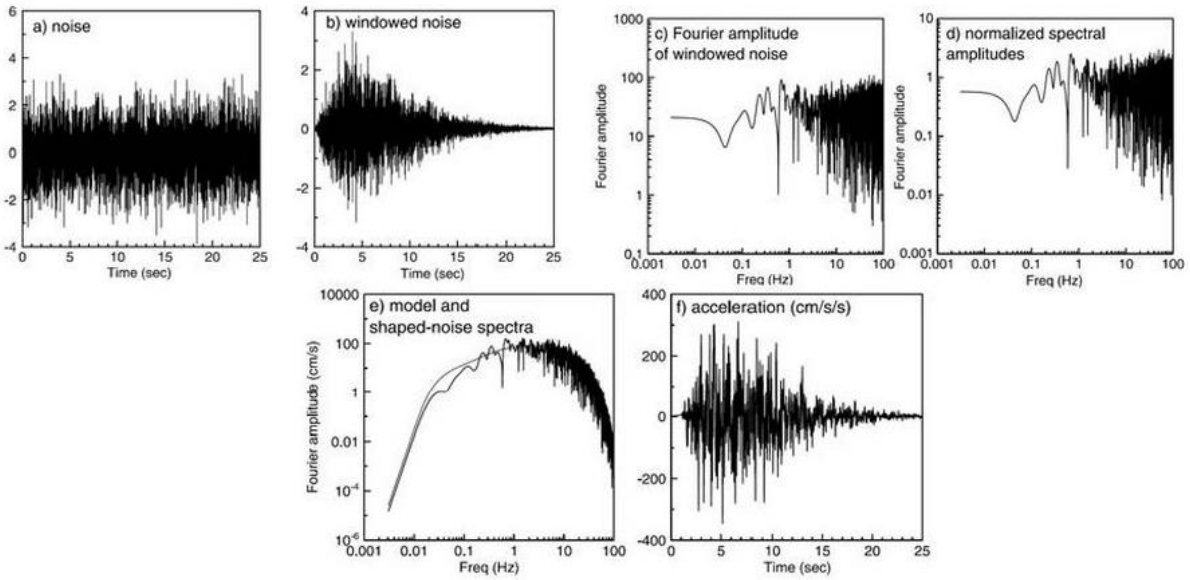

Figure 3.2-1 Figures illustrating the steps in the steps in the stochastic method for SMSIM. (From Ebrahimian (2013)).

The calculated point-source spectrum from point 5, observed as the recording site, is defined as:

$$Acc(M_0, R, f) = Source(M_0, f) \times Path(R, f) \times Site(f), \qquad 3.2.1\text{-}1$$

where R is the distance between source and site; f is the frequency; and M_0 is the seismic moment. The different factors in Equation 3.2.1-1 are as follows: $Source(M_0,f)$ is the source spectrum at unit distance; $Path(R,f)$ is the effects caused by the path, including the effects of geometrical spreading and anelastic attenuation; and $Site(f)$ is the response operator of the site, including the effects of both amplification and deamplification, and the high-frequency amplification (Atkinson et al., 2009).

The spectrum is produced by the seismic source at a given distance in a lossless medium, and it is modeled by multiplying a deterministic function by the Fourier spectrum of windowed Gaussian noise. The spectrum of angular frequency gets the

mean shape and amplitude from the deterministic function, and the realistic random time character to the simulated time series from the stochastic function (Beresnev and Atkinson, 1997)

This program is a stochastic model, meaning that the ground motion acceleration is determined randomly based on the input parameters describing the properties of the earthquake and the crust. Such an approach to model the possible ground motion in an area uses one frequency range, and the stochastic model gives the best result if it is used on frequencies higher than 1 Hz. This is probably because the effects of scattering becomes of more importance at high frequencies (Motazedian and Atkinson, 2005).

3.2.2 FINSIM

Considering the source of the ground motion as a point is useful when the ground motion is calculated at great distances from the source. However, when the distance from the source gets smaller, the effects of the finite-fault become important. These effects are related to the rupture velocity; the rupture starts at a point and then propagate along the fault, causing the released energy to arrive faster near the point of rupture. As the seismic energy is being released when the slip propagates, the delayed waves will interfere with earlier waves and increase the amplitude, causing the directivity effect (Beresnev and Atkinson, 1998). This is accounted for by dividing the fault into several subfault or subsources, and each subfault is then treated as a point source in the modeling. Afterward, the radiation from the subfaults is added with proper time delay to account for the rupture propagation along the fault, Equation 3.2.2-1 (Beresnev and Atkinson, 1998). This method became the FINSIM program, which uses the basis of a stochastic model set by Boore (1983).

The main fault is divided into *N* subfaults, and the ground motion acceleration, $a(t)$, from the entire fault is obtained by summation:

$$a(t) = \sum_{i=1}^{nl} \sum_{j=1}^{nw} a_{ij}\left(t + \Delta t_{ij}\right), \quad \text{3.2.2-1}$$

where *nl* and *nw* are the number of subfaults along the length and width of the fault and $nl * nw = N$; Δt_{ij} is the relative time delay for the radiated wave from the *ij*th subfault to reach the observation point; and finally is each of the $a_{ij}(t)$ calculated by the stochastic method (Motazedian and Atkinson, 2005). The subfault area and the main fault area ratio control the moment for each subfault:

$$M_{oij} = M_0/N \qquad 3.2.2\text{-}2$$

where M_0 is the seismic moment of the entire fault. This formula is only true if the subfaults are identical.

FINSIM sets the subfaults as point sources and uses the ω^2-spectrum to model the radiation from the fault, and ω is the angular frequency.

3.2.3 EXSIM

The FINSIM program is very reliable and gives realistic and plausible results, but the radiated energy at high frequencies is dependent on the size of the subfaults, the magnitude range is smaller, and the FINSIM program lack control of the relative amplitude when it comes to higher versus lower frequencies (Motazedian and Atkinson, 2005). Therefore, Motazedian and Atkinson (2005) uses the same method for simulation of ground motion as in FINSIM, and in addition, they modified the FINSIM approach and added the factor of the dynamic corner frequency. In this approach, the parameter of time is included because the dynamic corner frequency is a function of time. The frequency of each subfault is controlled by the rupture history of the simulated time series. Rupture along a fault begins with a high corner frequency that decrease as the ruptured area increase. The dynamic corner frequency is inverse proportional to the ruptured area and thus it is inverse proportional with the magnitude. This new parameter in the FINSIM method has advantages over earlier methods for the stochastic methods, and the most notable is that the radiated energy is not lost for large subfaults sizes. In addition, the adding of the corner frequency leads to a wider magnitude range and control of the relative amplitude of higher versus lower frequencies (Motazedian and Atkinson, 2005).

Adding the dynamic corner frequency resulted in another change in the code of the original program developed by Boore (1983), and this new branch became the EXSIM program, which is the program I will use in my ground motion simulations. Parts of the method of EXSIM is similar to that of FINSIM in which the total ground motion triggered by the earthquake is the sum of the ground motion triggered on each subfault, where each is calculated using the stochastic point-source method with a proper time delay to account for directivity in the time domain.

The corner frequency is inversely proportional to the faulted area, which is the number of subfaults that ruptures during the earthquake. This means that the corner frequency can be used as a function of time because the corner frequency is dependent on how many subfaults that ruptured, because the rupture stops at a time, thus defining the corner frequency for that earthquake. This theory also means that the corner frequency should decrease as the duration of the earthquake increase (Motazedian and Atkinson, 2005). The dynamic corner frequency was added to the FINSIM code by the equation

$$f_{0ij}(t) = N_R(t)^{-1/3}\, 4.9E + 6\beta\left(\frac{\Delta\sigma}{M_{0ave}}\right)^{1/3} \qquad 3.2.3\text{-}1$$

where f_{0ij} is the dynamic corner frequency of the ijth subfault; $N_R(t)$ is the cumulative number of ruptured subfaults at time t; $4.9E + 6\beta(\Delta\sigma/M_{011})$ is the corner frequency of the first subfault near the beginning of rupture, where M_{011} is the seismic moment of the first subfault. Thus, $M_{0ave} = M_0/N$ is the average seismic moment for subfaults. The number of ruptured faults is $N_R(t)^{-1/3} = N^{-1/3}$ for $t = t_{end}$. At the end of the rupture the corner frequency therefore will be

$$f_{0ij}(t_{end}) = N^{-1/3}\, 4.9E + 6\beta\left(\frac{\Delta\sigma}{M_0}/N\right)^{1/3} \qquad 3.2.3\text{-}2$$

which leads to

$$f_{0ij}(t_{end}) = f_0 \qquad 3.2.3\text{-}3$$

Where f_0 is the corner frequency of the entire fault. Equation 1.3.3-3 says that the corner frequency for the entire fault is the lower limit of the corner frequency.

The input parameters needed for EXSIM to calculate the ground motion at a site are as follows:

- Geometry of the fault (strike, sip, length, width, depth of upper edge)
- Magnitude targeted for the simulation
- Location of the fault (geographic coordinates of one of the corners in the fault)
- Geographic corner of the observation point
- Number of subfaults along the strike and dip
- Position of the hypocenter, where the rupture propagation was initiated
- Distribution of slip (if this is not specified will the program generate random slip
- Crustal density and velocity of the S-wave

- Radiation-strength factor, z (maximum rate of slip)
- Quality factor of the crust in the form of $Q(f) = Q_0 f^{\eta}$
- Model for geometric attenuation, $1/R^{\alpha}$
- Model for the duration of the radiation from the subfaults
- Parameter of f_{max} or κ filter
- Options for window used in the simulation (tapered boxcar or Saragoni-Hart window)
- Interval of sampling
- Frequency interval and percentage of critical damping for response spectrum calculation
- Dynamic flag (which is 1 for dynamic corner frequencies)
- Pulsing percent
- Time step
- Number of simulation trials for calculating average response spectrum
- Name of the ASCII-file that contains the frequency-dependent amplification function. Two separate amplifications are allowed, for example crustal amplification and response of the local site

Obtaining and deciding the values for the parameters can be challenging as the data from a fault usually lack many of the desired values. Some can be calculated using the empirical relationship between length, width and magnitude calculated by Wells and Coppersmith (1994). Their method is commonly used to find some of the fault geometry parameters necessary for EXSIM to run. Other data can be found from the seismogram, as the magnitude and stress drop, while some of the data has to be guessed using experience and assumptions, like the dip of the fault. Tveit (2013) performed a study of the sensitivity of the different parameters, meaning that she evaluated how changes in a parameter affected the result of the hazard study in the Øygarden Fault Zone. I will use these results to define the values necessary in my hazard simulations as well.

The output of the EXSIM12 simulation is a file that gives the peak ground acceleration for each site in the simulation, presented in columns. Particularly one of the output-files for each simulations that is useful and it states the coordinates for each sites with time and the ground motion in peak velocity and peak acceleration. I then use MatLab to extract the site coordination and the peak acceleration at each site to make a new file.

This file is then used to plot the ground motion in a color-coded map covering the affected area around the fault, using Generic Mapping Tool (Wessel et al., 2013).

4 DATA

4.1 FAULTS AND MAGNITUDES

The faults used in the earthquake scenarios are chosen based on location and seismicity. The seismicity in Norway is moderate to low, but there are earthquakes of smaller magnitudes occurring regularly. The basis of my study is three counties: Nordland located in Northern Norway, because there is more seismic activity there than in the rest of Norway; Oslo Rift Zone located in Eastern Norway, because this is where one of the largest earthquakes in Norway occurred in 1904 and because the capitol of Norway is located in this old rift zone; Hordaland located in Western Norway, because it shows slightly higher seismic activity in this area and because Bergen, the second largest city in Norway, is located here. Based on a comprehensive literature survey, I have identified many faults in these three areas, and I have chosen 13 faults to use in my ground motion simulations.

The ground motion is simulated for three different earthquake scenarios for all of the faults, and four scenarios for the largest faults. The magnitudes in the earthquake scenarios are the highest magnitude possible for each fault length, ranging between M_W 7.7 and M_W 6.9, magnitude 7.0 earthquakes (for the four largest faults only), magnitude 6.5 earthquakes and finally magnitude 6.0 earthquakes. I have used formulas calculated by Wells and Coppersmith (1994), Table 4-1, to calculate the maximum magnitude based on the fault lengths, and to find the length of the faults when the magnitude is reduced. All magnitudes are given as moment magnitude, M_W. Table 4-2, Table 4-3, Table 4-4 and Table 4-5 lists the length, width and locations of the faults for each of the magnitudes in the earthquake scenarios.

Table 4-1 Relations calculated by Wells and Coppersmith (1994), used to calculate the fault length, fault width and magnitude of the earthquake scenarios.

Formula	Rupture type
Magnitude = 4.86 + 1.32 * log (length)	Normal rupture
Magnitude = 5.00 + 1.22 * log (length)	Reverse rupture
Magnitude = 5.16 + 1.12 * log (length)	Strike-slip rupture
Area = 10^(-2.87 + 0.82 * magnitude)	Normal rupture
Area = 10^(-3.99 + 0.98 * magnitude)	Reverse rupture
Area = 10^(-3.42 + 0.90 * magnitude)	Strike-slip rupture
Length = 10^(-2.01 + 0.50 * magnitude)	Normal rupture
Length = 10^(-2.86 + 0.63 * magnitude)	Reverse rupture
Length = 10^(-3.55 + 0.74 * magnitude)	Strike-slip rupture

The Oslo Rift Zone is located near the capital of Norway, and there are many normal faults in this area after the rift event. I chose Hamar Fault because it is a very long fault, the largest earthquake scenario for this fault is M_W 7.7, and it cuts through a large, populated part of Eastern Norway. There are also some seismic activity in the area around and along the fault. The faults for the M_W 7.0, M_W 6.5 and M_W 6.0 scenarios are located close to the middle of the Hamar Fault because there are some seismic activity associated with the area, and they are located close to cities like Oslo, Jevnaker and Lillestrøm. Drammen Fault was chosen because of its location, there is little seismicity near the fault. It is near Drammen, Hønefoss, and Oslo and its vicinity. The largest earthquake scenario is M_W 7.0 for Drammen fault, and the locations of the M_W 6.5 and M_W 6.0 scenarios were chosen based on population in the area; they are located parallel to Oslo. The last fault in the Oslo Rift Zone is Oslofjorden Fault. The largest earthquake scenario on this fault is M_W 7.4, and I chose this fault because it cuts through Oslofjorden and are close to several cities like Oslo, Lillestrøm, Drammen, Horten, Moss, Tønsberg, Fredikstad and vicinity. In addition, the M_S = 5.4 earthquake in 1904 occurred on one of the faults in Oslofjorden. This area is an old rift zone (Ro and Faleide, 1992), and the simulations on the faults are therefore performed as normal rupture. The faults for the M_W 7.0, M_W 6.5 and M_W 6.0 scenarios are located such that they will affect Oslo and surroundings if one of these earthquakes were to occur. Hamar Fault, Drammen Fault and Oslofjorden Fault with all scenarios and the seismic activity in the area are shown in Figure 4.1-1.

Hordaland is the largest populated county in Western Norway, and the second largest city in Norway, Bergen, is located here. The faults chosen for the ground motion simulations in Hordaland are Rustefjorden Fault, Hjeltefjorden Fault, Totland Fault, Sauda Fault, Northern Sunnhordland Fault and Sunnhordland Fault. Both Rustefjorden and Hjeltefjorden Fault are located near Bergen, and they cut through Sotra, which is a populated island west of Bergen. The largest earthquake scenario for these faults is M_W 7.0 for Rustefjorden Fault and M_W 7.2 for Hjeltefjorden Fault. The seismic activity is notable along these two fault, and the faults for the M_W 6.5 and M_W 6.0 scenarios were located based on the location of Bergen and the seismicity. Totland Fault is located approximately 10 km south of Bergen, and it was chosen for the simulation for its location. This is the shortest of all the faults and the largest earthquake scenario is therefore the smallest, M_W 6.9. There is some seismicity in the southwestern end of the fault, and this is where the faults for the M_W 6.5 and M_W 6.0 scenarios are located. Sauda Fault is among the five largest faults, the largest earthquake scenario is M_W 7.3, and it is located furthest from the coast (not including the faults in Oslo Rift Zone). There is some seismic activity in the area near the fault, which, together with the location and size, is the reason for adding Sauda Fault to the simulation list. There are no large cities located near this fault, but some rather small villages, so the faults for the M_W 6.5 and M_W 6.0 scenarios were located in the middle of the M_W 7.3 fault. Northern Sunnhordland Fault was chosen because it is located in an area where earthquakes occur regularly, it is located along the north-northeastern coast of Bømlo, Stord and Tysnes. The largest earthquake scenario for this fault is M_W 7.2, and the faults for the M_W 6.5 and M_W 6.0 scenarios were placed near Stord, close to the middle of the M_W 7.2 fault, because of the seismic activity on Stord. The last fault in Hordaland is Sunnhordland Fault. The largest earthquake scenario on Sunnhordland Fault is M_W 7.1, and this fault was chosen because it cuts through the city of Haugesund and there are some seismic activity in the area. The location of the faults for the M_W 6.5 and M_W 6.0 scenario was chosen because of the seismic activity and because of the location of Haugesund. These faults are simulated as normal faults. Rustefjorden Fault and Hjeltefjorden Fault are stated as normal faults, while Totland Fault is most likely a pure strike-slip fault (Fossen, 1998), and Northern Sunnhordland and Sunnhordland Fault are normal faults according to Andersen and Jansen (1987). Because most of these faults are normal faults, and because the majority of the faults were reactivated into normal faults after collapse of the Caledonian

Orogeny, Sauda Fault is simulated as a normal fault as well. Figure 4.1-2 shows the location of the faults in Hordaland with the location of all the different earthquake scenarios simulated on the faults and the seismic activity in the area.

Nordland is the third area in my study, and the faults chosen for the ground motion simulations here are Vestfjorden Fault, Nesna Fault, Båsmoen Fault and Mosjøen Fault. Vestfjorden fault is one of the longest faults in the simulation; the largest earthquake scenario is M_W 7.5. This fault was chosen because it is located far north in Nordland, near Bodø and Sortland. There is also quite a lot of seismic activity just west of the fault, and the location of the faults for the M_W 7.0, M_W 6.5 and M_W 6.0 were chosen based on this seismicity. I chose Båsmoen Fault because there were conducted several studies on the seismic activity on this fault in the early 1990's, and because it is located in Mo i Rana. The largest earthquake scenario on Båsmoen Fault is M_W 7.1, and the faults for the M_W 6.5 and M_W 6.0 scenarios are placed close to Mo i Rana. Nesna Fault is located west of Båsmoen Fault, and it was chosen because of the seismic activity in the area. The largest earthquake scenario on Nesna Fault is M_W 7.2, and the locations of the M_W 6.5 and M_W 6.0 were chosen based on the seismicity in the area. The final fault chosen for the ground motion simulations is Mosjøen Fault. Mosjøen Fault is located due south of the seismic activity in Nordland, and it was chosen because it is a long fault that potentially can cause a M_W 7.5 earthquake and because there are some seismic activity west of the fault. The faults for the M_W 7.0 M_W 6.5 M_W 6.0 scenarios are located based on this seismic activity. Båsmoen Fault is a reverse structure (Olesen, 1994) and it is simulated as such. The other faults are simulated as normal fault because the faults in Nordland were reactivated to normal fault during the collapse of the Caledonian Orogeny, and in addition, Olesen et al. (2002) mapped the faults in Nordland as normal Mesozoic structures. Figure 4.1-3 shows the locations of the faults and their earthquake scenarios with the seismic activity in Nordland.

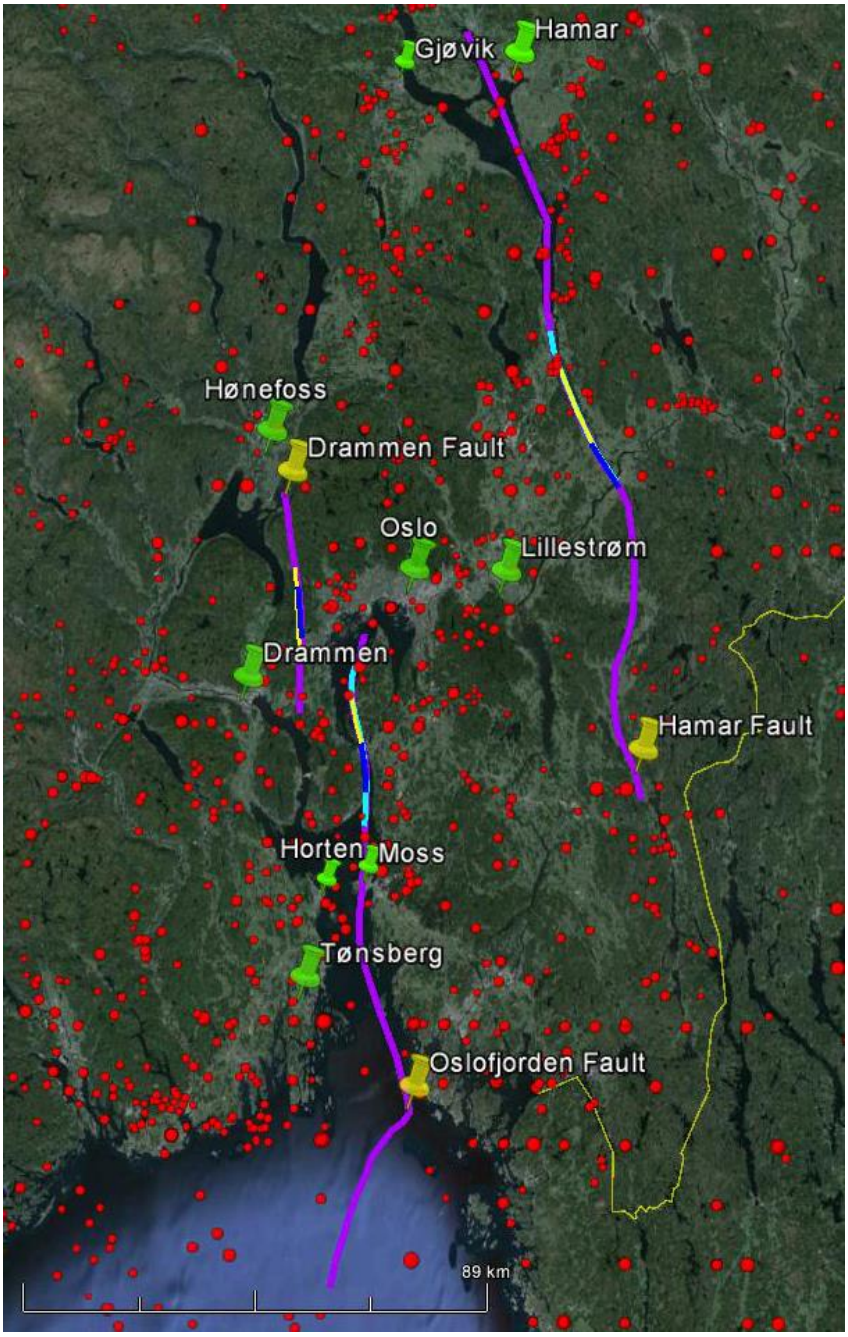

Figure 4.1-1 Faults and seismicity in the Oslo Rift Zone. All of the faults are drawn from Ro and Faleide (1992). The purple faults are the faults as they are drawn in the references, and they show the fault length that can result in an earthquake with highest magnitude possible for that length, calculated using Wells and Coppersmith (1994). The turquoise fault is the fault length that can result in a magnitude 7.0 earthquake. The yellow and blue faults are the lengths that can rupture in 6.5 and 6.0 earthquakes, respectively. The Yellow pins marks the faults and the green pins are cities located close to the faults. The red dots are the seismicity shown as earthquakes. The size of the red dot indicates the magnitude of the event.

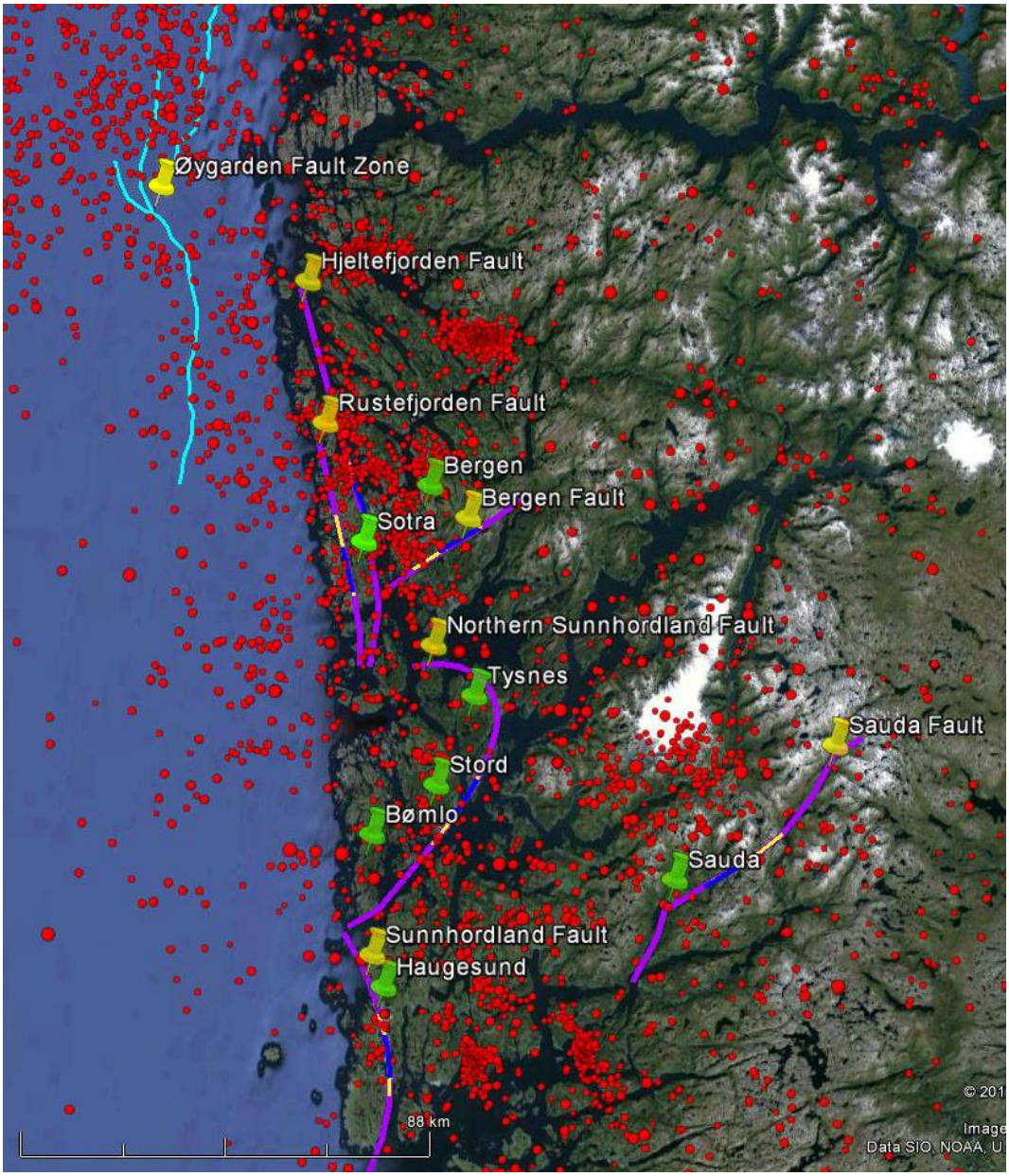

Figure 4.1-2 The faults chosen for the ground motion simulations, drawn from Fossen (1998) and Fossen (2000). The purple faults are the faults as they are drawn in the references and they constitute the earthquake scenarios with the highest possible magnitude for that fault length (based on calculations performed by Wells and Coppersmith (1994)). The yellow faults are the faults with the length that would result in a M_W 6.5 earthquake scenario, while the blue faults are the faults that would result in a M_W 6.0 scenario. The turquoise fault north of Bergen is the Øygarden Fault Zone, which is an important fault, but it is not modeled here because it has already been done by Tveit (2013). The yellow pins in the figure places the faults, and the green pins are cities near the faults. The red dots are the seismic activity, and the size of the dot indicates the magnitude of the earthquake.

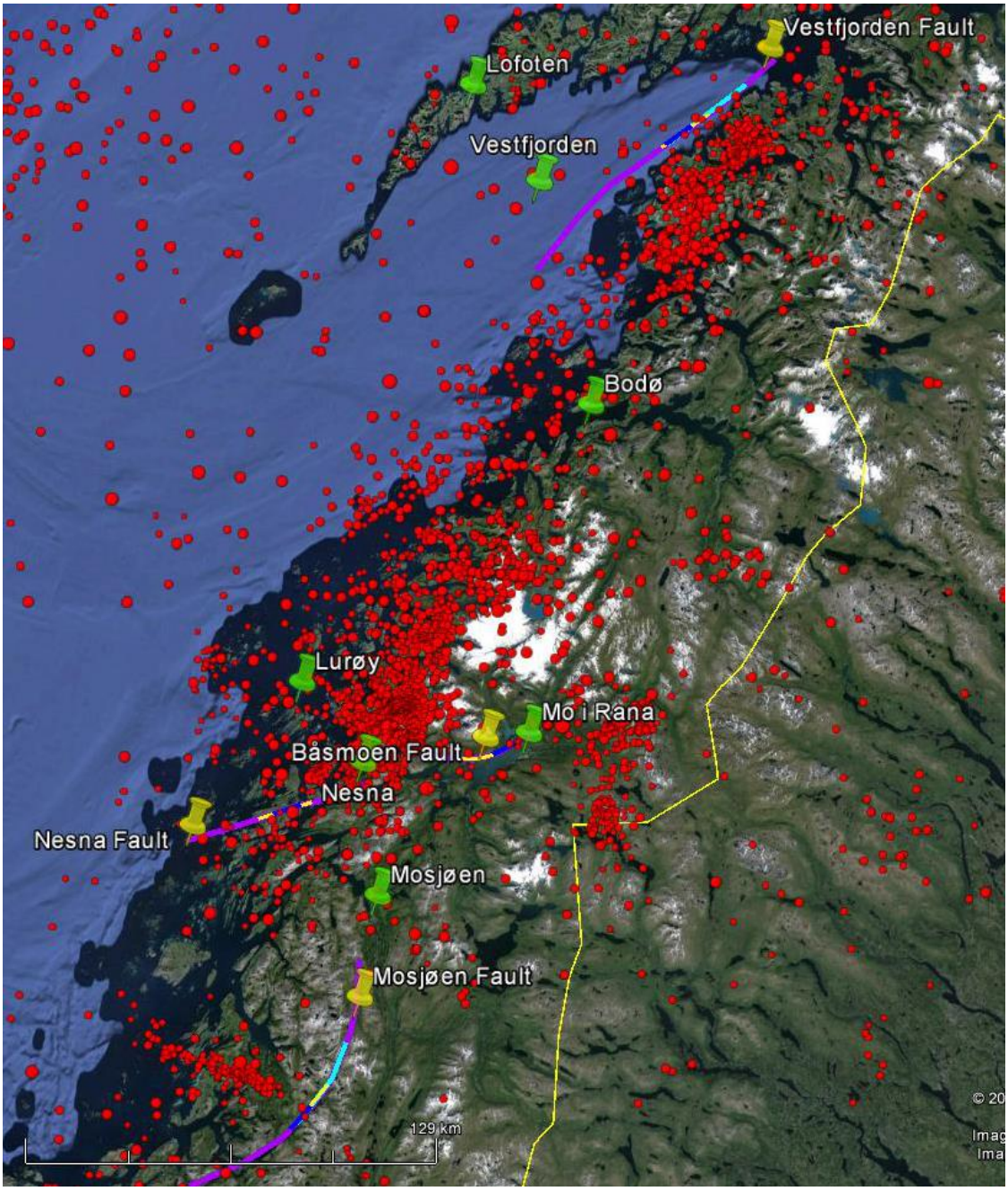

Figure 4.1-3 Faults and seismicity in Nordland. The faults are drawn from Olesen et al. (2010). The purple faults are the faults as they are drawn in the references, and they show the fault length that can result in an earthquake with the highest magnitude possible for that length, calculated using Wells and Coppersmith (1994). The Turquoise fault is the fault length that can result in a magnitude 7.0 earthquake. The yellow and blue faults are the lengths that can rupture in 6.5 and 6.0 earthquakes, respectively. The Yellow pins marks the faults and the green pins are cities located close to the faults. The red dots are the seismicity shown as earthquakes. The size of the red dot indicates the magnitude of the event.

			Maximum magnitude event			
Fault name	**Fault type**	**Maximum MW**	**Fault length**	**Fault width**	**Latitude**	**Longitude**
Hamar Fault	Normal	7.7 M	150.0 km	18.5 km	60.874167	10.920278
Mosjøen Fault	Normal	7.5 M	100.0 km	19.0 km	65.711944	13.139444
Vestfjorden Fault	Normal	7.5 M	98.0 km	19.4 km	68.248611	15.609722
Oslofjorden Fault	Normal	7.4 M	90.0 km	18.0 km	59.855278	10.610833
Sauda Fault	Normal	7.3 M	75.0 km	17.4 km	59.961944	7.173611
Nesna Fault	Normal	7.2 M	60.0 km	18.0 km	66.198611	13.088333
Hjeltefjorden Fault	Normal	7.2 M	60.0 km	18.0 km	60.811944	4.721667
Northern Sunnhordland Fault	Normal	7.2 M	60.0 km	18.0 km	60.046944	5.623056
Sunnhordland Fault	Normal	7.1 M	50.0 km	18.0 km	59.563333	5.179444
Båsmoen Fault	Reverse	7.1 M	50.0 km	17.36 km	66.335000	14.105278
Rustefjorden Fault	Normal	7.0 M	46.0 km	16.0 km	60.458333	4.915278
Drammen Fault	Normal	7.0 M	44.0 km	16.8km	60.095833	10.326111
Totland Fault	Strike-slip	6.9 M	35.0 km	17.9 km	60.418889	5.600278

Table 4-2 List of the faults and their maximum potential magnitude. The table also lists the fault lengths and widths, and the coordinates of the upper edge of the fault. These are the purple faults in Figure 4.1-1 - Figure 4.1-3.

			Magnitude 7 event			
Fault name	**Fault type**	**Maximum MW**	**Fault length**	**Fault width**	**Latitude**	**Longitude**
Hamar Fault	Normal	7.7 M	30.90 km	23.99 km	60.699167	11.068333
Mosjøen Fault	Normal	7.5 M	30.90 km	23.99 km	65.486111	13.098889
Vestfjorden Fault	Normal	7.5 M	30.90 km	23.99 km	68.177222	15.424722
Oslofjorden Fault	Normal	7.4 M	30.90 km	23.99 km	59.822222	10.581667
Sauda Fault	Normal	7.3 M				
Nesna Fault	Normal	7.2 M				
Hjeltefjorden Fault	Normal	7.2 M				
Northern Sunnhordland Fault	Normal	7.2 M				
Sunnhordland Fault	Normal	7.1 M				
Båsmoen Fault	Reverse	7.1 M				
Rustefjorden Fault	Normal	7.0 M				
Drammen Fault	Normal	7.0 M				
Totland Fault	Strike-slip	6.9 M				

Table 4-3 List of the faults that are simulated for a magnitude 7.0 earthquake, with the fault lengths and widths and the coordinates of the upper edge of the fault. These are the turquoise faults in Figure 4.1-1 - Figure 4.1-3.

			Magnitude 6.5 event			
Fault name	**Fault type**	**Maximum MW**	**Fault length**	**Fault width**	**Latitude**	**Longitude**
Hamar Fault	Normal	7.7 M	17.37 km	16.90 km	60.306111	11.253611
Mosjøen Fault	Normal	7.5 M	17.37 km	16.90 km	65.361667	13.009167
Vestfjorden Fault	Normal	7.5 M	17.37 km	16.90 km	68.088611	15.171389
Oslofjorden Fault	Normal	7.4 M	17.37 km	16.90 km	59.752222	10.569167
Sauda Fault	Normal	7.3 M	17.37 km	16.90 km	59.776111	6.788056
Nesna Fault	Normal	7.2 M	17.37 km	16.90 km	66.122222	12.761667
Hjeltefjorden Fault	Normal	7.2 M	17.37 km	16.90 km	60.454722	5.010556
Northern Sunnhordland Fault	Normal	7.2 M	17.37 km	16.90 km	59.867222	5.585556
Sunnhordland Fault	Normal	7.1 M	17.37 km	16.90 km	59.401389	5.2991670
Båsmoen Fault	Reverse	7.1 M	17.18 km	13.96 km	66.341111	14.214444
Rustefjorden Fault	Normal	7.0 M	17.37 km	16.90 km	60.340556	4.985556
Drammen Fault	Normal	7.0 M	17.37 km	16.90 km	59.962500	10.373056
Totland Fault	Strike-slip	6.9 M	18.20 km	14.79 km	60.345000	5.536944

Table 4-4 List of the faults that are simulated for a magnitude 6.5 earthquake, with the fault lengths and widths and coordinates of the upper edge of the fault. These faults are yellow in Figure 4.1-1 - Figure 4.1-3.

			Magnitude 6 event			
Fault name	**Fault type**	**Maximum MW**	**Fault length**	**Fault width**	**Latitude**	**Longitude**
Hamar Fault	Normal	7.7 M	9.77 km	11.50 km	60.179722	11.370278
Mosjøen Fault	Normal	7.5 M	9.77 km	11.50 km	65.296111	12.908611
Vestfjorden Fault	Normal	7.5 M	9.77 km	11.50 km	68.051667	15.056944
Oslofjorden Fault	Normal	7.4 M	9.77 km	11.50 km	59.671944	10.583333
Sauda Fault	Normal	7.3 M	9.77 km	11.50 km	59.726389	6.624722
Nesna Fault	Normal	7.2 M	9.77 km	11.50 km	66.106667	12.691944
Hjeltefjorden Fault	Normal	7.2 M	9.77 km	11.50 km	60.424444	5.035833
Northern Sunnhordland Fault	Normal	7.2 M	9.77 km	11.50 km	59.860556	5.579444
Sunnhordland Fault	Normal	7.1 M	9.77 km	11.50 km	59.362500	5.312222
Båsmoen Fault	Reverse	7.1 M	8.3 km	9.35 km	66.333611	14.141111
Rustefjorden Fault	Normal	7.0 M	9.77 km	11.50 km	60.280833	5.020278
Drammen Fault	Normal	7.0 M	9.77 km	11.50 km	59.933333	10.382778
Totland Fault	Strike-slip	6.9 M	7.76 km	12.30 km	60.336111	5.545556

Table 4-5 List of the faults that are simulated for a magnitude 6.0 earthquake, with the fault lengths and widths and coordinates of the upper edge of the faults. These faults are blue in Figure 4.1-1 - Figure 4.1-3.

4.2 INPUT PARAMETERS IN EXSIM12

EXSIM12 calculates the ground motion based on parameters describing the fault and properties of the crust in the area. The program calculates the ground motion time histories based on information about stress drop, magnitude, velocity of the S-wave and quality factor. The most critical parameters are the ones that describe the fault: magnitude, fault length, fault width and the location of the fault. These values are discussed in the previous subchapter. I have used set values for the stress drop, velocity, path duration, time step, geometric spreading and quality factor; meaning that I use the same value for all the faults in Norway. The values of quality factor, path duration and geometric spreading are taken from Boore (2009), and are based on the properties of the hard rocks in the Eastern North American crust.

Tveit (2013) used EXSIM12 to simulated peak ground acceleration in Øygarden Fault Zone, Figure 4.1-2, and in doing so, she performed a sensitivity study of the input parameters in EXSIM12. Given that the Øygarden Fault Zone is located off the coast of Norway, I find it appropriate to assume that the earthquake scenarios in my simulations have the same properties as Øygarden Fault Zone.

In the sensitivity study, Tveit (2013) found that the value of stress drop ($\Delta\sigma$), kappa (κ) and the moment magnitude are the three parameters that affect the ground motion acceleration the most. I therefore use the values that she concluded as the best options for Øygarden Fault Zone: 0.02 for κ and 80 for $\Delta\sigma$. The depth of the faults also has major impact of the result close to the fault, but due to lack of information, and the fact that most earthquakes in Norway occur deep in the crust, the depth of the rupture is set to 15.0 km for all the faults in my simulations. The velocity of the S-wave is set to 3.7 km/s and the density of the crust is 2.8 gm/cm^3 , which is the velocity of the S-wave and density in Eastern North America used by Boore (2009) and suggested as the best option by Tveit (2013).

The location of the hypocenter location along the fault is chosen to be random in my simulations because this is a predictive study, and not a study of a known earthquake or earthquakes. For the same reason, and because it is impossible to know how the slip occurs along the fault, the slip distribution is also set to be random.

The length and width of the subfaults are set to be between 10.0 and 2.5 km, dependent on the size of the fault area. The largest faults, Hamar, Oslofjorden, Mosjøen and Vestfjorden have 10.0 x 10.0 km subfaults, while the rest of the faults are set to 5.0 km for the maximum magnitude. All of the faults have the same length and width for the magnitude 6.5 and 6.0 events and the size of the subfaults are set to be 2.5 x 2.5 km for the magnitude 6.5 scenarios, and 2.0 x 2.0 km for the magnitude 6.0 scenarios. Tveit (2013) found that setting the subfault length too small will cause the peak ground acceleration to increase near the fault, and if the subfault width is too small, the opposite will occur; the ground motion acceleration will decrease near the fault. During an earthquake, not all of the subfaults in the fault plane will be active at the same time. I use the pulsing percent suggested by Boore (2009), which is 50 %, meaning that 50 % of the subfaults are active at the same time.

The coordinates and number of sites in the simulation are the points in which EXSIM12 calculates the ground motion time histories. This means that the sites need to form a grid with several points to cover the area that is affected by the earthquake. The coordinates cannot be too far apart, as this will make the interpolation between the points inaccurate when the plots are made using Generic Mapping Tool, GMT (Wessel et al., 2013). Therefore, the simulations are run with sites that form a grid with 0.1° between each point.

I used the crustal amplification file that came with the installation of EXSIM12 because it is given for a hard rock site, which Norway is. There is no site amplification in the simulation because it is not needed for a hard rock site because the amplitude is not reduced by the crust. As for the empirical filter, this is also not needed in my simulations as I do not need to apply an instrument-response function or an additional site-response function, and both the site amplification file and the empirical filter file that followed the installation of the EXSIM12 program are applied. Table 4-6 lists the input parameters used in EXSIM12, and where the parameters are taken from.

Table 4-6 Input parameters used in the simulations in EXSIM12

Parameter	**Value used in the simulations**	**Reference**
Moment Magnitude, M_W	The value ranges between M_W 7.7 to M_W 6.0, based on the length of the faults and the desired earthquake scenario.	M_W is calculated using formulas calculated by Wells and Coppersmith (1994). The formulas are listed in Table 4-1.
Stress drop, $\Delta\sigma$	80 bar	Tveit (2013)
Kappa, κ	0.02	Tveit (2013)
Coordinates of the upper edge of the fault	Dependent on the location of the fault	
Fault length	Varies	The length is calculated using formulas calculated by Wells and Coppersmith (1994). The formulas are listed in Table 4-1.
Fault width	Varies	The width is calculated using formulas calculated by Wells and Coppersmith (1994). The formulas are listed in Table 4-1.
Depth of the fault	15.0 km	
Fault dip	45, 60 or 70	
Subfault length	Between 10 and 2, dependent on the fault length	
Subfault width	Between 10 and 2, dependent on the fault length	
Rupture velocity / S-wave velocity	0.8	From the example following the installation of EXSIM12
Hypocenter location	-1.0 -1.0 (Random)	
Rise time	1	
Density	2.8 gm/cm^3	Boore (2009)
S-wave velocity	3.7 km/sec	Boore (2009)
Geometric spreading	R^b : b = 1.0 3 1.3 (10 - 70 km) 0.2 (70 -140 km) -0.5 (>140 km)	Boore (2009)
Quality factor	Q = max [1000, 893 $f^{0.32}$]	Boore (2009)
Distance depending on duration	dR, d = 3 0.16 (10 - 70 km) -0.03 (70 – 130 km) 0.04 (> 130 km) 0.05	Boore (2009)

Type of window	1 (Saragoni-Hart window)	
Low-cut filter corner (Hz)	0.05 (the filer removes frequencies lower than 0.05 Hz)	From the example following the installation of EXSIM12
Output ground motion frequencies	PGA, PGV 0.5 5.0	From the example following the installation of EXSIM12
Pulsing percent	50	Boore (2009)
Iterations per site	3	
Slip distribution	1 (Random slip)	

An example of a file containing the needed parameters ready for simulation in EXSIM12 can be found in Appendix A.

5 RESULTS

5.1 GROUND MOTION SIMULATIONS

I have simulated the ground motion for three earthquake scenarios on each of the 13 faults with the highest magnitude possible for each fault length (M_W 7.7 – M_W 6.9, calculated using Wells and Coppersmith (1994)), M_W 6.5 and M_W 6.0. The four largest fault have an additional scenario, M_W 7.0, to accommodate the large span between the highest potential magnitude and M_W 6.5. This adds up to 43 earthquake scenarios. This chapter presents all of the faults, but only one fault from each area (Oslo Rift Zone, Hordaland and Nordland) are shown with earthquake scenario for all of the magnitudes. The other faults are shown with one or two earthquake scenario for a selected magnitude, and the remaining earthquake scenarios can be found in Appendix B.

5.2 EARTHQUAKE SCENARIOS AND PEAK GROUND MOTION ACCELERATION

This chapter shows the earthquake scenarios that illustrates the distribution of the peak ground acceleration around the fault. The results from all of the different magnitudes in the earthquake scenarios are presented for three faults, one from each of the three areas in this study. These faults are Hamar Fault, Vestfjorden Fault and Sunnhordland Fault. The other faults are presented with selected earthquake scenarios, and the rest of the scenarios can be found in Appendix B. The results will be discussed in the next chapter. The ground acceleration is given in cm/s^2, and Stein and Wysession (2012) have used Bolt (1999) to link the Modified Mercalli Intensity Scale to peak ground acceleration values:

Table 5.2-1 Modified Mercalli Intensity Scale (from (Stein and Wysession, 2012)).

Modified Mercalli Intensity Scale		
Intensity	**Effects**	**Approx. PGA**
I	No shaking felt, no damage: Not felt except for a few under very favorable conditions	
II	Weak shaking, no damage: Felt only by few people resting, especially on upper floors of buildings. Delicately suspended objects may swing.	
III	Some shaking, no damage: Felt quite noticeably indoors, especially on upper floors of buildings. Many people does not recognize it as an earthquake. Standing automobiles may rock slightly, vibration like passing truck. Duration estimated.	

IV	Light shaking, no damage: Felt indoor by many during the day, outdoors by few. At night, some are awakened. Dishes, windows, doors are disturbed; walls make creaking sound. Sensation like heavy truck striking building. Standing automobiles rocked noticeably.	15 - 20 cm/s^2
V	Moderate shaking, very light damage: Felt by nearly everyone, many are awakened. Some dishes, windows, and so on are broken; cracked plaster in few places; unstable objects overturned. Disturbances of trees and poles, and other tall objects sometimes noticed. Pendulum clocks may stop.	30 - 40 cm/s^2
VI	Strong shaking, light damage: Felt by all, many are frightened and run outdoors. Some heavy furniture are moved; a few instances of fallen plaster and damaged chimneys. Slight damage.	60 - 70 cm/s^2
VII	Very strong shaking, moderate damage: Everybody runs outdoors. Damage are negligible in buildings of good design and construction; slight to moderate in well-built ordinary structures; considerable in poorly built or badly designed structures; some chimneys are broken. Noticed by persons driving cars.	100 - 150 cm/s^2
VIII	Severe shaking, moderate to heavy damage: Damage slight in specially designed structures; considerable in ordinary substantial buildings with partial collapse; great in poorly built structures. Panel walls are thrown out of frame structures. Fall of chimneys, factory stacks, columns, monuments, walls. Heavy furniture are overturned. Sand and mud are ejected in small amount. Changes in well water. Persons driving cars are disturbed.	250 - 300 cm/s^2
IX	Violent shaking, heavy damage: Damage considerable in specially designed structures; well-designed frame structures are thrown out of plump; great in substantial buildings, with partial collapse. Buildings are shifted off foundations. Ground are cracked conspicuously. Underground pipes are broken.	500 - 550 cm/s^2
X	Extreme shaking, very heavy damage: Some well-built wooden structures are destroyed; most masonry and frame structures are destroyed with foundations; ground are badly cracked. Rails are bent. Landslides are considerable from riverbanks and steep slopes. Shifted sand and mud, water splashed and slopped over banks.	More than 600 cm/s^2
XI	Few, if any, (masonry) structures remain standing. Bridges are destroyed. Broad fissures in the ground. Underground pipelines are completely out of service. Earth slumps and the land slips in soft ground. Rails are bent greatly.	
XII	Total damage. Waves are seen on ground surfaces. Lines of sight and level are destroyed. Objects are thrown in the air.	

Table 5.2-2 lists the maximum peak ground acceleration (PGA) in cm/s^2 for each earthquake scenario. The table shows that the peak ground acceleration for the maximum magnitude earthquake scenarios goes from 308.4 cm/s^2 on Hamar Fault to 200.7 cm/s^2 on Rustefjorden Fault. This result was expected as the magnitude is dependent on the fault length, leading to different magnitudes for the faults. Also for the scenarios with the same magnitude do the maximum PGA vary, for example for M_W 7.0 does Hamar Fault have 244.8 cm/s^2 while Mosjøen Fault has 319.4 cm/s^2 as the highest value. Such differences are also found in the M_W 6.5 and M_W 6.0 scenarios. These results were not expected because the input parameters are very similar for the same magnitude, which should result in more equal results. However, the results do decrease with magnitude for each fault, which is expected as higher magnitude releases more energy resulting in higher peak ground acceleration. Båsmoen Fault is the only reverse fault and Totland Fault is the only strike-slip fault in the simulations, and the ground motion acceleration may therefore deviate some from the other results. All of the other fault are normal faults. The PGA values in the scenarios are linked to the Modified Mercalli Intensity Scale, Table 5.2-1 by giving estimated intensities, because the actual intensity during an earthquake are dependent on the duration of the shaking, the distance from the source and local site effects like lithology and density of the crust.

Table 5.2-2 List of the faults and the maximum PGA for each earthquake scenario.

Faults	Max mag	Fault type	Length	Dip	Maximum peak ground acceleration (cm/s^2)			
					Max Mag	M 7.0	M 6.5	M 6.0
Hamar	M 7.7	Normal	150.0 km	60	308.4000	244.8000	191.1000	105.3000
Mosjøen	M 7.5	Normal	100.0 km	60	272.8000	319.4000	191.4000	111.5000
Vestfjorden	M 7.5	Normal	98.0 km	60	317.6000	251.2000	173.2000	92.5000
Oslofjorden	M 7.4	Normal	90.0 km	60	267.4000	235.4000	178.2000	106.3000
Sauda	M 7.3	Normal	75.0 km	60	280.7000		177.7000	129.4000
Nesna	M 7.2	Normal	60.0 km	60	239.5000		179.4000	117.7000
Hjeltefjorden	M 7.2	Normal	60.0 km	45	267.0000		154.5000	115.7000
Northern Sunnhordland	M 7.2	Normal	60.0 km	60	217.3000		180.0000	91.1100
Sunnhordland	M 7.1	Normal	50.0 km	60	206.5000		178.5000	98.6100
Båsmoen	M 7.1	Reverse	50.0 km	60	239.9000		157.6000	139.6000
Rustefjorden	M 7.0	Normal	46.0 km	70	200.7000		188.9000	96.1200
Drammen	M 7.0	Normal	44.0 km	60	228.6000		164.6000	91.4400
Totland	M 6.9	Strike-slip	35.0 km	60	214.4000		171.4000	132.0000

5.2.1 Oslo Rift Zone, Eastern Norway

In this subchapter the Oslofjorden Fault is represented by the earthquake scenarios of M_W 7.4 and M_W 6.5; the scenarios of M_W 7.0 and M_W 6.0 can be found in Appendix B. Hamar Fault is represented by all four earthquake scenarios (M_W 7.7, M_W 7.0, M_W 6.5 and M_W 6.0) in this subchapter. One of the earthquake scenarios, M_W 7.0, represents Drammen Fault; the scenarios of M_W 6.5 and M_W 6.0 can be found in Appendix B.

5.2.1.1 Oslofjorden Fault M_W 7.4

Figure 5.2.1-1 shows the earthquake scenario for Oslofjorden Fault, with the PGA that would occur following a M_W 7.4 event. The maximum PGA is estimated to be 267.5 cm/s^2. The distribution of the PGA in Figure 5.2.1-1 shows that the center of the distribution gets acceleration values above 100 cm/s^2, covering an area of approximately 7600 km^2. 100 cm/s^2 could correspond to intensity VII on the Modified Mercalli Intensity Scale, Table 5.2-1. Within this area Oslo, the largest city and capital of Norway, Horten, Moss, Sandefjord, Tønsberg and Drammen are situated. In addition are several cities located outside the 100 cm/s^2 contour line, experiencing PGA above 50 cm/s^2, which may indicate to shaking of intensity V and VI on the Modified Mercalli Intensity Scale. This area is much larger, approximately 45 000 km^2, and cities located in this area are Lillestrøm, Hønefoss and Jevnaker.

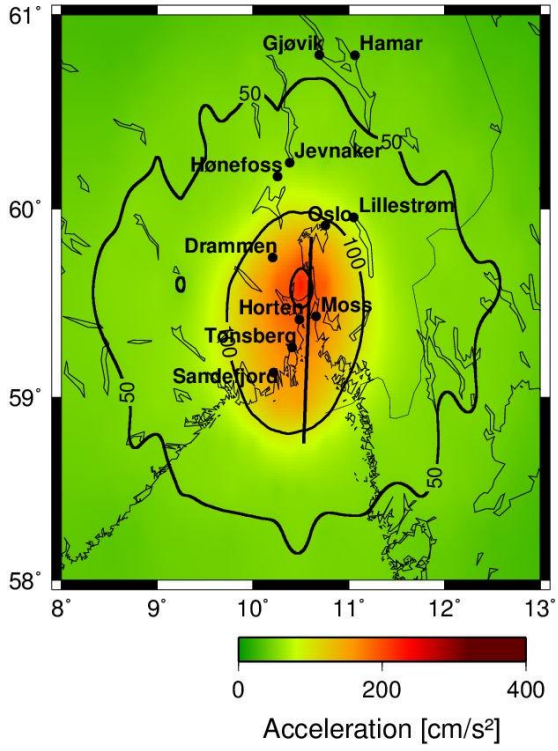

Figure 5.2.1-1 Peak ground acceleration distribution for a M_W 7.4 earthquake scenario on Oslofjorden Fault.

5.2.1.2 Oslofjorden Fault M_W 6.5

Figure 5.2.1-2 shows the earthquake scenario for Oslofjorden Fault, with the PGA that would occur following a M_W 6.5 event. The maximum PGA is estimated to be 178.2 cm/s^2. The distribution of the PGA in Figure 5.2.1-2 shows that an area of approximately 5400 km^2 would be exposed to PGA values of 50 – 178.2 cm/s^2. The area in the center would be exposed to shaking that exceeds 100 cm/s^2, which may indicate intensity VII, is approximately be 950 km^2. This value of PGA may indicate shaking of intensity VII on the Modified Mercalli Intensity Scale, Table 5.2-1. Oslo, Drammen, Moss and Horten are located within the 50 cm/s^2 contour line, where the PGA could correspond to VI on the Modified Mercalli Intensity Scale.

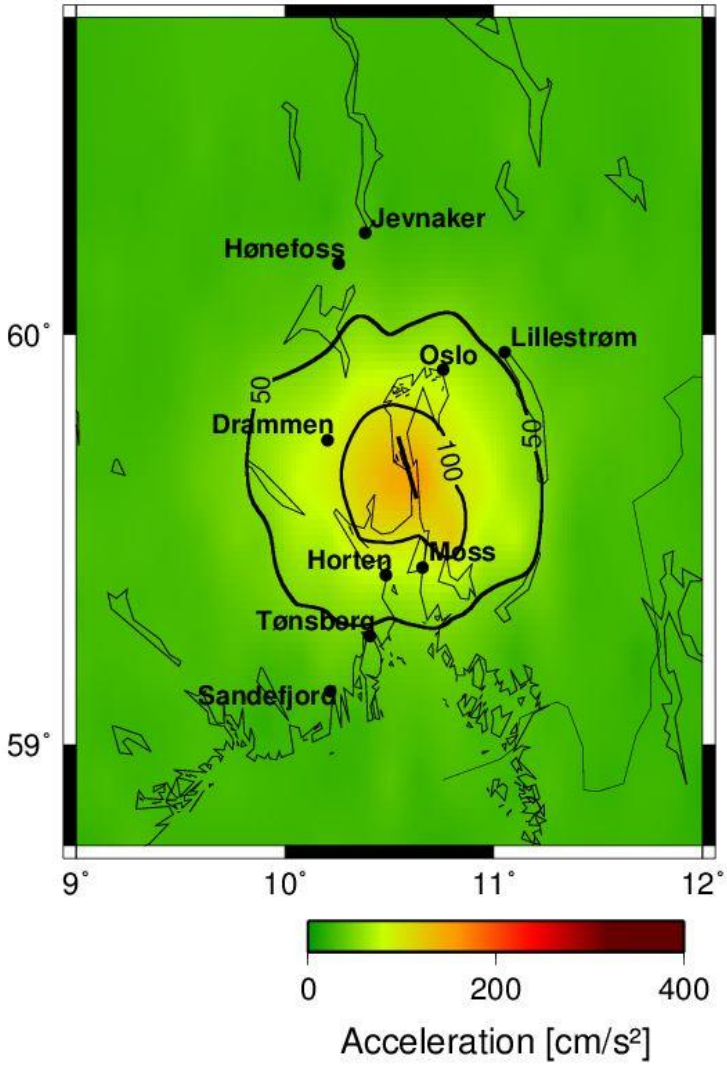

Figure 5.2.1-2 Peak ground acceleration distribution for a M_W 6.5 earthquake scenario on Oslofjorden Fault.

5.2.1.3 Hamar Fault M_W 7.7

This is the largest earthquake of all the scenarios. Figure 5.2.1-3 shows that the 50 cm/s² contour line of PGA will cover a large area, approximately 60 300 km², and cross over the Swedish border. Cities within this area include Lillehammer, Sandefjord and Tønsberg. The maximum PGA is estimated to be 308.1 cm/s², which could correspond to ground shaking of intensity VIII on the Modified Mercalli Intensity Scale (Table 5.2-1). The area affected by ground acceleration between 100 and 308.1 cm/s² is approximately 9200 km², and Gjøvik, Hamar, Oslo and Lillestrøm are situated within this area.

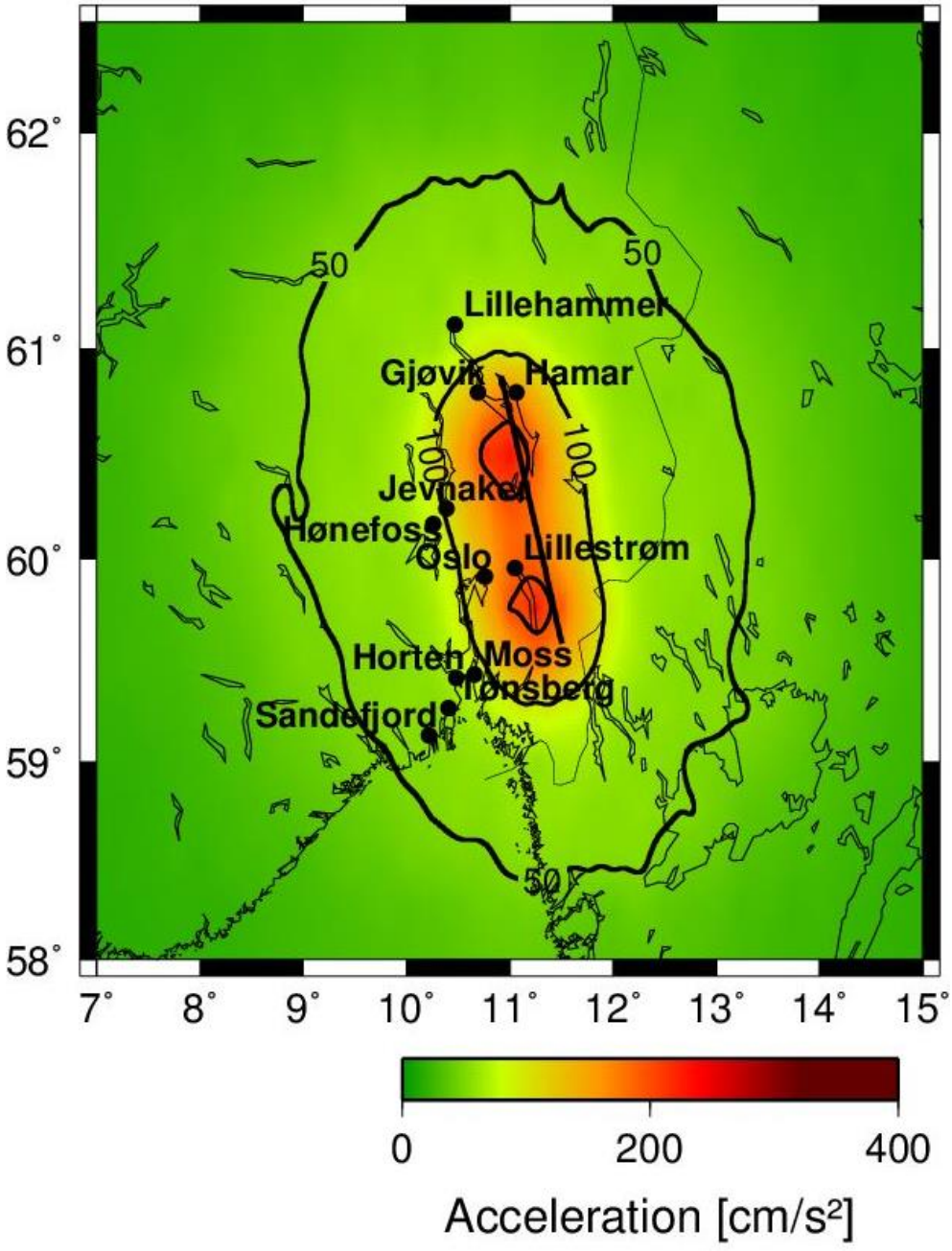

Figure 5.2.1-3 Peak ground acceleration distribution for a M_W 7.7 earthquake scenario on Hamar Fault.

5.2.1.4 Hamar Fault M_W 7.0

The M_W 7.0 earthquake scenario for Hamar Fault has a maximum PGA of 244.8 cm/s^2, which may indicate shaking of intensity VII on the Modified Mercalli Intensity Scale (Table 5.2-1). Figure 5.2.1-4 show the PGA following the earthquake would affect a 10 900 km^2 large area with 50 cm/s^2, while 2600 km^2 would be exposed to ground acceleration 100 – 244.8 cm/s^2. Within this area, Hamar and Gjøvik are situated, in addition to Mjøsa, Norway's largest lake.

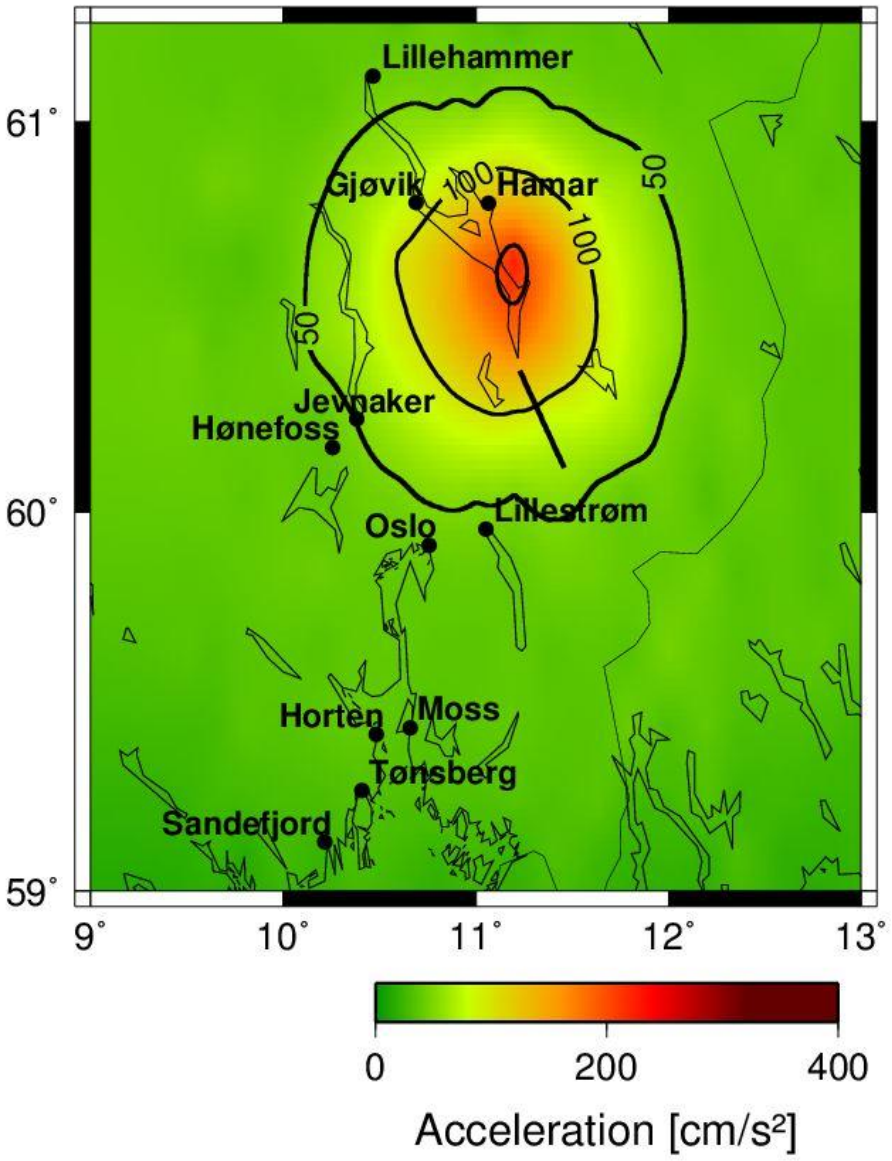

Figure 5.2.1-4 Peak ground acceleration distribution for a M_W 7.0 earthquake scenario on Hamar Fault.

5.2.1.5 Hamar Fault M_W 6.5

Figure 5.2.1-5 shows that approximately 6200 km^2 would be affected by PGA of 50 – 191.1 cm/s^2 after a M_W 6.5 earthquake on Hamar Fault. The area within the 100 cm/s^2 contour line could experience shaking of intensities between VII and VIII on the Modified Mercalli Intensity Scale (Table 5.2-1) during the earthquake. The maximum PGA is estimated to be 191.1 cm/s^2.

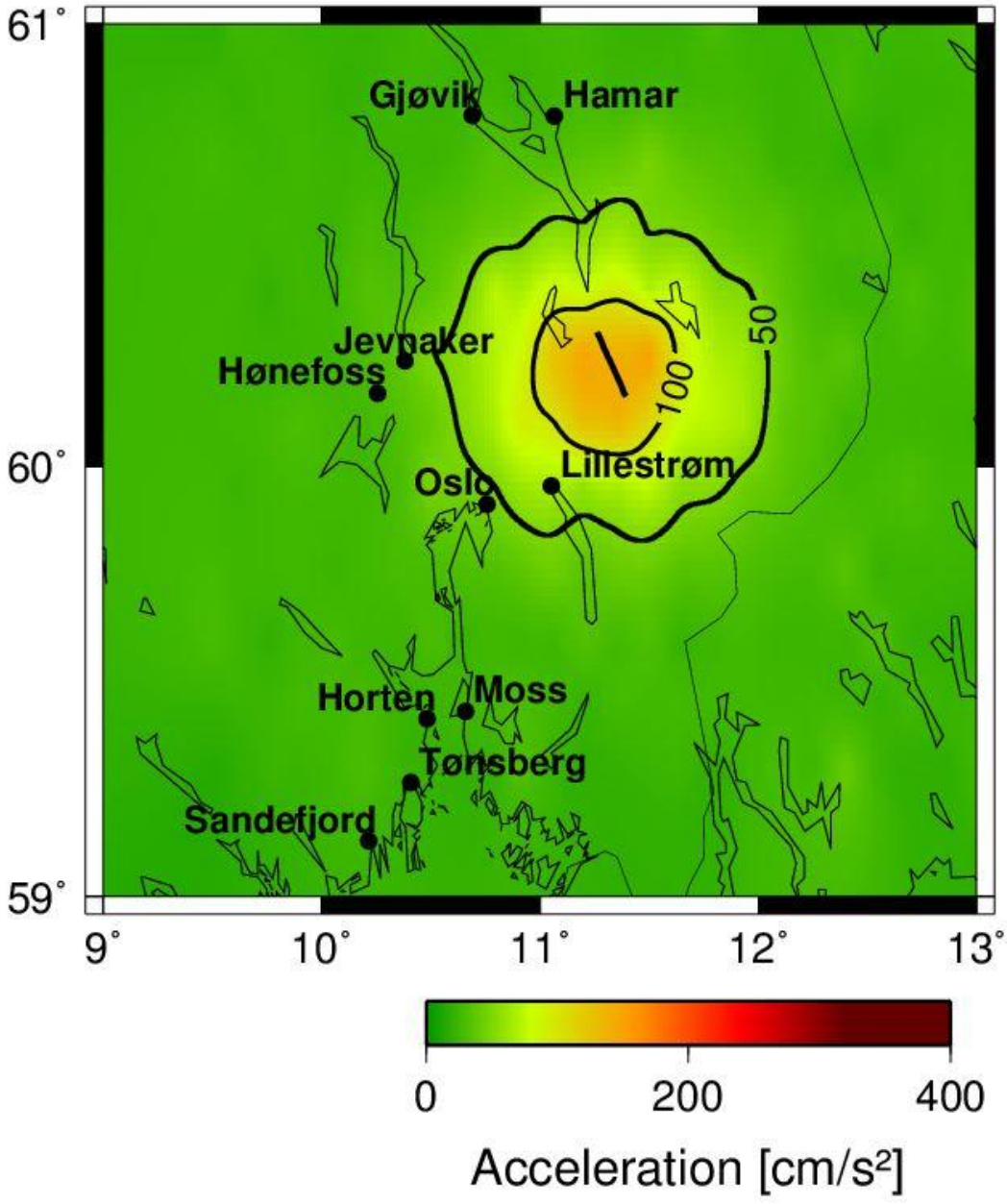

Figure 5.2.1-5 Peak ground acceleration distribution for a M_W 6.5 earthquake scenario on Hamar Fault.

5.2.1.6 Hamar Fault M_W 6.0

Figure 5.2.1-6 shows the PGA following a M_W 6.0 earthquake on Hamar Fault. The area affected by 50 -100 cm/s^2, which may indicate shaking of intensities between VI and VII on the Modified Mercalli Intensity Scale (Table 5.2-1), is approximately 2700 km^2. Lillestrøm is located just within this area. The maximum PGA is estimated to be 105.3 cm/s^2.

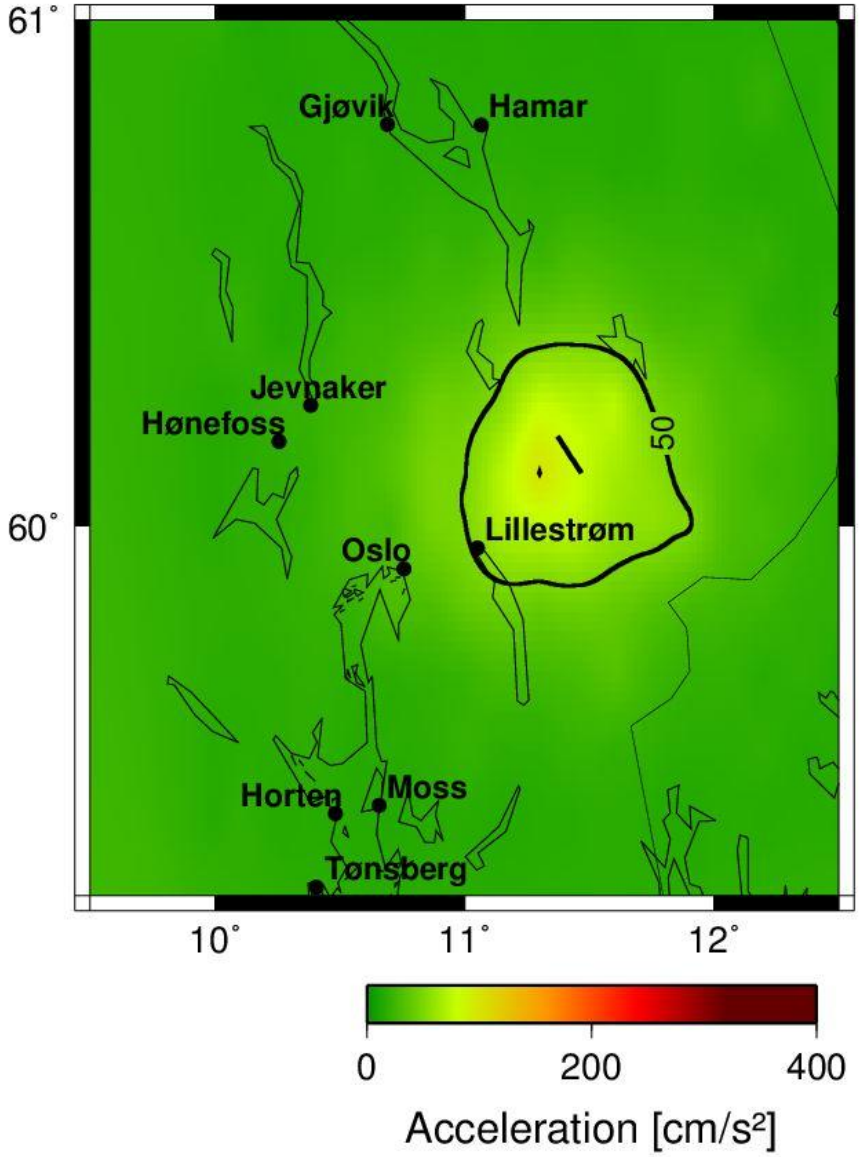

Figure 5.2.1-6 Peak ground acceleration distribution for a M_W 6.0 earthquake scenario on Hamar Fault.

5.2.1.7 Drammen Fault M_W 7.0

The maximum PGA is estimated to be 228.6 cm/s² for an earthquake of M_W 7.0 occurring on Drammen Fault. Figure 5.2.1-7 shows that cities like Hønefoss, Jevnaker, Oslo and Drammen would be exposed to PGA between 100 and 228.6 cm/s², while an area of 12 500 km², which includes Lillestrøm, Horten and Moss, would be affected by PGA of 50 cm/s². The center of the ground motion (150 – 221.3 cm/s²) could correspond to shaking of intensity VII to VIII on the Modified Mercalli Intensity Scale, Table 5.2-1.

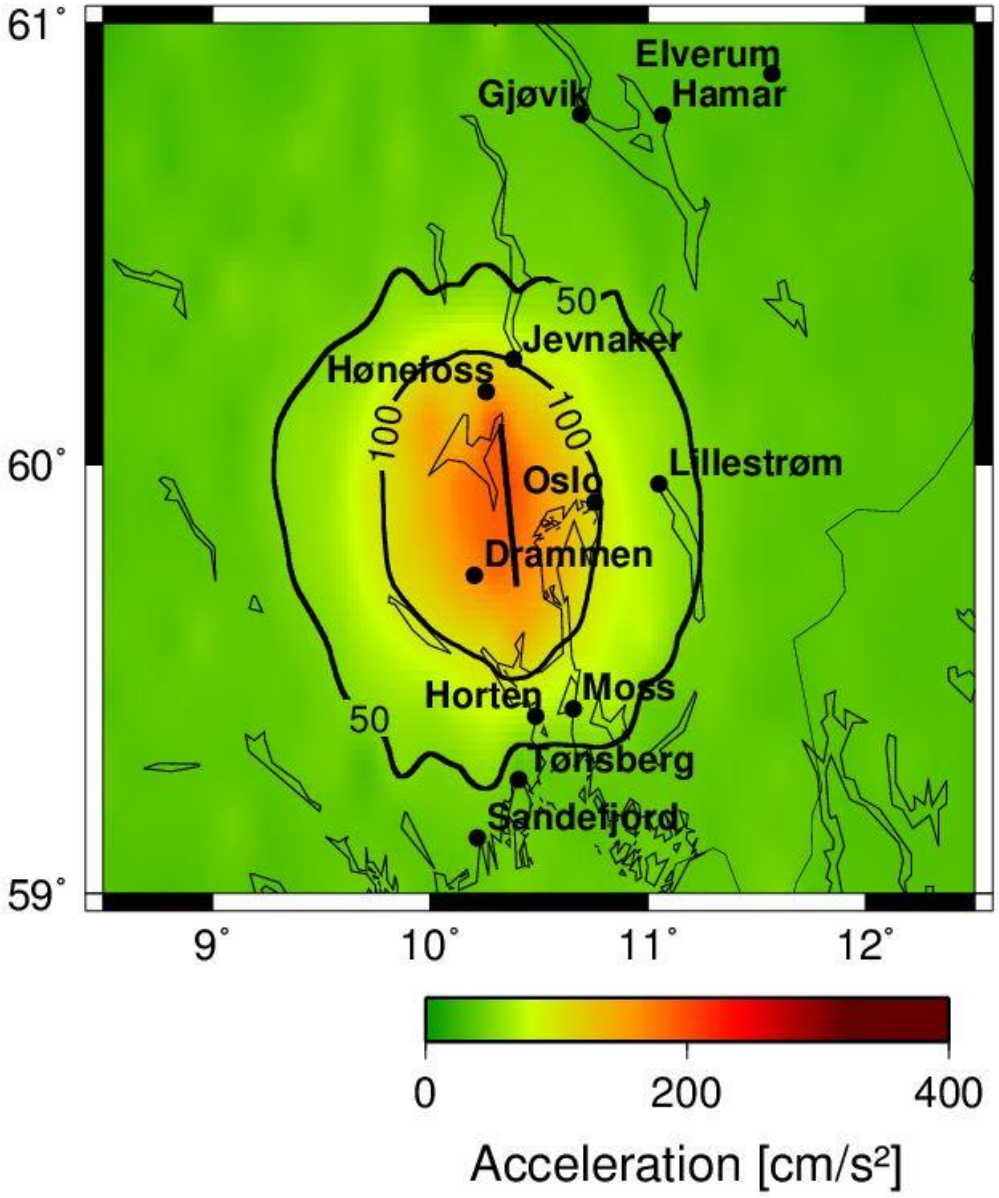

Figure 5.2.1-7 Peak ground acceleration distribution for a M_W 7.0 earthquake scenario on Drammen Fault

5.2.2 Hordaland, Western Norway

Hjeltefjorden Fault is here represented by the earthquake scenarios of M_W 6.5 and M_W 6.0, while the scenario for M_W 7.2 can be found in Appendix B. Rustefjorden Fault is represented by the earthquake scenario of M_W 7.0 in this subchapter; the scenarios for M_W 6.5 and M_W 6.0 can be found in Appendix B. The earthquake scenarios of M_W 6.9 and M_W 6.0 on Totland Fault are represented here, while the scenario for M_W 6.5 can be found in Appendix B. Northern Sunnhordland Fault is represented by the earthquake scenario of M_W 6.0 in this chapter; the scenarios of M_W 7.2 and M_W 6.5 can be found in Appendix B. All of the earthquake scenarios (M_W 7.1, M_W 6.5 and M_W 6.0) on Sunnhordland Fault are represented here. Sauda Fault is in this subchapter represented by the earthquake scenario of M_W 7.3, while the scenarios of M_W 6.5 and M_W 6.0 can be found in Appendix B.

5.2.2.1 Hjeltefjorden Fault M_W 6.5

Figure 5.2.2-1 shows the PGA that would follow a M_W 6.5 earthquake on Hjeltefjorden Fault. The maximum PGA is estimated to be 154.5 cm/s^2. Approximately 6300 km^2 would be affected by ground acceleration between 50 and 154.5 cm/s^2, which may indicate shaking of intensity VII on the Modified Mercalli Intensity Scale (Table 5.2-1). Within this area is Bergen situated, the second largest city in Norway.

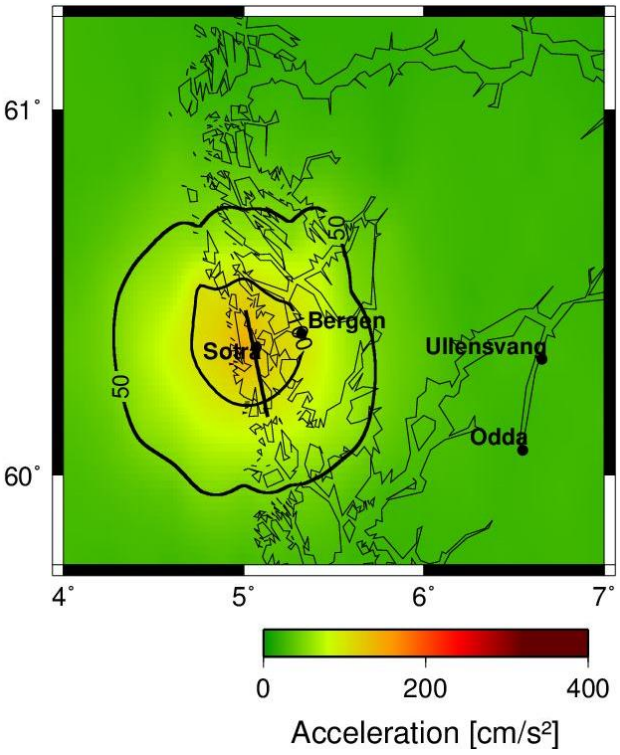

Figure 5.2.2-1 Peak ground acceleration distribution for a M_W 6.5 earthquake scenario on Hjeltefjorden Fault.

5.2.2.2 Hjeltefjorden Fault M_W 6.0

Figure 5.2.2-2 shows the PGA that would follow a M_W 6.0 earthquake on Hjeltefjorden Fault. The maximum PGA is estimated to be 115.7 cm/s^2, which may indicate intensity VII on the Modified Mercalli Intensity Scale (Table 5.2-1). The maximum PGA would only occur in the very center of the earthquake; approximately 2900 km^2 would be affected by intensity between V and VI, above 50 cm/s^2. This fault runs through Sotra, an island west of Bergen. The area affected by the ground acceleration includes Bergen, the second largest city in Norway.

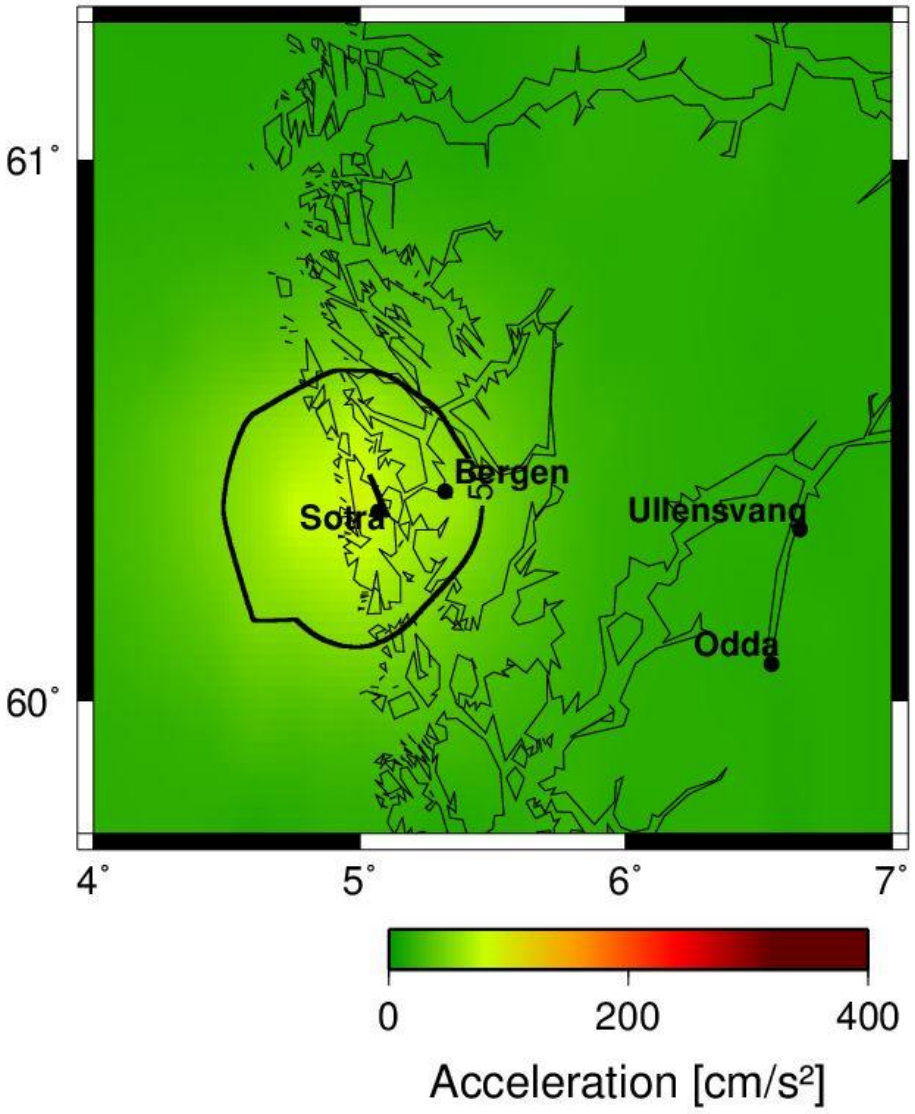

Figure 5.2.2-2 Peak ground acceleration distribution for a M_W 6.0 earthquake scenario on Hjeltefjorden Fault.

5.2.2.3 Rustefjorden Fault M_W 7.0

Figure 5.2.2-3 shows the PGA that would occur if Rustefjorden Fault ruptures in a M_W 7.0 earthquake. Rustefjorden Fault is located 4 km west of Hjeltefjorden Fault, and it runs through Sotra as well. The maximum PGA is estimated to be 200.7 cm/s^2 for such an event. An area of approximately 14 500 km^2 would be exposed to PGA between 50 – 200.7 cm/s^2, which could correspond to intensity VI – VII. Bergen is located within the 100 cm/s^2 contour line where the PGA reaches 200 cm/s^2 or approximately intensity VII on the Modified Mercalli Intensity Scale (Table 5.2-1). Bremnes on Bømlo and Leirvik on Stord are situated within the 50 cm/s^2 contour line, and would experience shaking that could correspond to intensity VI on the Modified Mercalli Intensity Scale.

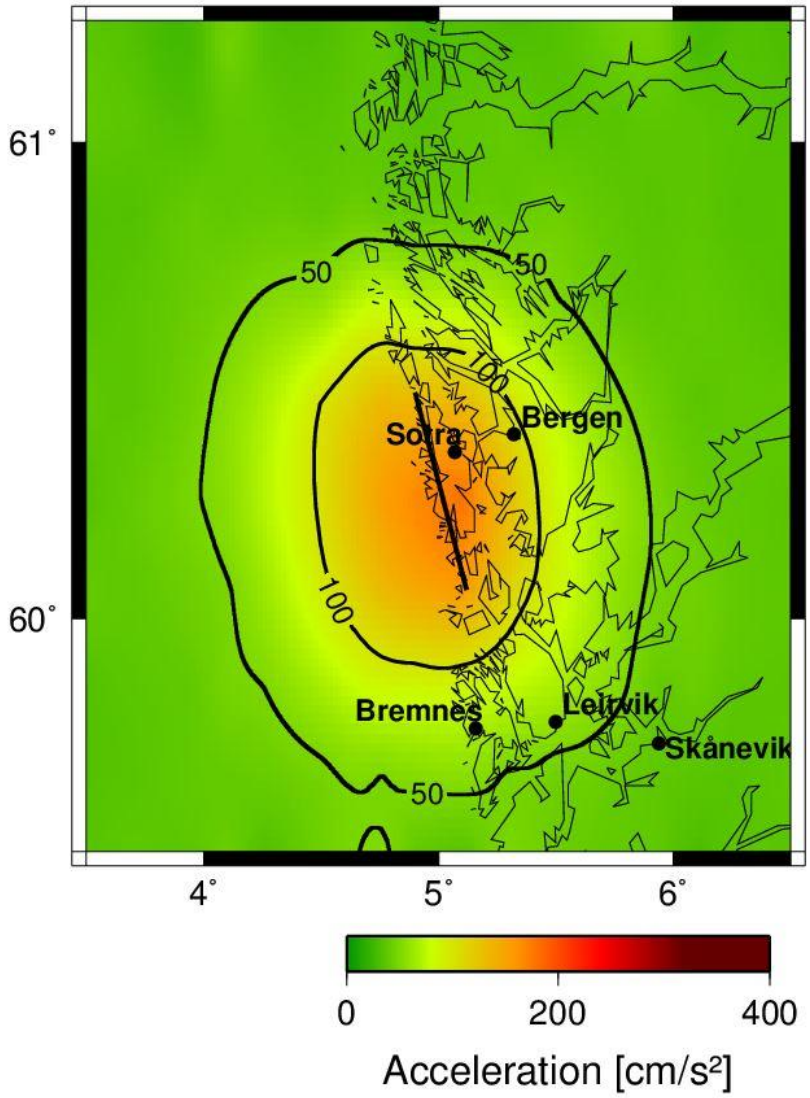

Figure 5.2.2-3 Peak ground acceleration distribution for a M_W 7.0 earthquake scenario on Rustefjorden Fault.

5.2.2.4 Totland Fault M_W 6.9

This is the only strike-slip fault in the simulations. Figure 5.2.2-4 shows the distribution of PGA that could occur after an M_W 6.9 earthquake on Totland Fault. The maximum PGA for this event is estimated to be 214.4 cm/s^2. Bergen is located within the 50 cm/s^2 contour line, an area of approximately 8800 km^2, and would be exposed to ground shaking that could correspond to intensity VI – VII on the Modified Mercalli Intensity Scale, Table 5.2-1.

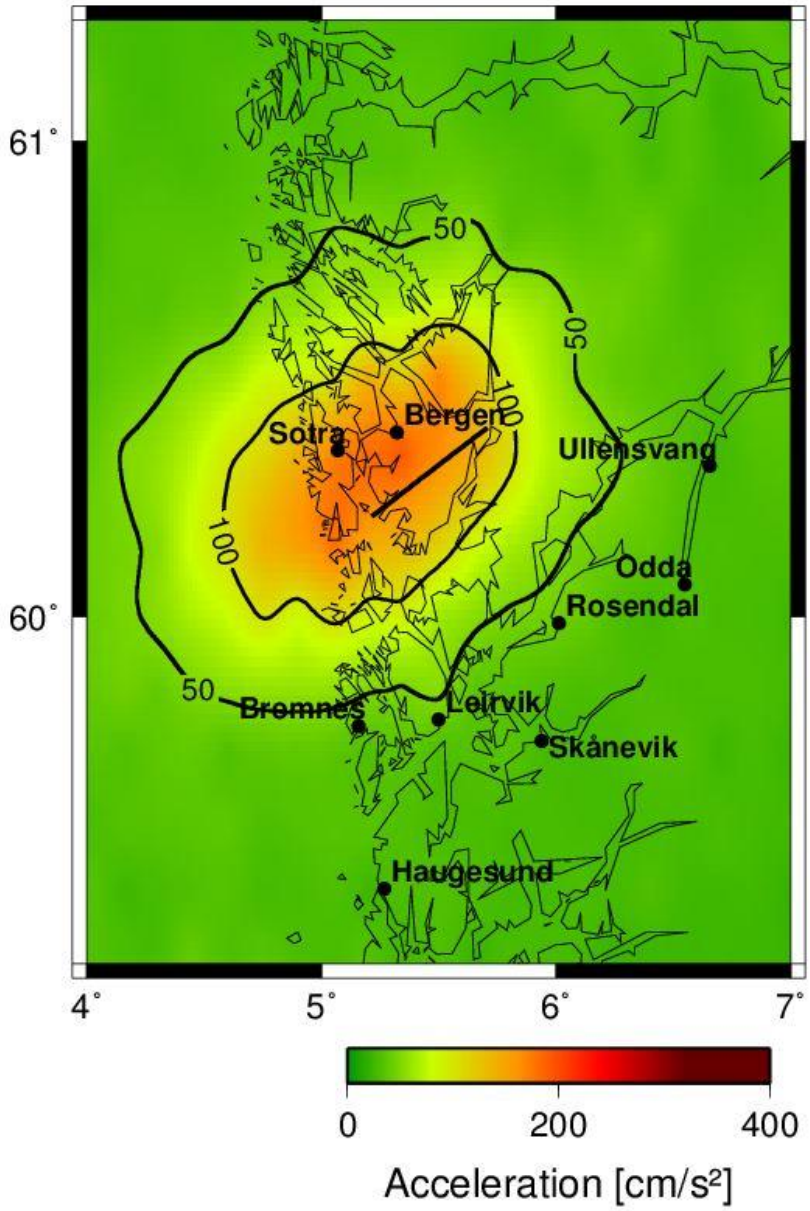

Figure 5.2.2-4 Peak ground acceleration distribution for a M_W 6.9 earthquake scenario on Totland Fault.

5.2.2.5 Totland Fault M_W 6.5

Figure 5.2.2-5 shows the PGA for an earthquake scenario rupturing in a M_W 6.5 event on Totland Fault. The area affected by PGA between 50 – 171.4 cm/s^2 is approximately 5700 km^2 with Bergen located within the 100 cm/s^2 contour line. Bergen would therefore experience intensity that could correspond to VII, from the Modified Mercalli Intensity Scale (Table 5.2-1) during this earthquake scenario.

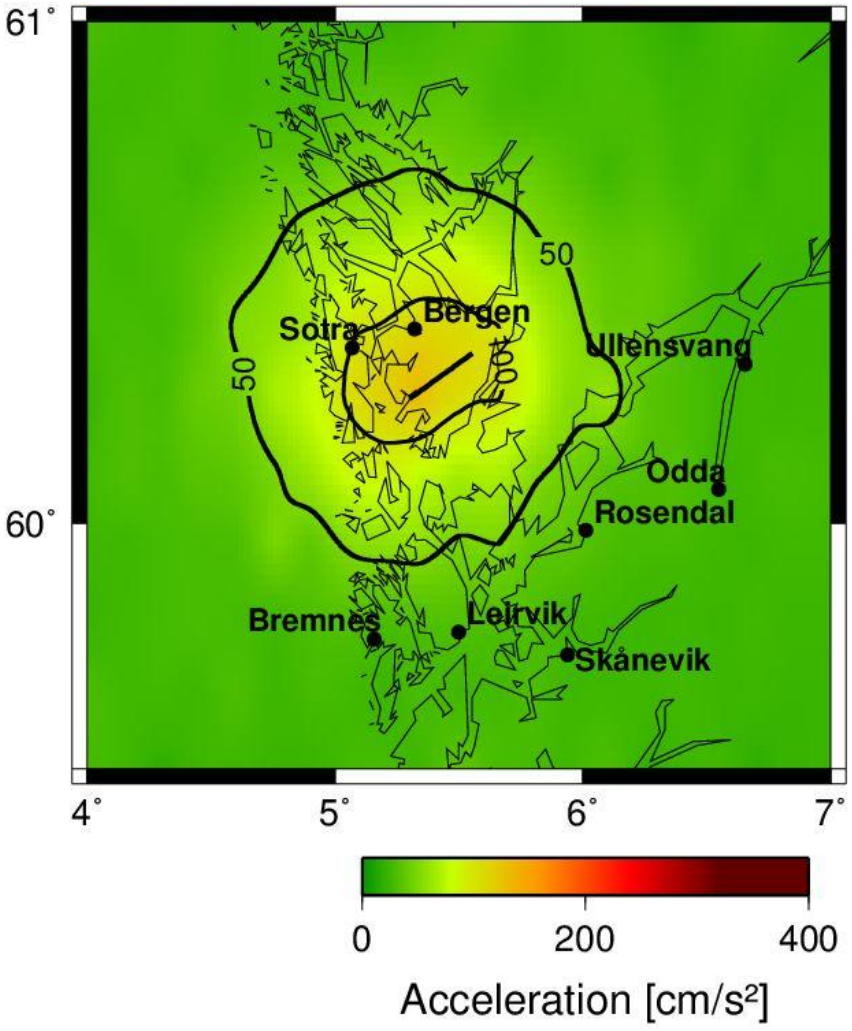

Figure 5.2.2-5 Peak ground acceleration distribution for a M_W 6.5 earthquake scenario on Totland Fault.

5.2.2.6 Northern Sunnhordland Fault M_W 6.0

Figure 5.2.2-6 shows the PGA that would be caused by an earthquake of M_W 6.0 on Northern Sunnhordland Fault. The maximum PGA is estimated to be 91.11 cm/s^2 for this event, and the area affected by ground shaking that could correspond of intensity V – VII is approximately 2700 km^2. This area covers the outlet of Hardangerfjorden where towns like Bremnes on Bømlo and Leirvik on Stord. The intensities are from the Modified Mercalli Intensity Scale, Table 5.2-1.

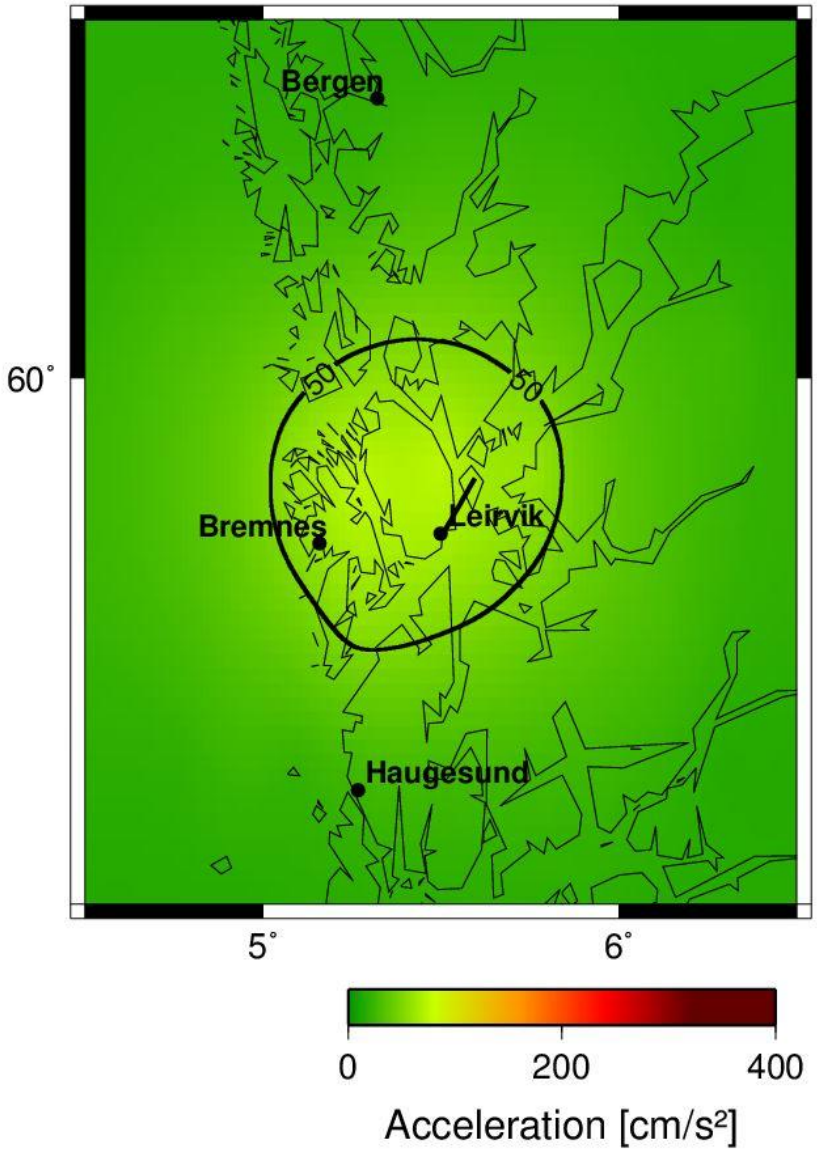

Figure 5.2.2-6 Peak ground acceleration distribution for a M_W 6.0 earthquake scenario on Northern Sunnhordland Fault.

5.2.2.7 Sunnhordland M_W 7.1

Figure 5.2.2-7 shows that the PGA would affect approximately 2500 km² with values between 100 and 206.5 cm/s², which may indicate to intensity VII on the Modified Mercalli Intensity Scale (Table 5.2-1). Within this area, Haugesund is situated. Stord, Bømlo and Skånevik falls within the 50 cm/s² contour line and is exposed to PGA that exceeds 50 cm/s² and intensity of approximately VI, in an area of approximately 11 200 km². The maximum PGA is estimated to be 206.5 cm/s².

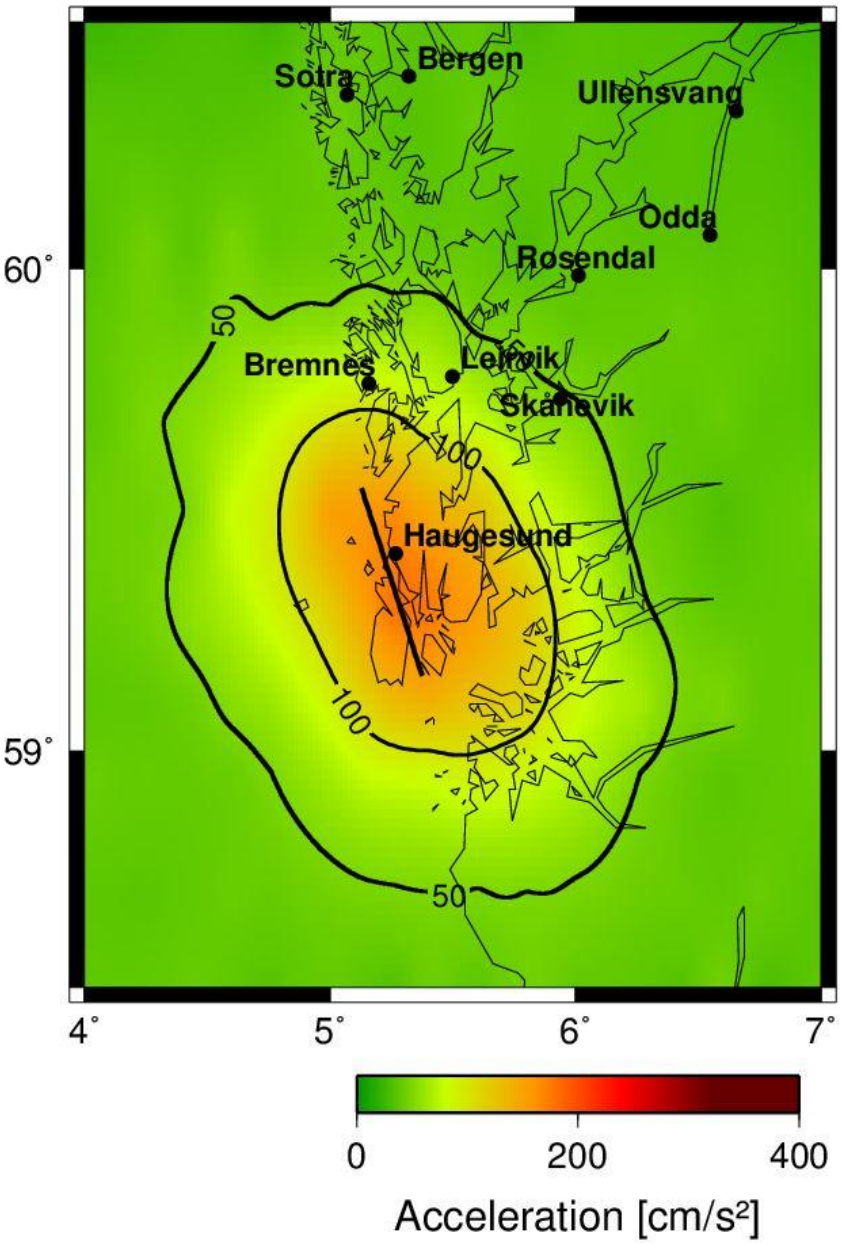

Figure 5.2.2-7 Peak ground acceleration distribution for a M_W 7.1 earthquake scenario on Sunnhordland Fault

5.2.2.8 Sunnhordland M_W 6.5

The maximum PGA is estimated to be 178.5 cm/s² for an earthquake of M_W 6.5 on Sunnhordland Fault. Approximately 6700 km² would be exposed to PGA between 50 and 178.5 cm/s², Figure 5.2.2-8. Haugesund is the largest city in the affected area, and it is located almost in the center of the 100 cm/s² contour line, in which the PGA exceeds 100 cm/s² and the intensity could correspond to VII (Modified Mercalli Intensity Scale, Table 5.2-1).

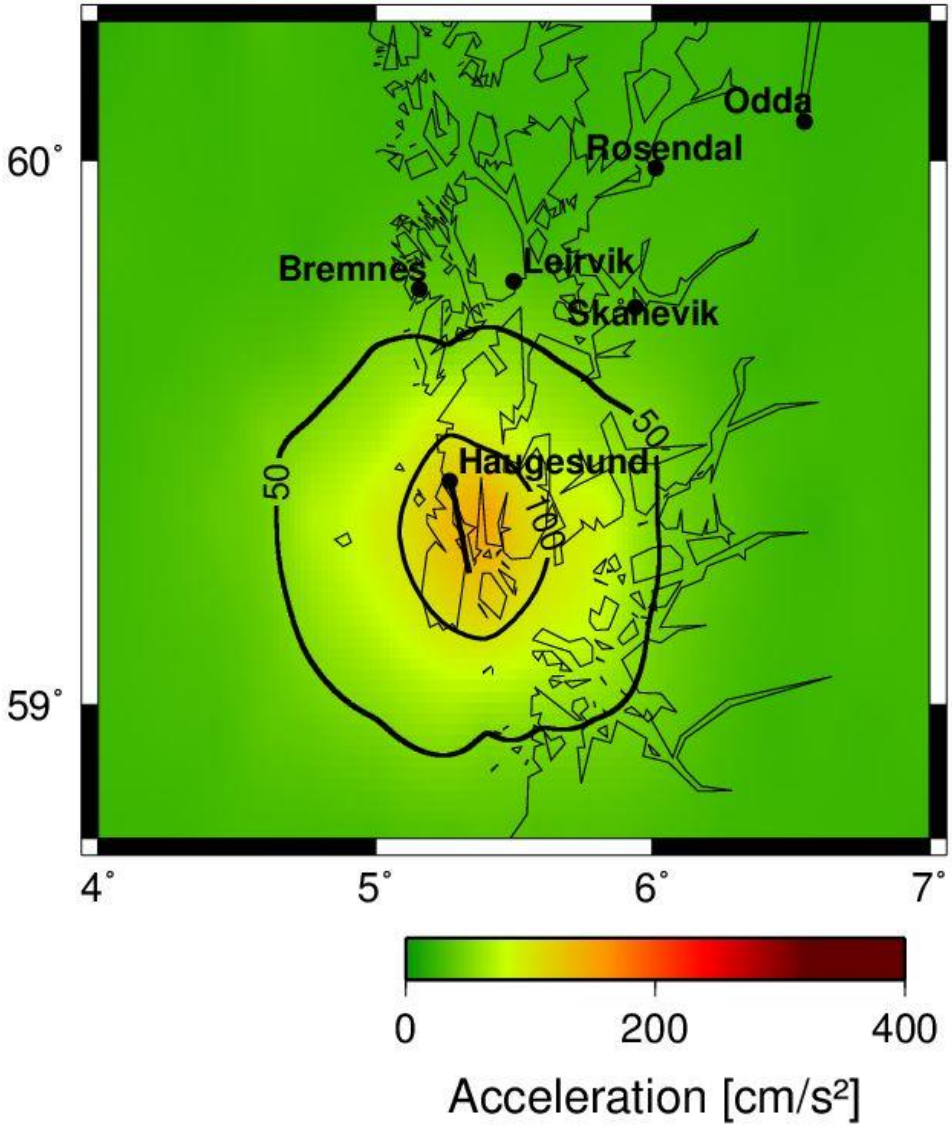

Figure 5.2.2-8 Peak ground acceleration distribution for M_W 6.5 earthquake scenario on Sunnhordland Fault.

5.2.2.9 Sunnhordland M_W 6.0

Figure 5.2.2-9 shows the ground acceleration distribution following a M_W 6.0 earthquake on Sunnhordland Fault. The maximum PGA is estimated to be 98.61 cm/s^2 for this event. The area affected by PGA between 50 and 98.61 cm/s^2, which may indicate intensity VI – VII on the Modified Mercalli Intensity Scale (Table 5.2-1), is approximately 2200 km^2 and the city of Haugesund is located near the center of the PGA.

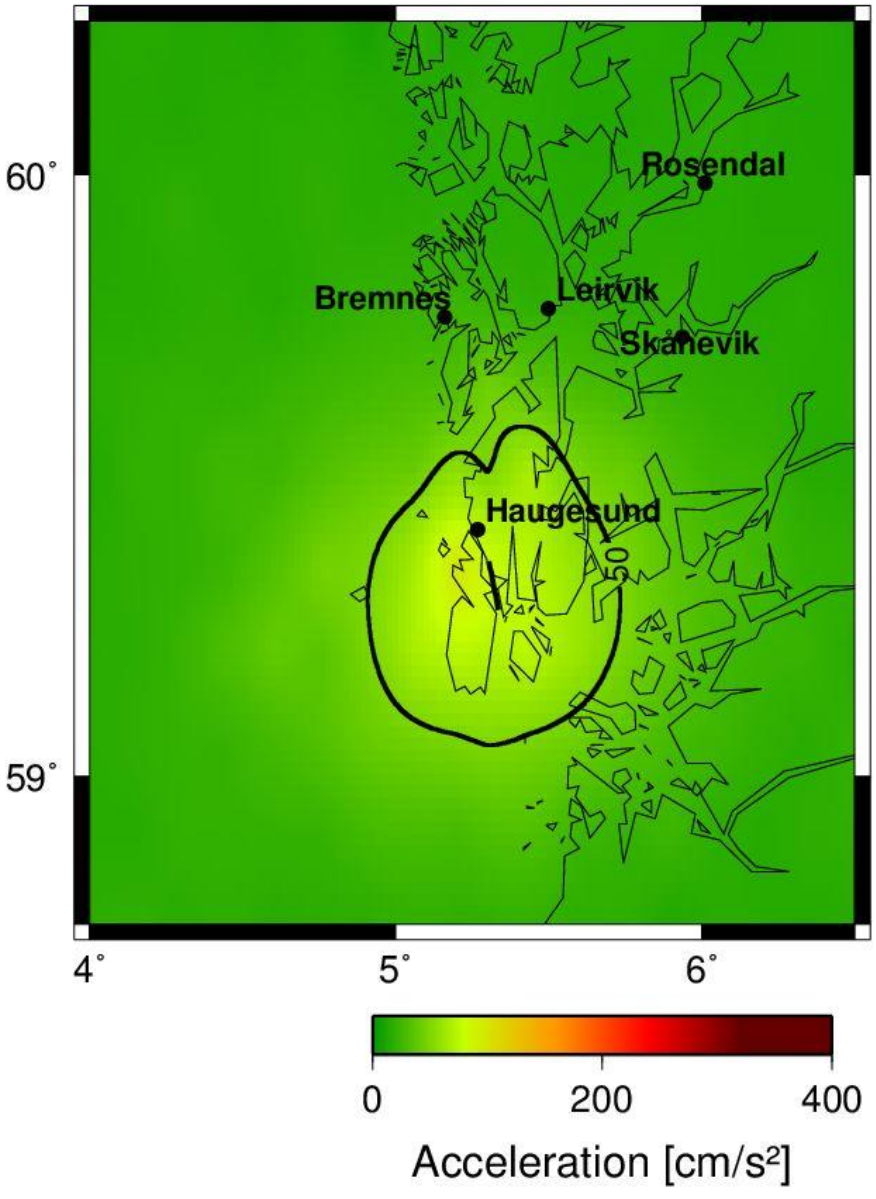

Figure 5.2.2-9 Peak ground acceleration distribution for a M_W 6.0 earthquake scenario on Sunnhordland Fault.

5.2.2.10 Sauda Fault M_W 7.3

Figure 5.2.2-10 shows the PGA distribution following a M_W 7.3 earthquake on Sunnhordland Fault. The maximum PGA is estimated to be 280.7 cm/s^2 for this event. The area affected by PGA between 50 and 280.7 cm/s^2 is approximately 21 200 km^2. Odda and Ullensvang are located within the outer area where the PGA exceeds 50 cm/s^2. The PGA exceeds 200 cm/s^2 in the center in an area that is approximately 450 km^2 where the town of Sauda is situated, and this would be exposed to shaking that could correspond to intensity VIII on the Modified Mercalli Intensity Scale, Table 5.2-1.

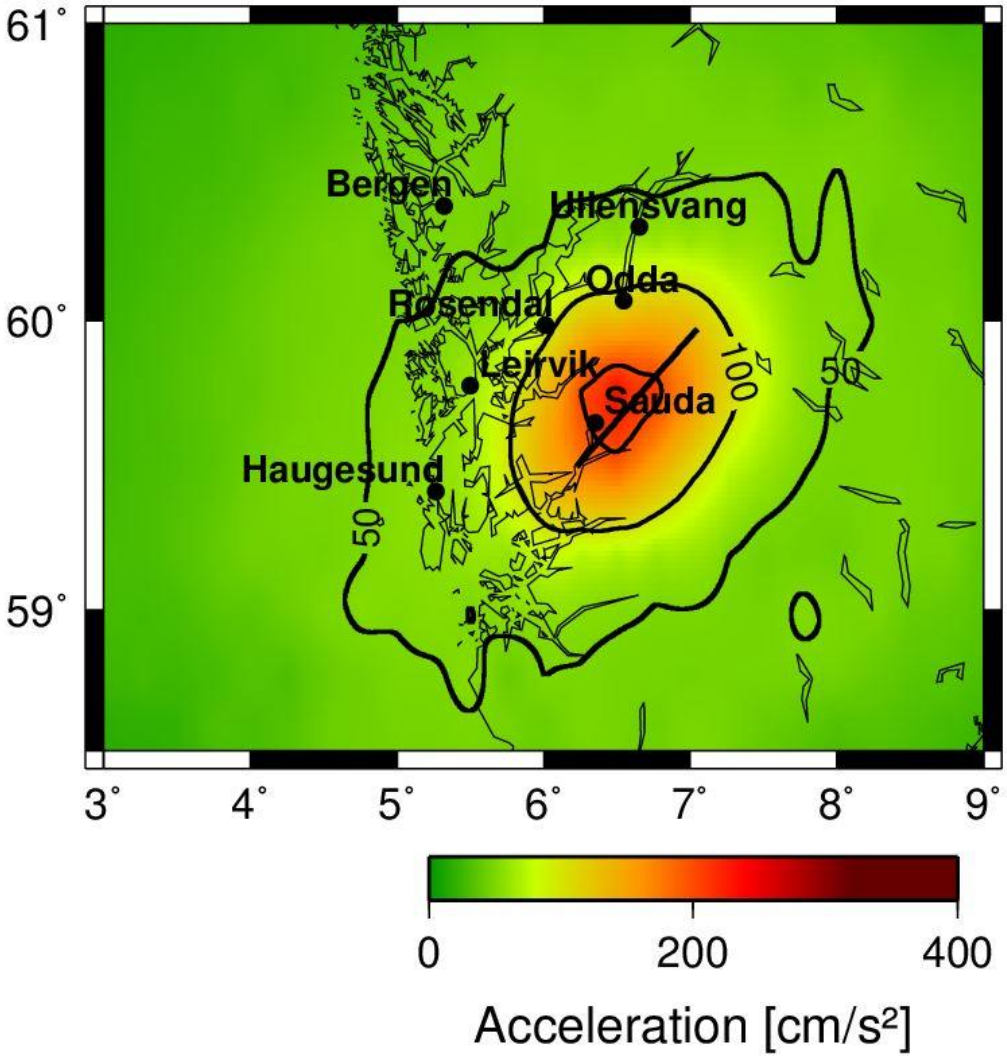

Figure 5.2.2-10 Peak ground acceleration distribution for a M_W 7.3 earthquake scenario on Sauda Fault.

5.2.3 Nordland, Northern Norway

In this subchapter is Vestfjorden Fault represented by all four earthquake scenarios (M_W 7.5, M_W 7.0, M_W 6.5 and M_W 6.0). Båsmoen Fault is represented by the earthquake scenarios of M_W 7.1 and M_W 6.0 in this chapter; the scenario of M_W 6.5 can be found in Appendix B. Nesna Fault is here represented by the earthquake scenario of M_W 6.5, while the scenarios of M_W 7.2 and M_W 6.0 can be found in Appendix B. Mosjøen Fault is here represented by the earthquake scenarios of M_W 7.5 and M_W 6.5; the scenarios of M_W 7.0 and M_W 6.0 can be found in Appendix B.

5.2.3.1 Vestfjorden Fault M_W 7.5

Figure 5.2.3-1 shows the distribution of PGA that would follow a M_W 7.5 earthquake on Vestfjorden Fault. The estimated maximum PGA is 317.6 cm/s^2 for this event. The area affected by PGA between 50 – 317.6 cm/s^2 is approximately 83 500 km^2, and it includes cities and towns like Sortland, Svolvær and Lofoten. Approximately 9500 km^2 would be exposed to PGA between 100 – 317.6 cm/s^2, which may indicate ground shaking of intensity VII – VIII on the Modified Mercalli Intensity Scale, Table 5.2-1.

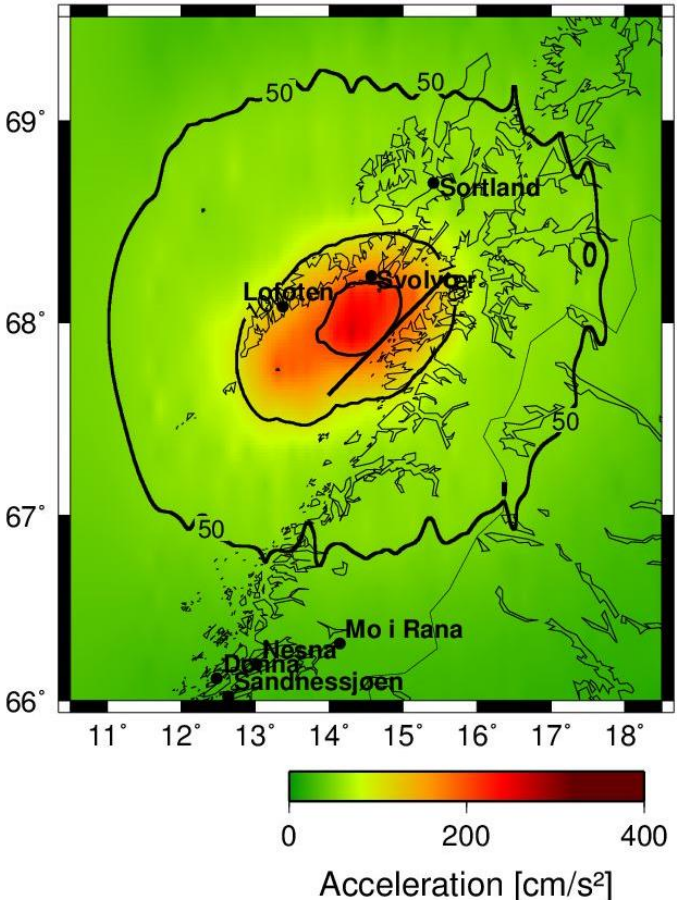

Figure 5.2.3-1 Peak ground acceleration distribution for a M_W 7.5 earthquake scenario on Vestfjorden Fault.

5.2.3.2 Vestfjorden Fault M_W 7.0

Figure 5.2.3-2 shows the PGA that would follow a Mw 7.0 earthquake on Vestfjorden Fault. It would cover an area of approximately 14 500 km^2 and affect Svolvær the most. Lofoten and Sortland are situated just outside the 50 cm/s^2 and would experience PGA below this value. The maximum PGA estimated for this scenario is 251.2 cm/s^2. Approximately 3500 km^2 would be exposed to PGA between 100 and 251.2 cm/s^2 and shaking that could correspond to intensity VII – VIII on the Modified Mercalli Intensity Scale, Table 5.2-1.

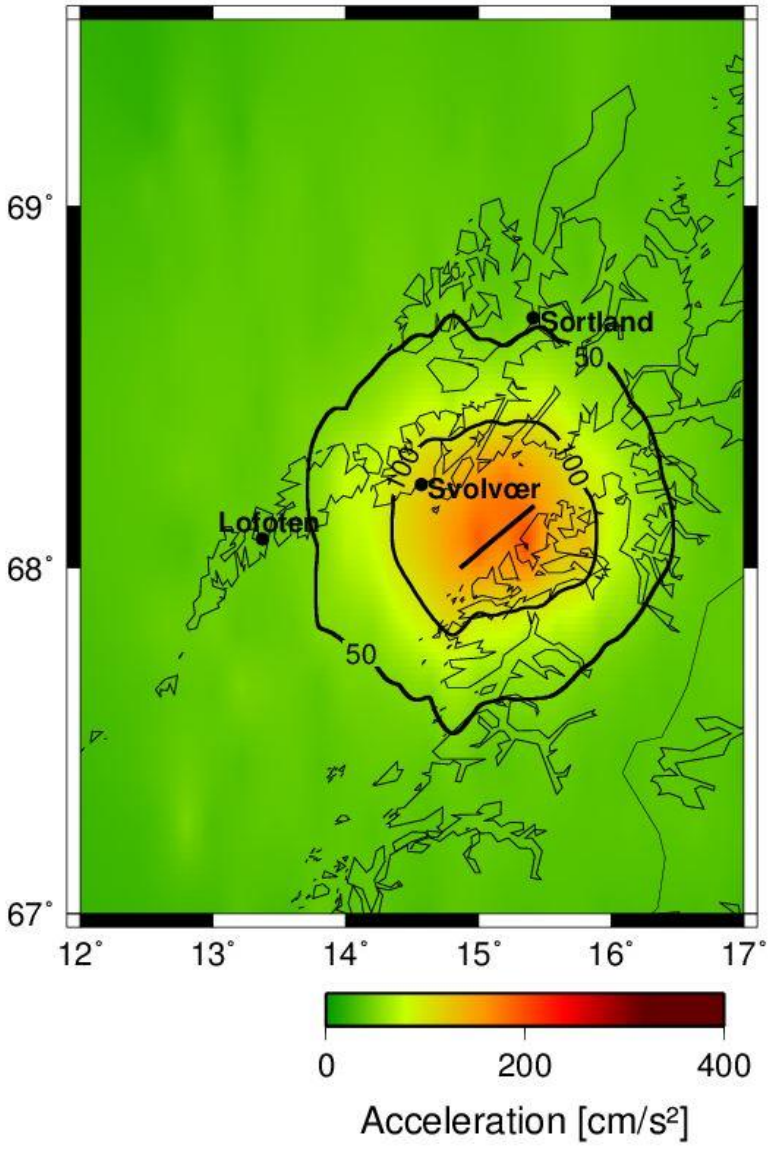

Figure 5.2.3-2 Peak ground acceleration distribution for a M_W 7.0 earthquake scenario on Vestfjorden Fault.

5.2.3.3 Vestfjorden Fault M_W 6.5

Figure 5.2.3-3 shows the distribution of PGA for Vestfjorden Fault if it ruptures in a M_W 6.5 earthquake. The maximum PGA is estimated to be 172.2 cm/s^2. The area affected by PGA between 50 and 172.2 cm/s^2 is approximately 6500 km^2, and Svolvær, located just outside the 100 cm/s^2 contour line, would be exposed to ground shaking that could correspond to intensity VI - VII, while the intensity could correspond to VII within the 100 cm/s^2 contour line (Modified Mercalli Intensity Scale, Table 5.2-1).

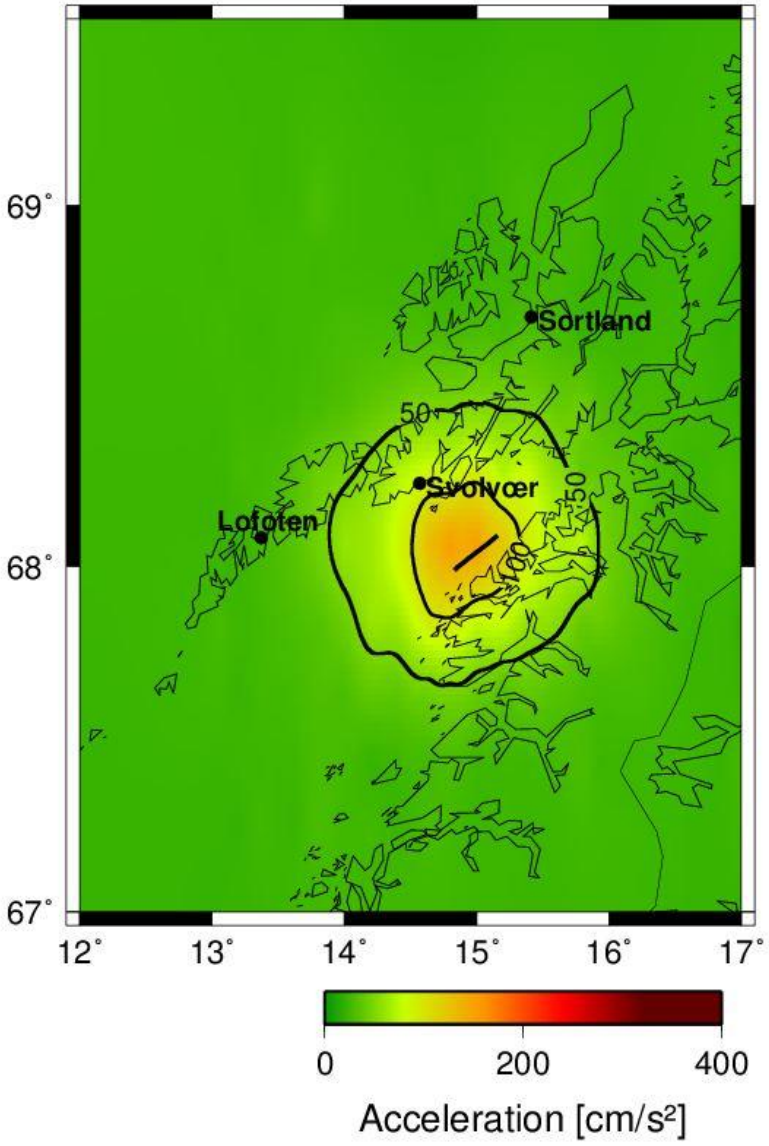

Figure 5.2.3-3 Peak ground acceleration distribution for a M_W 6.5 earthquake scenario on Vestfjorden Fault.

5.2.3.4 Vestfjorden Fault M_W 6.0

The M_W 6.0 earthquake scenario for Vestfjorden Fault has a maximum PGA of 92.5 cm/s^2. Approximately 2100 km^2 would be exposed to PGA between 50 – 100.6 cm/s^2, which may indicate shaking of intensity V – VI on the Modified Mercalli Intensity Scale, Table 5.2-1. Svolvær is located on the 50 cm/s^2 contour line and would be exposed to PGA around 50 cm/s^2 and Figure 5.2.3-4 shows the PGA that would follow such an earthquake.

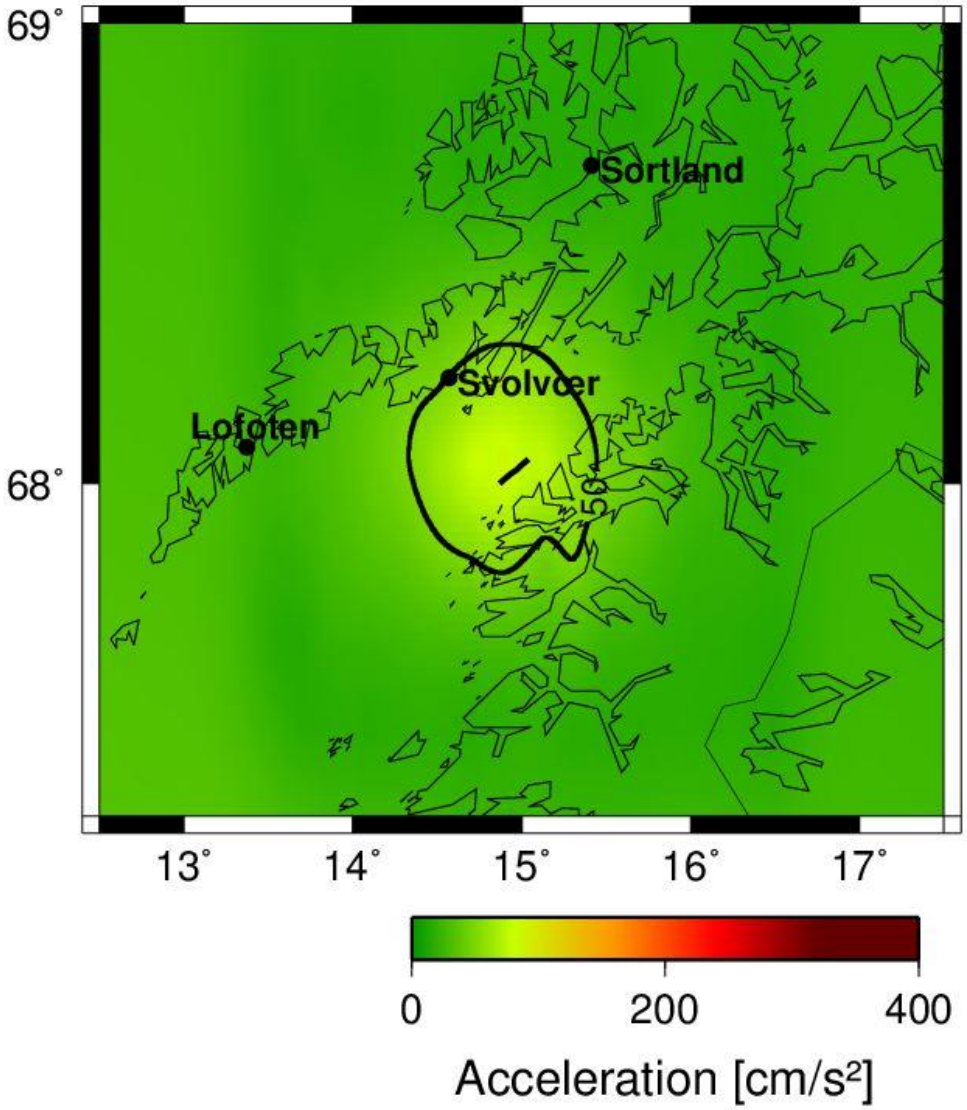

Figure 5.2.3-4 Peak ground acceleration distribution for a M_W 6.0 earthquake scenario on Vestfjorden Fault.

5.2.3.5 Båsmoen Fault M_W 7.1

Figure 5.2.3-5 shows the PGA that would occur after a M_W 7.1 earthquake on Båsmoen Fault. The maximum PGA is estimated to be 239.9 cm/s^2 for this event. The area affected by the most PGA, between 100 and 229.9 cm/s^2, is approximately 3900 km^2 and it includes the city of Mo i Rana, located at the head of Ranafjorden, near the center of the ground motion. In addition are the towns Nesna, Dønna, Sandnessjøen and Mosjøen located within the area that would experience PGA above 50 cm/s^2. This could correspond to ground shaking of intensity VII on the Modified Mercalli Intensity Scale, Table 5.2-1, for Mo i Rana and intensity V – VI for the other towns. Mo i Rana is the largest city in Nordland. Båsmoen Fault is the only reverse fault in the earthquake simulations.

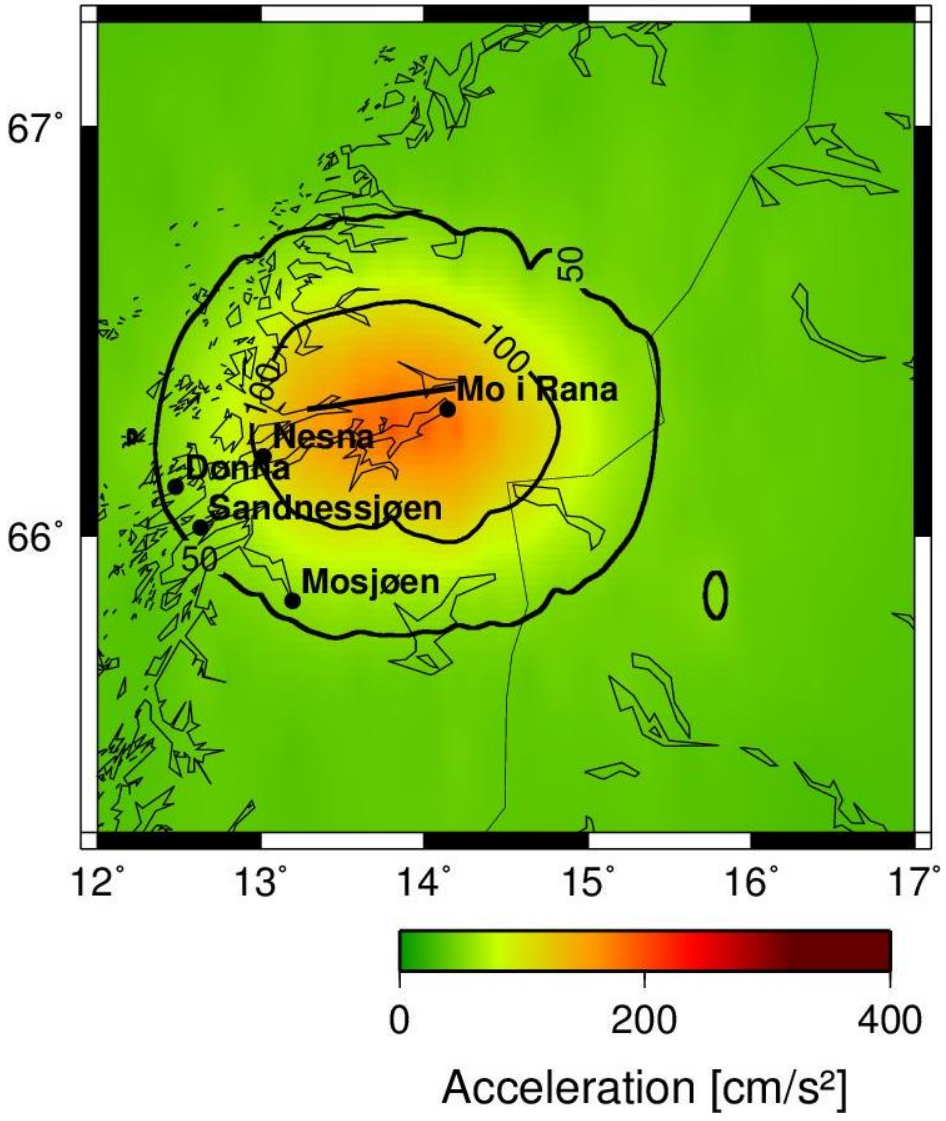

Figure 5.2.3-5 Peak ground acceleration distribution for a M_W 7.1 earthquake scenario on Båsmoen Fault.

5.2.3.6 Båsmoen Fault M_W 6.0

Figure 5.2.3-6 shoes the distribution of the PGA that would occur after a M_W 6.0 earthquake on Båsmoen Fault. The maximum PGA is estimated to be 139.6 cm/s^2. The PGA following the earthquake would affect approximately 2700 km^2 with shaking between 50 and 139.9 cm/s^2, where Mo i Rana is located in the center of this area. This area would be exposed to shaking that could correspond to intensity V – VII on the Modified Mercalli Intensity Scale, Table 5.2-1.

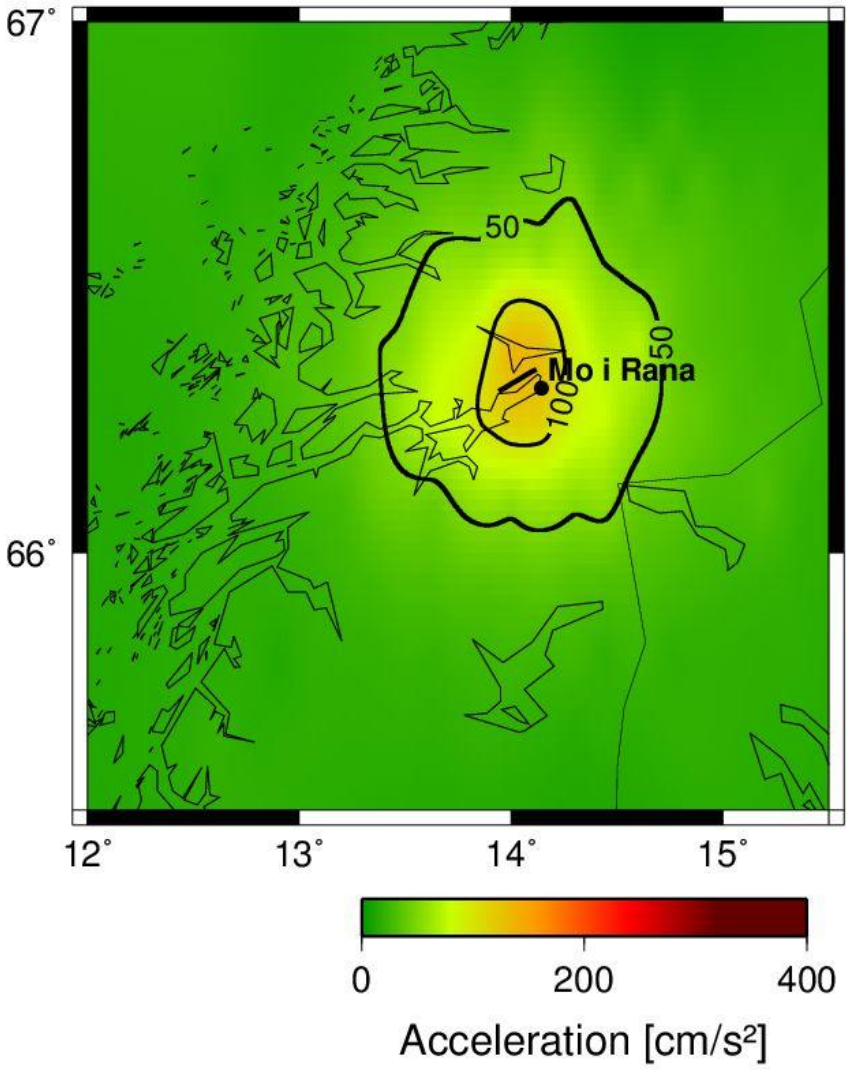

Figure 5.2.3-6 Peak ground acceleration distribution for a M_W 6.0 earthquake scenario on Båsmoen Fault.

5.2.3.7 Nesna Fault M_W 6.5

Figure 5.2.3-7 shows the PGA that would occur with a M_W 6.5 earthquake on Nesna Fault. The maximum PGA is estimated to be 179.4 cm/s^2. The area affected by PGA between 50 and 179.4 cm/s^2 is approximately 4900 km^2, and it would be exposed to shaking that could correspond to intensity VI – VII (Modified Mercalli Intensity Scale, Table 5.2-1). Dønna and Sandnessjøen are located within the area that would have PGA exceeding 100 cm/s^2, and Nesna and Mosjøen are located within the area that would have PGA exceeding 50 cm/s^2.

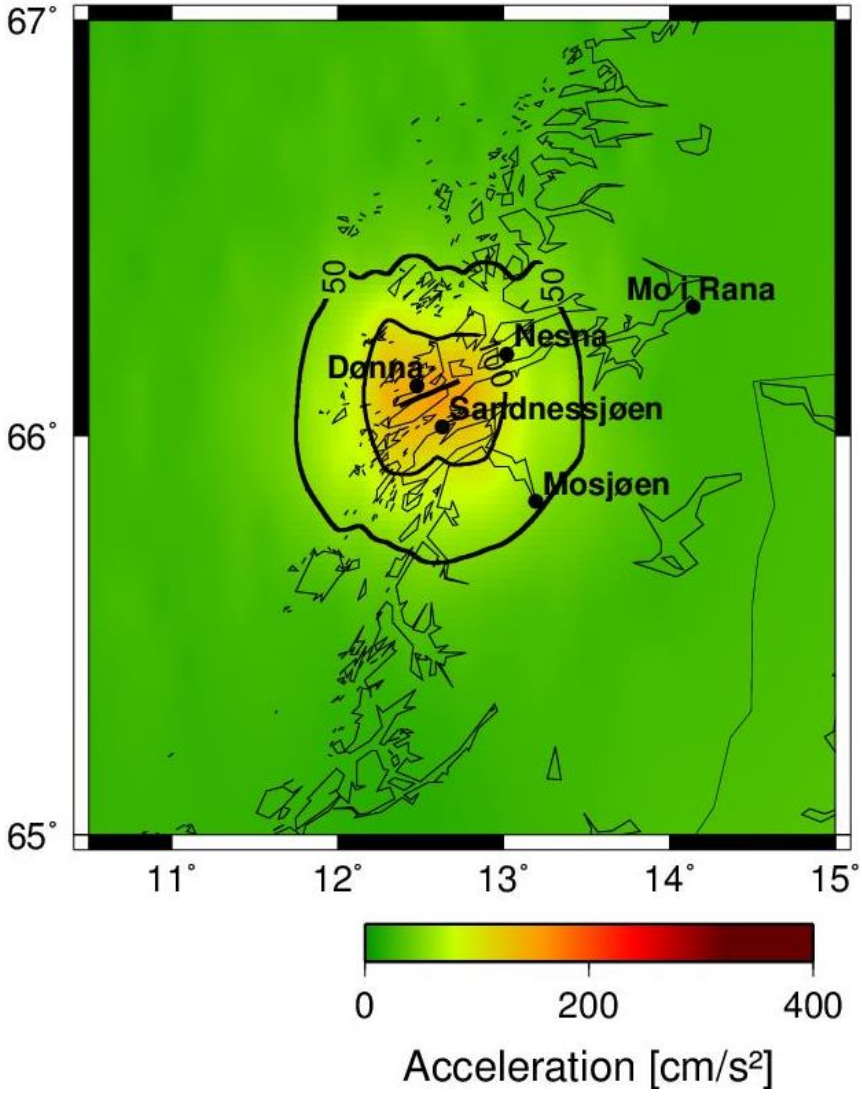

Figure 5.2.3-7 Peak ground acceleration distribution for a M_W 6.5 earthquake scenario on Nesna Fault.

5.2.3.8 Mosjøen Fault M_W 7.5

Figure 5.2.3-8 shows the PGA that would occur after a M_W 7.5 earthquake on Mosjøen Fault. The 50 cm/s² contour line covers an area of approximately 61 900 km², and the highest PGA values are centered between Ranafjorden and Mosjøen. This area would be exposed to ground shaking that could correspond to intensity VIII on the Modified Mercalli Intensity Scale, Table 5.2-1, and the maximum PGA is estimated to be 272.8 cm/s² for this scenario. Approximately 8300 km² is affected by PGA between 100 – 272.8 cm/s², which may indicate intensity VII on the Modified Mercalli Intensity Scale. Brønnøysund and Mosjøen are located within this area, while Sandnessjøen, Dønna and Nesna are situated in the area that would have PGA exceeding 50 cm/s² but below 100 cm/s².

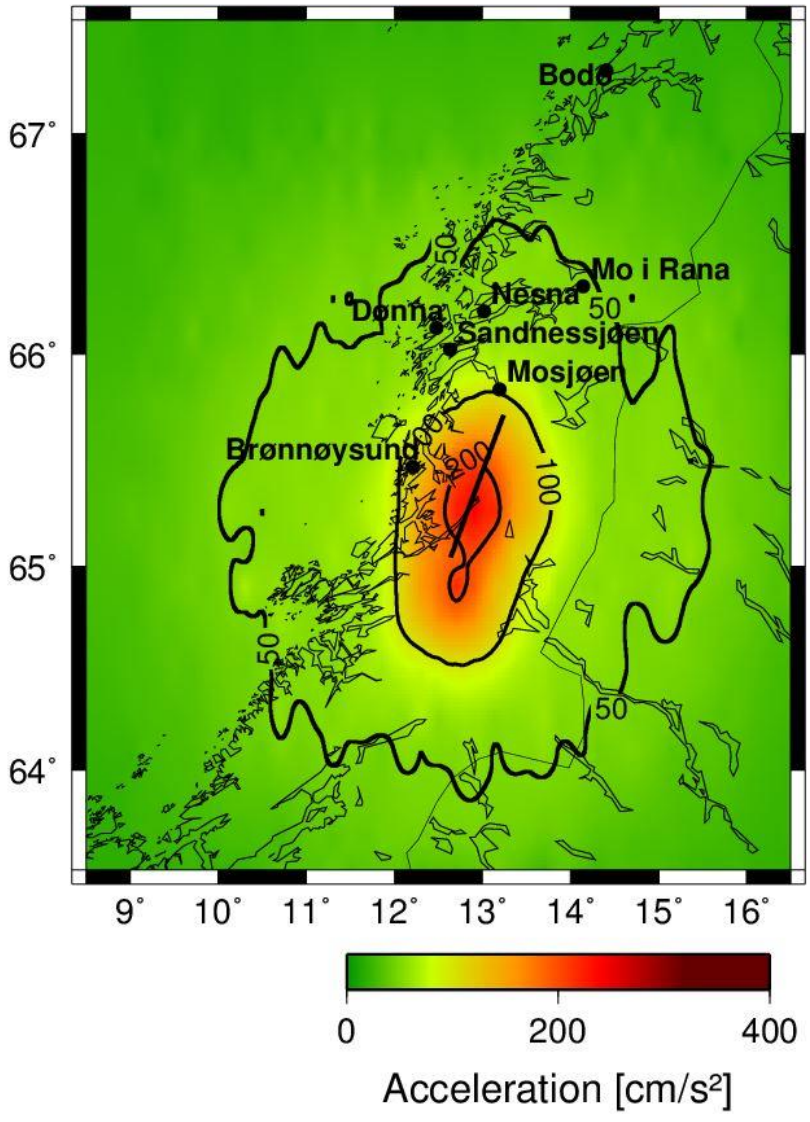

Figure 5.2.3-8 Peak ground acceleration distribution for a M_W 7.5 earthquake scenario on Mosjøen Fault.

5.2.3.9 Mosjøen Fault M_W 6.5

Figure 5.2.3-9 shows the PGA distribution that would occur if Mosjøen Fault ruptures in a M_W 6.5 earthquake. The maximum PGA is estimated to be 191.4 cm/s^2 for this scenario. The PGA between 50 and 191.4 cm/s^2 would cover an area approximately 6600 km^2 where the intensity could correspond to VI - VII on the Modified Mercalli Intensity Scale, Table 5.2-1. Mosjøen is located outside the 50 cm/s^2 contour line and Brønnøysund is situated just within the line.

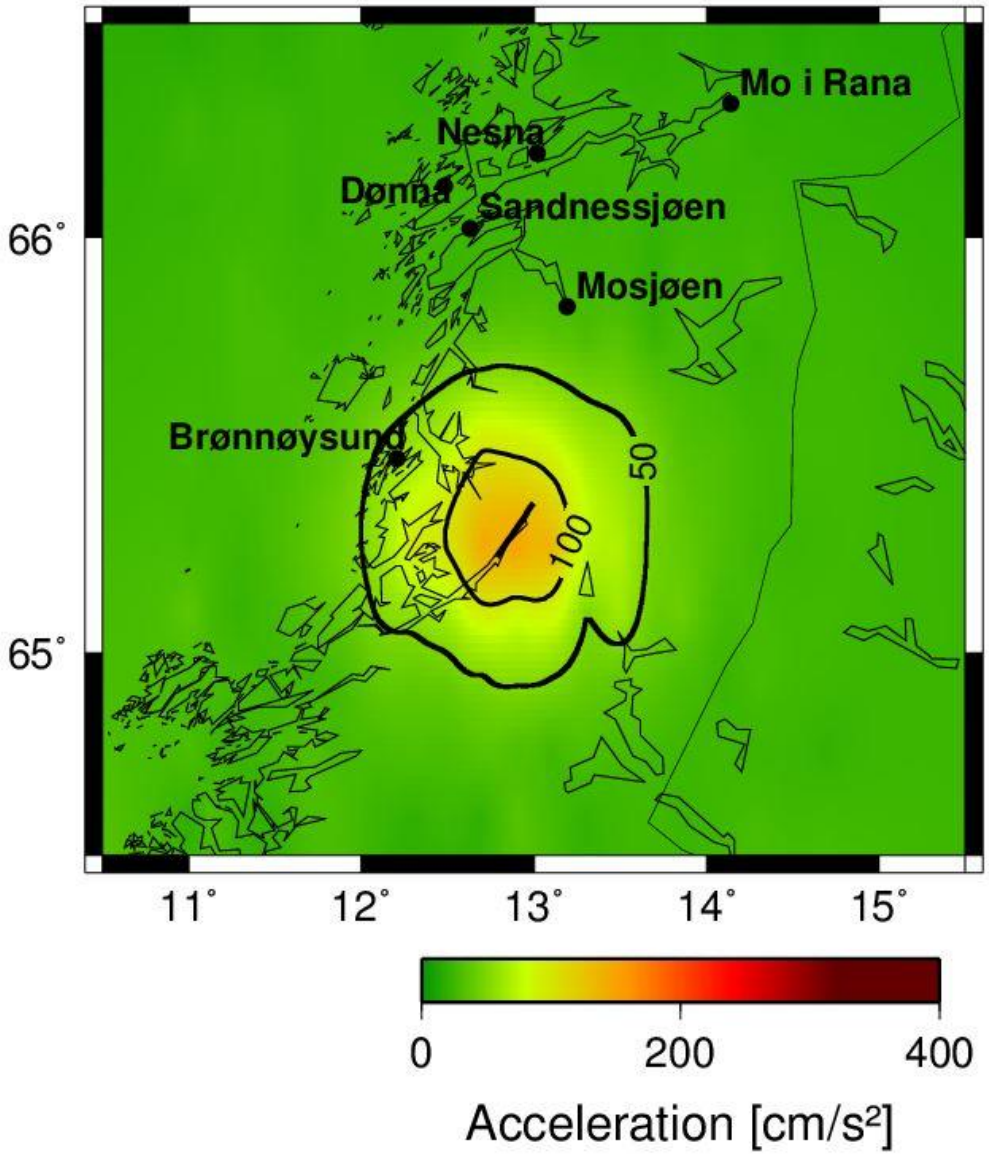

Figure 5.2.3-9 Peak ground acceleration distribution for a M_W 6.5 earthquake scenario on Mosjøen Fault.

5.3 SEISMOGRAMS

Several of these earthquake scenarios are located near the two largest cities in Norway, Oslo and Bergen. In addition to the plots showing the distribution of the peak ground acceleration after an earthquake, I have plotted two seismograms for Oslo and two for Bergen that represents the seismograms for the largest earthquake and the M_W 6.0 scenario on Oslofjorden and Hjeltefjorden Fault.

5.3.1 Oslo

Figure 5.3.1-1and Figure 5.3.1-2 shows the seismograms from Oslo during an M_W 6.0 and M_W 7.4 earthquake on Oslofjorden Fault, Figure 11.1.1-2 and Figure 5.2.1-1 respectively.

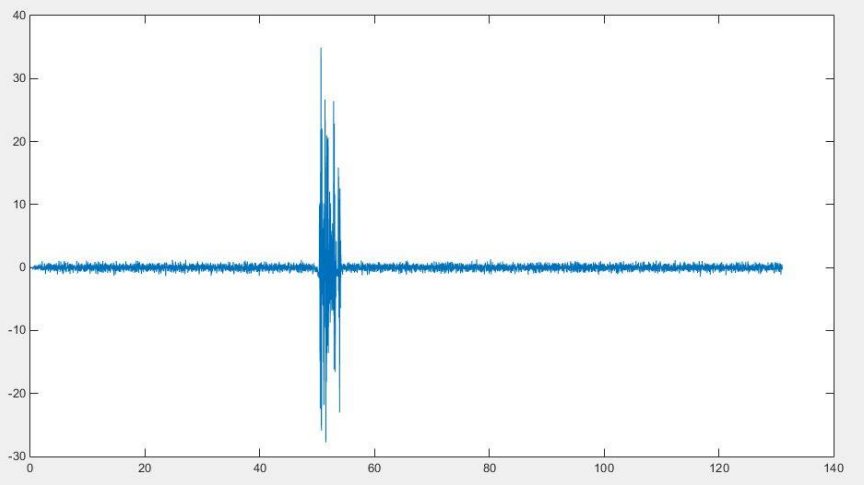

Figure 5.3.1-1 Seismogram from the M_W 6.0 earthquake scenario on Oslofjorden Fault. The location of the seismogram is Oslo. The x-axis shows time and the y-axis shows the peak ground acceleration.

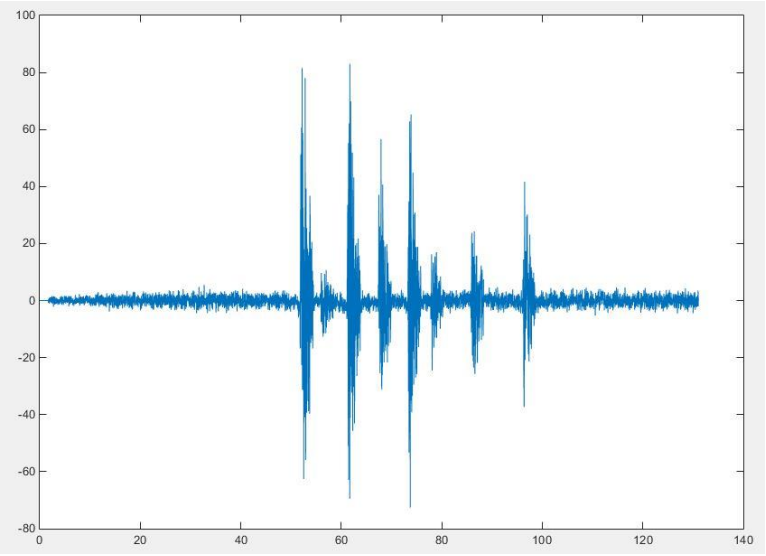

Figure 5.3.1-2 Seismogram from the M 7.4 earthquake scenario on Oslofjorden Fault. The location of the seismogram is Oslo. The x-axis shows time and the y-axis shows the peak ground acceleration.

5.3.2 Bergen

Figure 5.3.2-1 and Figure 5.3.2-2 shows the seismograms from Bergen during an M_W 6.0 and M_W 7.2 earthquake on Hjeltefjorden Fault, Figure 5.2.2-2 and Figure 11.1.2-1 respectively.

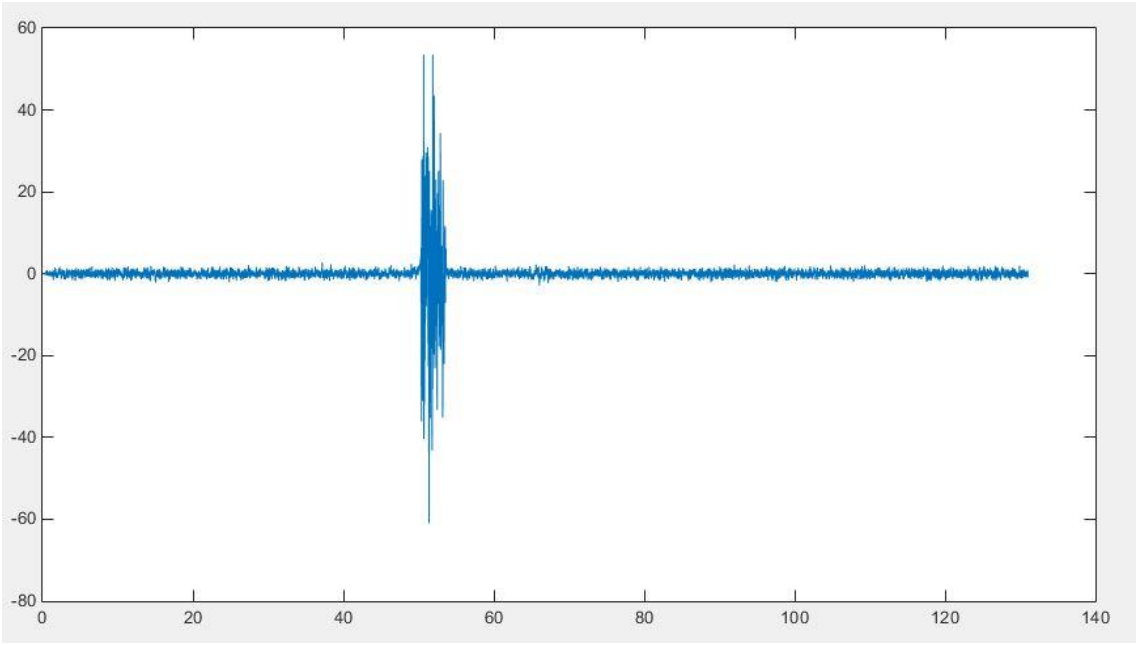

Figure 5.3.2-1 Seismogram from the M_W 6.0 earthquake scenario on Hjeltefjorden Fault. The location of the seismogram is Bergen. The x-axis shows time and the y-axis shows the peak ground acceleration.

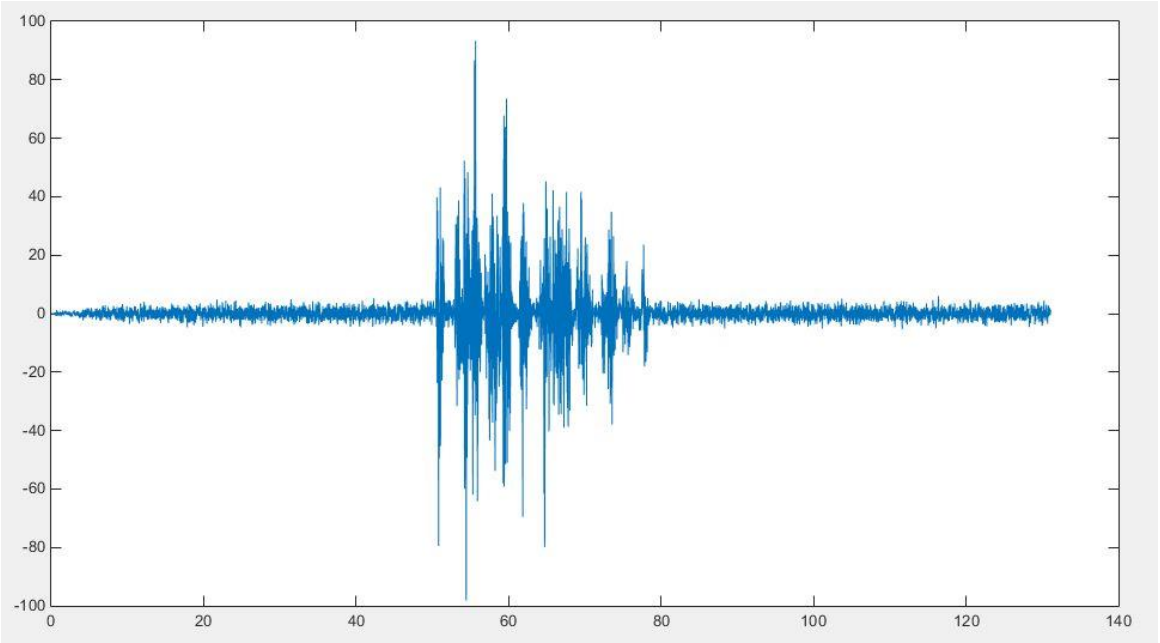

Figure 5.3.2-2 Seismogram from the M_W 7.2 earthquake scenario on Hjeltefjorden Fault. The location of the seismogram is Bergen. The x-axis shows time and the y-axis shows the peak ground acceleration.

6 DISCUSSION

This chapter contains the discussion of the results and possible reason for the variations in maximum PGA, the effect on the PGA caused by number of iterations, the effect on the PGA caused by random versus fixed hypocenter location, discussion of the probability of one of these earthquake scenarios actually occurring, and finally a comparison of my results with the results from the study performed by Tveit (2013) and Probabilistic Seismic Hazard Assessments.

6.1 DISCUSSION OF THE RESULTS

The results of the ground motion simulations show that if an earthquake is to occur on one of these faults, the following ground motion will be quite high and could cause damage to buildings, even for M_W 6.0, which is the lowest magnitude considered in the simulations. I have found that the M_W 6.0 earthquake scenarios cause peak ground acceleration of approximately 100 ± 15 cm/s^2, which may indicate intensity VI – VII on the Modified Mercalli Intensity Scale, Table 5.2-1 in the previous chapter. Intensity VI – VII involves strong to very strong shaking and light to moderate damage. Everybody feels the earthquake and many are frightened and run outdoors. The intensity of the peak ground acceleration is dependent on the distance from the rupture and local site effects. Earthquakes in hard rocks will usually be felt over a large area because the seismic energy travels far because of poor attenuation. Therefore, earthquakes of M_W 2.0 are sometimes felt in Norway.

Table 6-1 lists the maximum value for the peak ground acceleration for each earthquake scenario.

Table 6-1 List of the maximum peak ground motion acceleration for each earthquake scenario.

Faults	Max mag	Fault type	Length	Dip	Maximum peak ground acceleration (cm/s^2)			
					Max Mag	M 7.0	M 6.5	M 6.0
Hamar	M 7.7	Normal	150.0 km	60	308.4000	244.8000	191.1000	105.3000
Mosjøen	M 7.5	Normal	100.0 km	60	272.8000	319.4000	191.4000	111.5000
Vestfjorden	M 7.5	Normal	98.0 km	60	317.6000	251.2000	173.2000	92.5000
Oslofjorden	M 7.4	Normal	90.0 km	60	267.4000	235.4000	178.2000	106.3000
Sauda	M 7.3	Normal	75.0 km	60	280.7000		177.7000	129.4000
Nesna	M 7.2	Normal	60.0 km	60	239.5000		179.4000	117.7000
Hjeltefjorden	M 7.2	Normal	60.0 km	45	267.0000		154.5000	115.7000
Northern Sunnhordland	M 7.2	Normal	60.0 km	60	217.3000		180.0000	91.1100
Sunnhordland	M 7.1	Normal	50.0 km	60	206.5000		178.5000	98.6100
Båsmoen	M 7.1	Reverse	50.0 km	60	239.9000		157.6000	139.6000
Rustefjorden	M 7.0	Normal	46.0 km	70	200.7000		188.9000	96.1200
Drammen	M 7.0	Normal	44.0 km	60	228.6000		164.6000	91.4400
Totland	M 6.9	Strike-slip	35.0 km	60	214.4000		171.4000	132.0000

The results were expected to be more similar for the same magnitudes. For example, the maximum peak ground acceleration for the M_W 6.5 earthquake scenarios does vary from 154.5 and up to 191.4 cm/s^2 for the normal faults. Because the input-parameters are identical except for the location of the fault, the maximum PGA results should the difference between them be smaller. One reason for the difference may be that the maximum PGA occurs in a point in between the given sites in the simulation. If this is the case the actual point for the maximum PGA would not be given in the output-file and the value appears lower than it really is. This theory, however, is not tested because it would involve adding more sites in the simulation, which would take too much time. In addition, the type of faulting affects the maximum PGA because it affects the length and width of the faults. The M_W 7.0 scenario on Mosjøen Fault stands out, the maximum PGA is higher than the other M_W scenarios. This may be caused by coincidences in the simulations because of the randomness in hypocenter location and slip distribution. Båsmoen Fault (reverse type) and Totland Fault (strike-slip type) stands out as well, especially in the M_W 6.0 scenario because the fault length and width are different from the other faults. Båsmoen Fault is 1 km shorter in length and 2 km shorter in width, and Totland Fault is 2 km shorter in length and 1 km longer in width than the normal faults. It therefore follows that the distribution of PGA would be slightly different for these two faults because the faults planes are smaller and the released energy will thus be more concentrated.

In addition to the plots showing the distribution peak ground acceleration, I tried to plot the peak ground velocity (PGV) for some of the scenarios. However, because EXSIM12 works best with high frequencies, and PGV usually has lower frequencies compared to the PGA, it was not possible to plot the PGV using the same simulations.

6.2 INFLUENCE OF FAULT LENGTH AND WIDTH

The values in Table 6-1 are quite variable, especially within the same magnitude, and this is especially evident for Vestfjorden and Mosjøen Fault in the M_W 7.5 scenarios. The reason for these differences are discussed in this subchapter.

Two of the earthquake scenarios with identical magnitudes gave different values for the maximum peak ground acceleration. Both Vestfjorden and Mosjøen Fault have M_W 7.5 as the highest potential magnitude for their fault length, but the maximum PGA for this earthquake scenario is in Vestfjorden Fault estimated to be 317.6 cm/s^2, Figure 6.2-1, and only 272.8 cm/s^2 for Mosjøen Fault, Figure 6.2-2. The difference of 44.8 cm/s^2 is too large for two earthquake scenarios of magnitude 7.5. This difference is also evident in Figure 6.2-1 and Figure 6.2-2, the center of the ground motion acceleration is darker in Vestfjorden Fault than in Mosjøen Fault, indicating higher values.

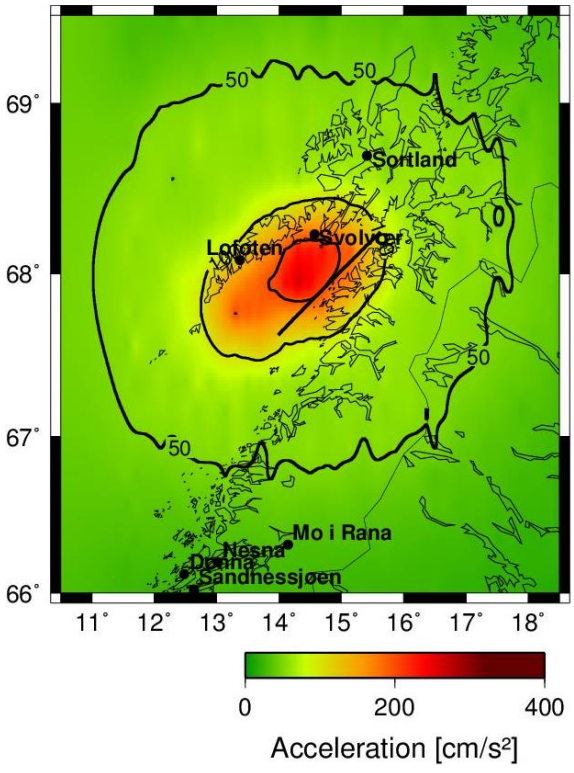

Figure 6.2-1 PGA distribution for a M_W 7.5 earthquake scenario on Vestfjorden Fault. The maximum PGA is estimated to be 317.6 cm/s^2.

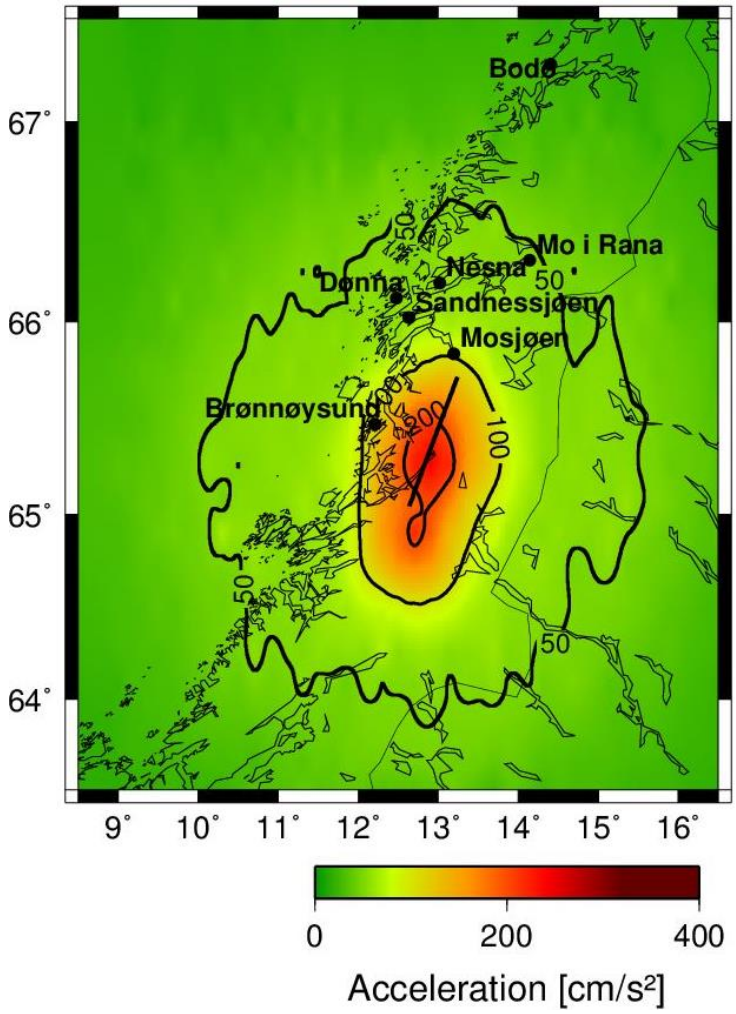

Figure 6.2-2 PGA distribution for a M_W 7.5 earthquake scenario on Mosjøen Fault. The maximum PGA is estimated to be 272.8 cm/s².

Based on the results in Table 6-1 a M_W 7.5 earthquake on Vestfjorden Fault would result in higher maximum PGA than a M_W 7.7 earthquake on Hamar Fault, 317.6 cm/s² versus 308.4 cm/s² respectively. It is therefore logical to assume that the earthquake scenario from Mosjøen Fault is the most correct, because a M_W 7.5 earthquake does not release more energy than a M_W 7.7 event.

To find out what could cause this difference, I compared the input-parameters for Vestfjorden and Mosjøen Fault, and it became evident that the only difference in the parameters are the length and width of the faults. Vestfjorden Fault is 98.0 km long and 19.4 km wide, while Mosjøen Fault is 100.0 km long and 19.0 km wide. To check whether this could be the reason for the difference in maximum PGA, I re-simulated both scenarios using the fault length and width of the other fault. The results of the re-simulations were 300.2 cm/s² for Vestfjorden Fault with the length and width from Mosjøen Fault, and 298.3 cm/s² for Mosjøen Fault with length and width from

Vestfjorden Fault. This difference can also be found in Figure 6.2-3 and Figure 6.2-4, which display the earthquake scenarios from the re-simulation.

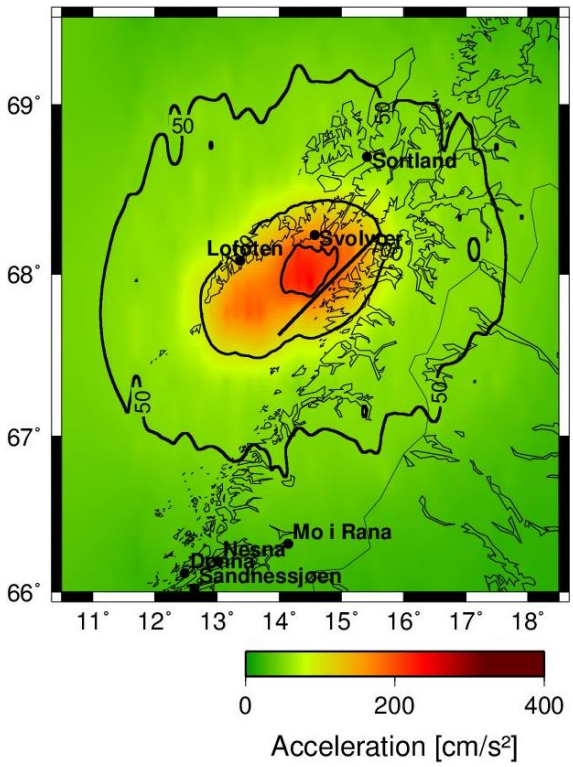

Figure 6.2-3 PGA distribution for a M_w 7.5 earthquake scenario on Vestfjorden Fault re-simulated with the length and width from Mosjøen Fault. The maximum PGA is estimated to be 300.2 cm/s² for this scenario.

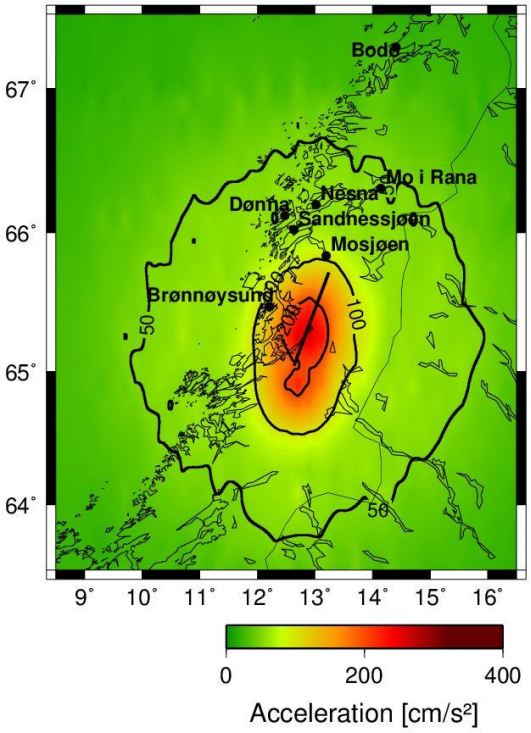

Figure 6.2-4 PGA distribution for a M_w 7.5 earthquake scenario on Mosjøen Fault re-simulated with the length and width from Vestfjorden Fault. The maximum PGA is estimated to be 298.3 cm/s² for this scenario.

To test whether the difference of 2.0 km in fault length actually was the cause of the high ground motion acceleration value, I edited Oslofjorden, initially a fault with the highest possible magnitude being M_W 7.4, to match Vestfjorden and Mosjøen Fault as well. The results of the re-simulations of Oslofjorden Fault are:

- Oslofjorden Fault re-simulated as a M_W 7.5 earthquake with fault length and fault width = 100.0 km and 19.0 km respectively, as Mosjøen Fault, the maximum peak ground motion acceleration is 275.7 cm/s^2, Figure 6.2-5 below.
- Oslofjorden Fault re-simulated as a M_W 7.5 earthquake with fault length and fault width = 98.0 km and 19.4 km respectively, as Vestfjorden Fault, the maximum peak ground motion acceleration is 277.7 cm/s^2, Figure 6.2-6 below.

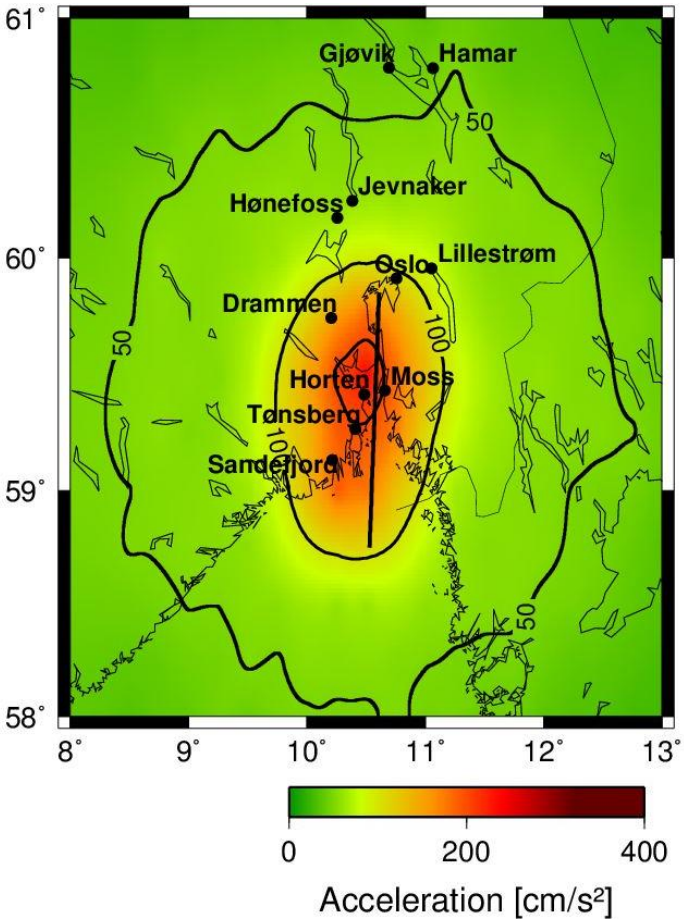

Figure 6.2-5 PGA distribution for Oslofjorden Fault, re-simulated as a M_W 7.5 earthquake with the fault length and width from Mosjøen Fault. The maximum PGA is estimated to be 275.7 cm/s^{2}for this scenario.

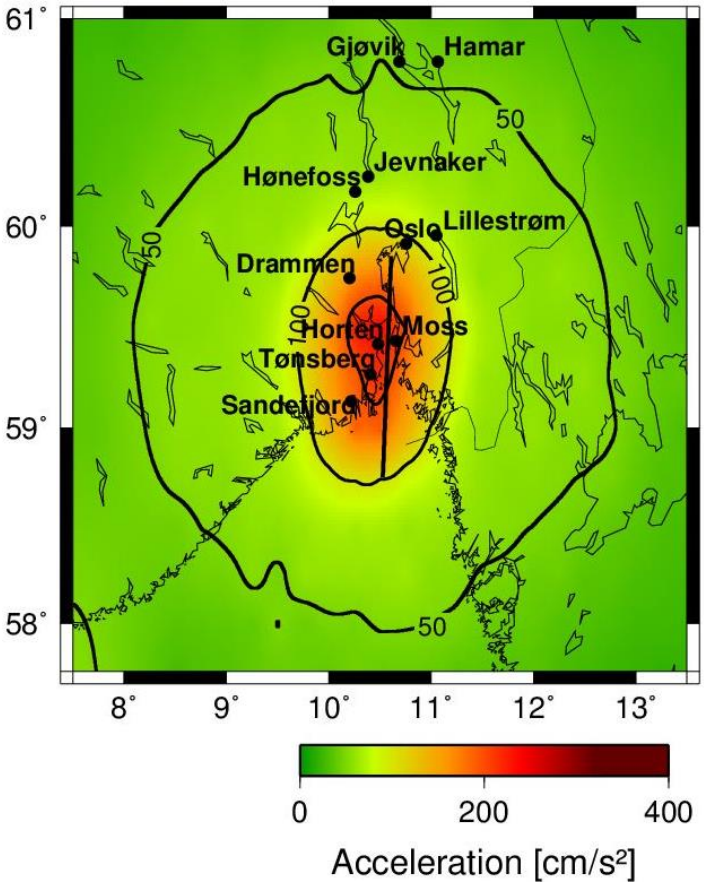

Figure 6.2-6 PGA for Oslofjorden Fault, re-simulated as a M_W 7.5 earthquake with the fault length and width from Vestfjorden Fault. The maximum PGA is estimated to be 277.7 cm/s²for this scenario.

The results from Vestfjorden and Mosjøen strongly suggests that a difference of 2 km in fault length and 0.4 km in fault width affects the earthquake scenarios by increasing the ground acceleration. The results from Oslofjorden Fault, however, did not show a large difference in maximum PGA when it was re-simulated with the fault length and width from Vestfjorden and Mosjøen Fault. The difference in Oslofjorden Fault is only 2 cm/s², and these results are therefore not compatible with the theory that the length and width are the reason for the large difference in PGA in the M_W 7.5 scenarios on Vestfjorden and Mosjøen Fault. The area affected by the ground motion appears to be slightly larger for the shorter fault length (Oslofjorden Fault re-simulated with the length and width from Vestfjorden Fault), Figure 6.2-6. This scenario also saw the highest PGA value.

The largest difference occurs on Mosjøen Fault, where the increase is 25.5 cm/s² between the scenarios with fault lengths of 100 km and 98 km. The maximum PGA on Vestfjorden Fault decreases by 17.4 cm/s² between the scenarios with fault lengths of 98 km and 100 km. This may occur because the PGA becomes more concentrated in the

area when the fault is shorter, even though the shortening only is by 2 km, and thus causing higher PGA, covering a larger area.

Between the M_W 7.5 scenarios on Oslofjorden Fault, however, the difference is very small, only 2 cm/s^2. These results may be caused because of the randomness in the simulations. Another possible explanation for the small difference in PGA when Oslofjorden Fault was edited to a M_W 7.5 scenario may be that the simulations are run with only 3 iterations and random hypocenter location. The results from Oslofjorden Fault can therefore be considered inconclusive.

The effect of these two parameters, number of iteration in the simulations and random versus fixed hypocenter location, are discussed in the following subchapters.

6.3 NUMBER OF ITERATIONS

My results from EXSIM12 are simulated using 3 iterations for each site, meaning that the program simulates the peak ground acceleration at each site three times with different random hypocenter location and then calculate the mean value of the peak ground acceleration. This value is used to plot the distribution of the ground motion acceleration. To test the theory that the number of trials could be the reason for the difference in maximum ground acceleration for earthquake scenarios with the same magnitude, I re-simulated all scenarios for two of the faults using 20 iteration.

I chose Northern Sunnhordland Fault and Nesna Fault to test this theory because these are two fault with identical input parameters, except for the location. They are both 60.0 km long and 18.0 km wide, and it follows that the highest potential magnitude calculated with formulas from Wells and Coppersmith (1994) are identical as well, M_W 7.2. It is therefore logical to expect close to identical results for these two earthquake scenarios, which is almost the case. The maximum PGA for the two scenarios with M_W 7.2 is 217.3 cm/s^2 for Northern Sunnhordland Fault and 239.5 cm/s^2 for Nesna Fault. In the M_W 6.5 scenarios, the maximum PGA values are 180.0 cm/s^2 and 179.4 cm/s^2 for Northern Sunnhordland and Nesna Fault respectively. The maximum PGA is 91.11 cm/s^2 for Northern Sunnhordland Fault and 117.7 cm/s^2 for Nesna Fault in the M_W 6.0 scenarios. These values are listed in Table 6-1 at the end of this subchapter. Figure 6.3-1 and Figure 6.3-2 shows the distribution of PGA that would follow a M_W 7.2 earthquake on Northern Sunnhordland and Nesna Fault.

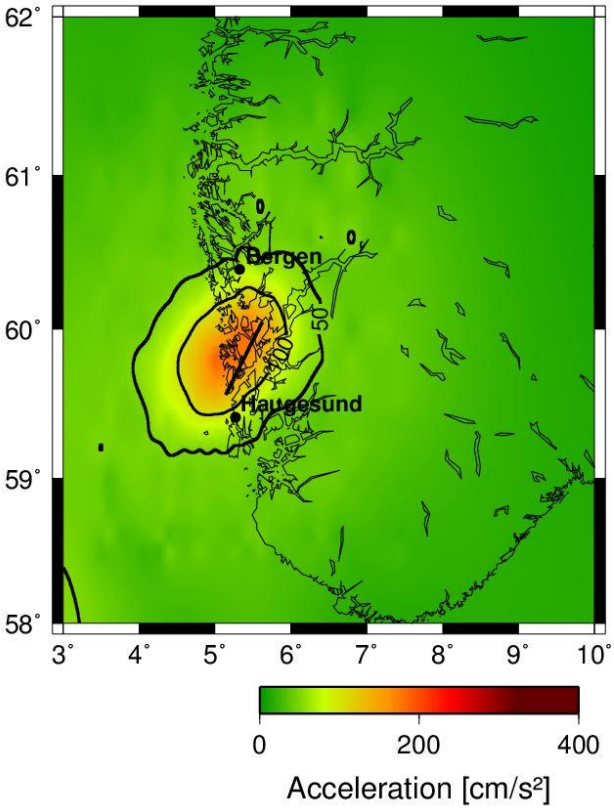

Figure 6.3-1 Distribution of PGA for a M_W 7.2 earthquake scenario on Northern Sunnhordland Fault simulated with 3 iterations for each site.

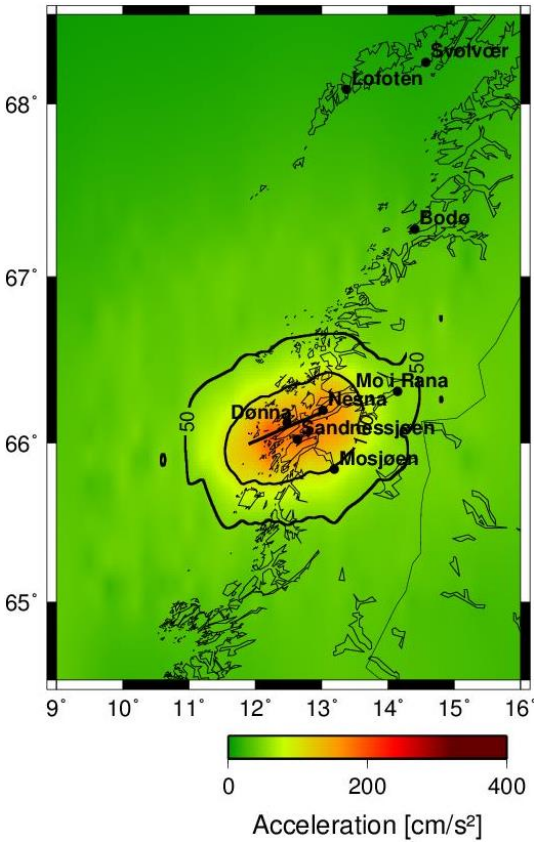

Figure 6.3-2 Distribution of PGA for a M_W 7.2 earthquake scenario for Nesna Fault simulated with 3 iterations for each site.

All earthquake scenarios on Nesna Fault and Northern Sunnhordland Fault were re-simulated, this time using 20 iterations for each site in the fault. Table 6-2 shows that there is an improvement in the PGA distributions from 3 to 20 iterations because the maximum PGA values for the scenarios are more similar, which is expected for two identical faults. The plots are also made using the same scale for the scenarios with the same magnitude, meaning that the number of degrees in latitude and longitude are similar, to make the comparison more accurate.

6.3.1 Nesna Fault

Figure 6.3-3 shows the earthquake scenarios for a M_W 7.2 event on Nesna Fault, simulated with 3 iterations (left) and 20 iterations (right). There is a difference of 14.7 cm/s^2 in the maximum PGA between the two plots in Figure 6.3-3; the scenario with 3 iterations has 239.5 cm/s^2 as the maximum PGA and the scenario with 20 iterations have 224.8 cm/s^2 as the maximum PGA. The area affected by the ground motion is approximately 16 000 km^2 for both simulations, but the contour lines are slightly smoother in the in the right plot (20 iterations), especially noticeable in the 50 cm/s^2 contour line.

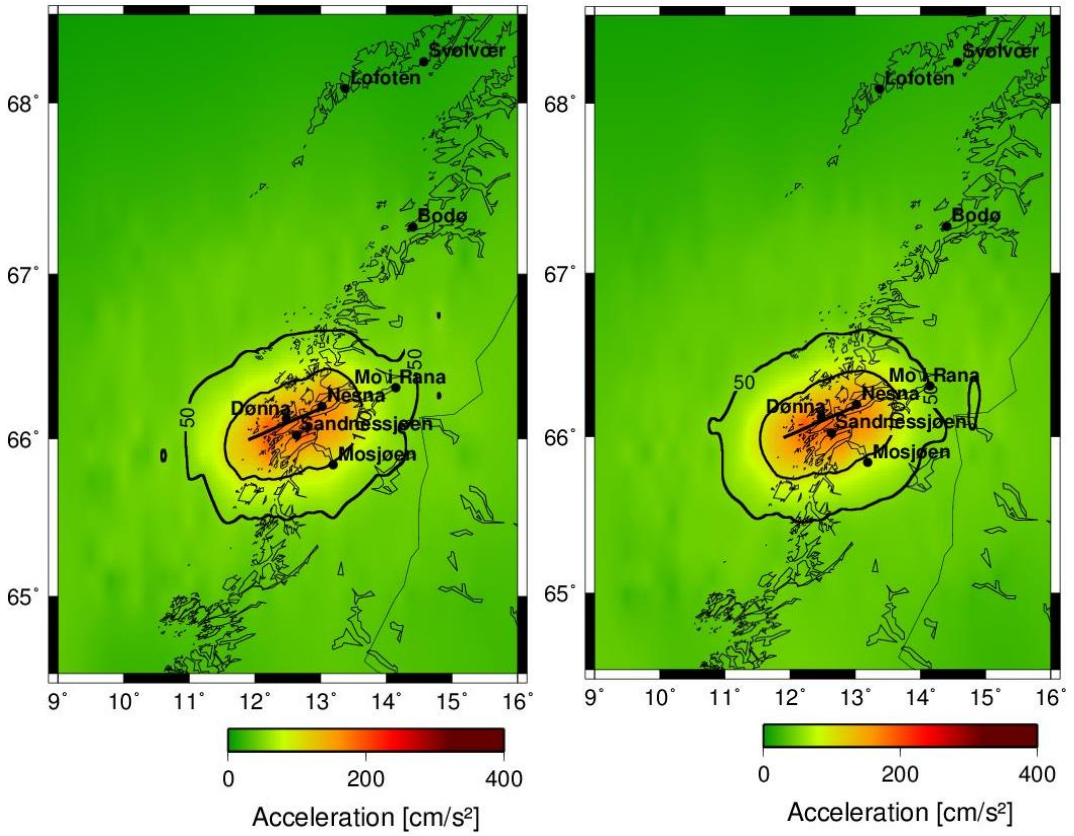

Figure 6.3-3 M_W 7.2 scenarios for Nesna Fault simulated with 3 iterations (left) and 20 iterations (right)

Figure 6.3-4 shows the earthquake scenarios for a M_W 6.5 event on Nesna Fault, simulated with 3 iterations (left) and 20 iterations (right). The earthquake scenario simulated with 20 iterations (right plot in Figure 6.3-4) has a smoother distribution of the PGA caused by the earthquake. The maximum PGA decreases by 20.6 cm/s² in the scenario simulated with 20 iterations; 158.8 cm/s² compared with the value from the simulation with 3 iteration that was 179.4 cm/s². The area affected by the ground acceleration is about the same size, approximately 4900 km².

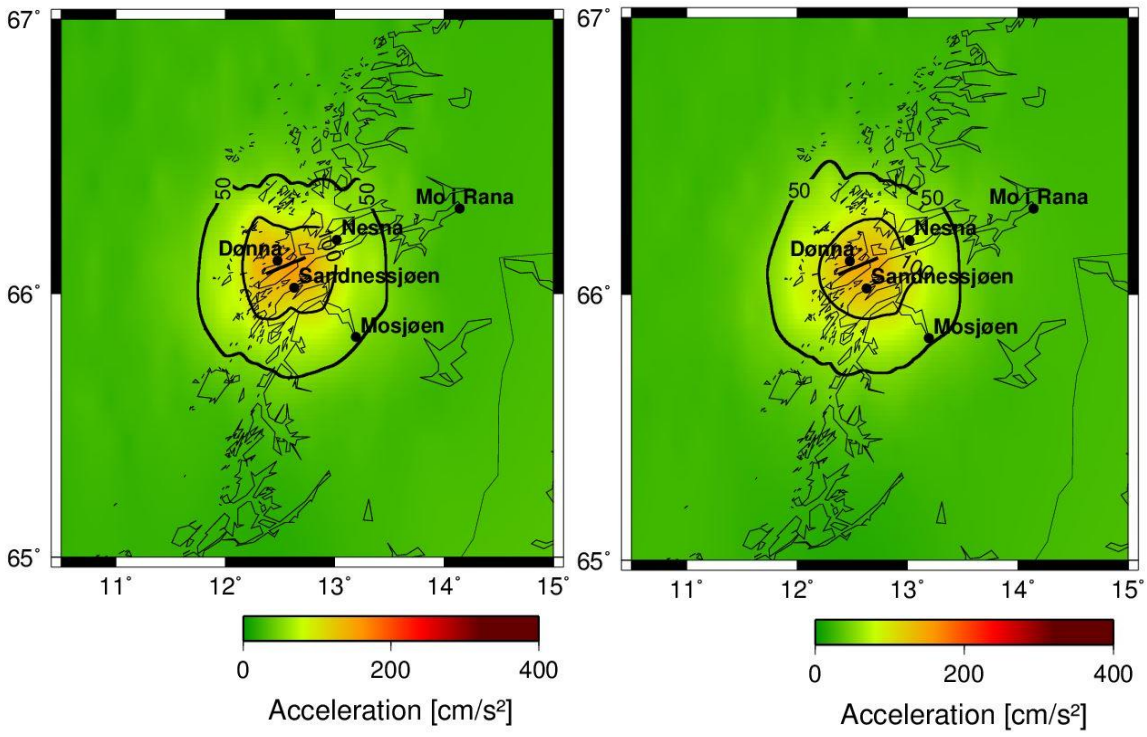

Figure 6.3-4 M_W 6.5 earthquake scenarios for Nesna Fault simulated with 3 iterations (left) and 20 iterations (right).

Figure 6.3-5 shows the earthquake scenarios for a M_W 6.0 event on Nesna Fault, simulated with 3 iterations (left) and 20 iterations (right). As for the M_W 7.2 and M_W 6.5 scenarios, the distribution of the peak ground acceleration is smoother and more even in the plot simulated with 20 iterations. The maximum PGA was reduced by 26.4 cm/s^2, from 117.7 cm/s^2 in the scenario simulated with 3 iteration to 93.3 cm/s^2 in the scenario simulated with 20 iterations. Despite this difference, the area affected by the ground acceleration is roughly the same size, approximately 2200 km^2.

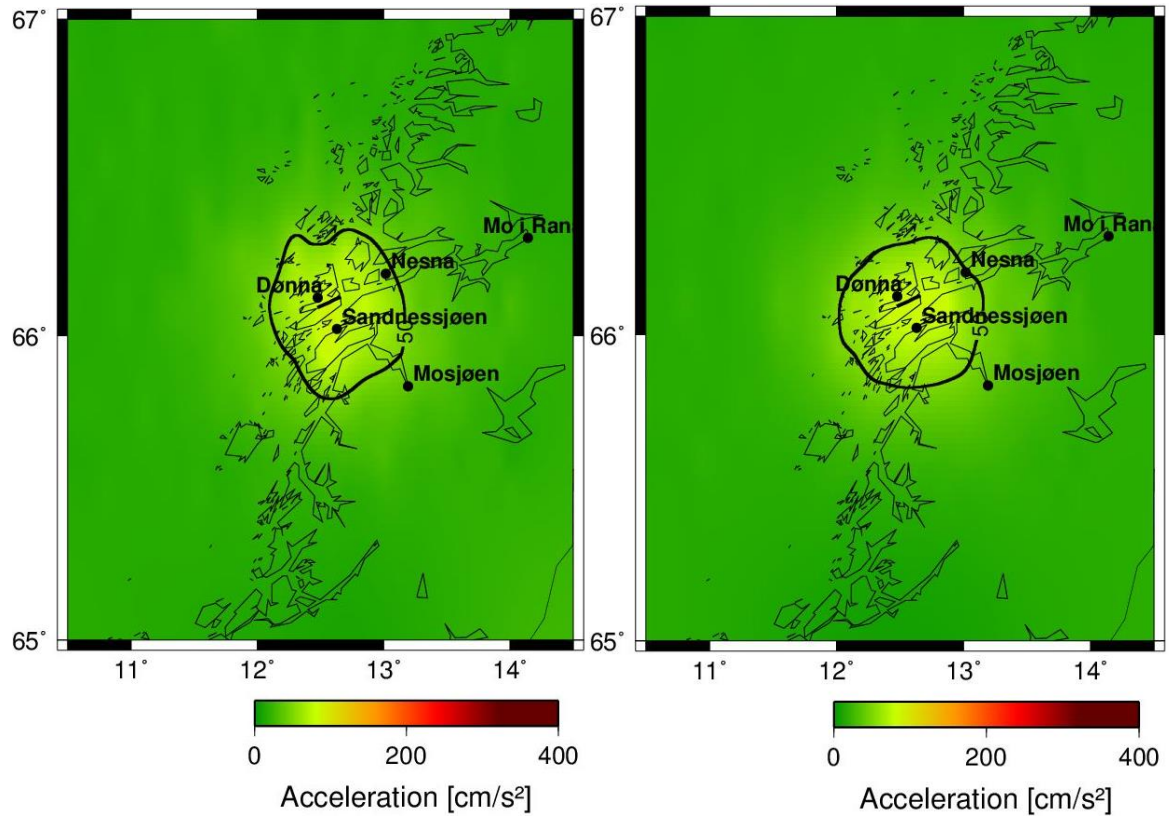

Figure 6.3-5 M_W 6.0 earthquake scenarios for Nesna Fault simulated with 3 iterations (left) and 20 iterations (right)

6.3.2 Northern Sunnhordland Fault

Northern Sunnhordland Fault was also re-simulated with 20 iterations instead of 3 to see if this could be the reason for the difference in the maximum PGA and the plots between the faults. The results of the re-simulations on Northern Sunnhordland Fault is slightly different from Nesna Fault: the M_W 7.2 and M_W 6.5 earthquake scenarios saw a decrease in maximum PGA in the scenario with 20 iterations, and the M_W 6.0 scenario had an increase in maximum PGA from the scenario with 3 to the scenario with 20 iteration.

Figure 6.3-6 shows the earthquake scenarios a M_W 7.2 event on Northern Sunnhordland Fault, simulated with 3 iterations (left) and 20 iterations (right). The maximum PGA value decreased by 4 cm/s^2 between the two simulations; 217.3 cm/s^2 for the initial simulation with 3 iterations compared to 213.2 cm/s^2 in the re-simulation with 20 iterations. The area affected by the earthquake is similar in both simulations, approximately 16 500 km^2, and the 50 cm/s^2 contour line is slightly smoother in the plot to the right.

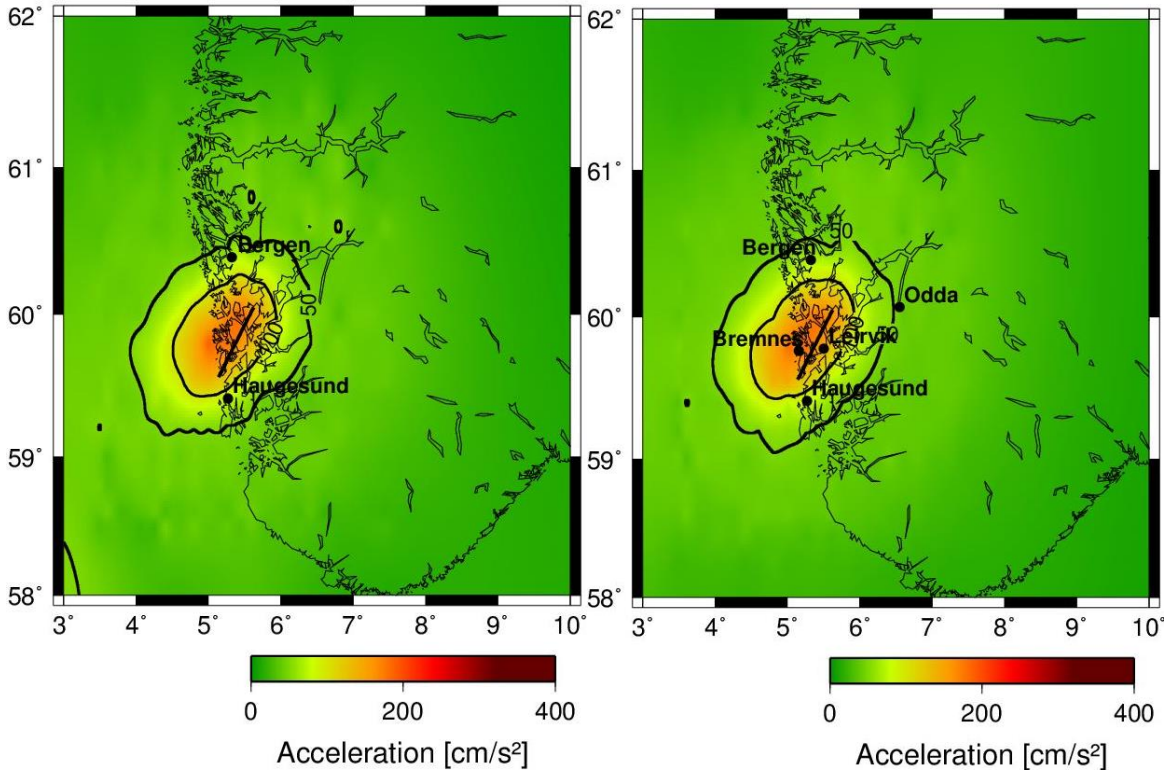

Figure 6.3-6 M_W 7.2 earthquake scenario for Northern Sunnhordland Fault simulated with 3 iterations (left) and 20 iterations (right).

Figure 6.3-7 shows the earthquake scenarios of a M_W 6.5 event on Northern Sunnhordland Fault, simulated with 3 iterations (left) and 20 iterations (right). The maximum PGA is reduced form 180.0 cm/s^2 to 173.7 cm/s^2 in the re-simulations with 20 iterations, a decrease of 6.3 cm/s^2. In addition, the distribution of the ground motion is affected; it is smoother and more circular in the re-simulation with 20 iterations. The size of the area affected by the PGA is roughly the same for both cases, approximately 6100 km^2.

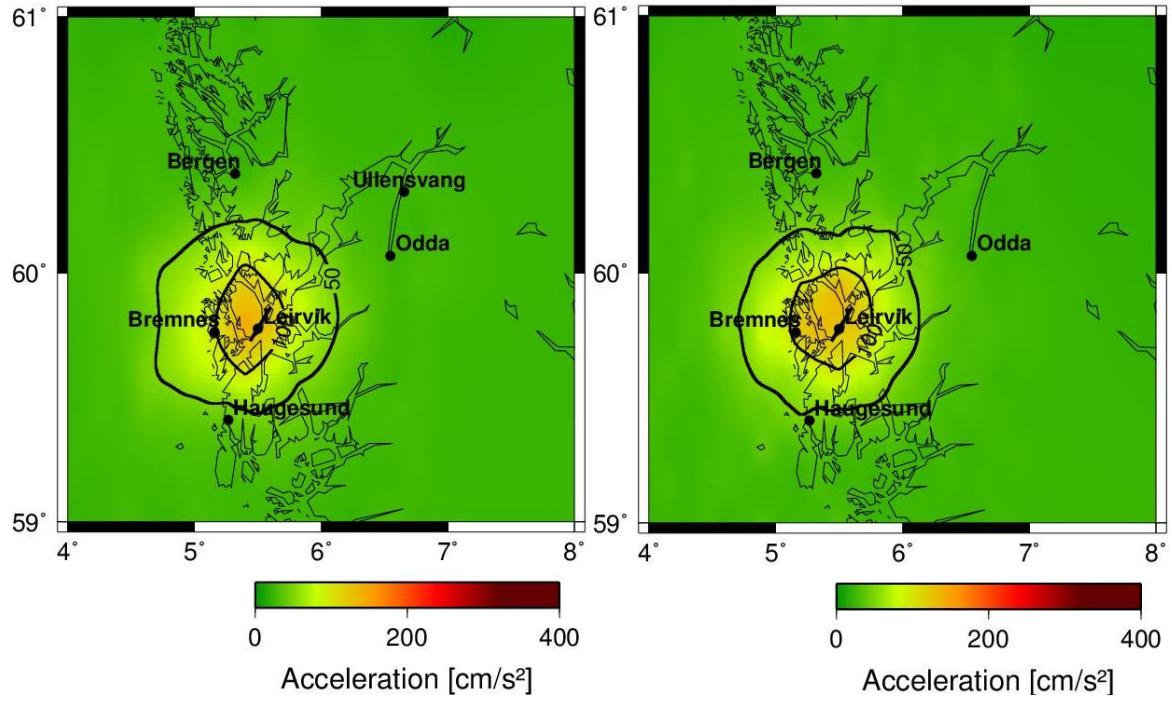

Figure 6.3-7 M_W 6.5 earthquake scenario for Northern Sunnhordland Fault simulated with 3 iterations (left) and 20 iterations (right).

Figure 6.3-8 shows the earthquake scenarios for Northern Sunnhordland Fault if it ruptures in a M_W 6.0 event, simulated with 3 iterations (left) and 20 iterations (right). The maximum PGA increased by 12.4 cm/s², from 91.11 cm/s² to 103.5 cm/s² in the re-simulation with 20 iterations per site. The area affected by PGA over 50 cm/s² is approximately the same size, roughly 2700 km² in both cases. This is the only scenario that saw an increase in maximum PGA after the re-simulation with 20 iterations.

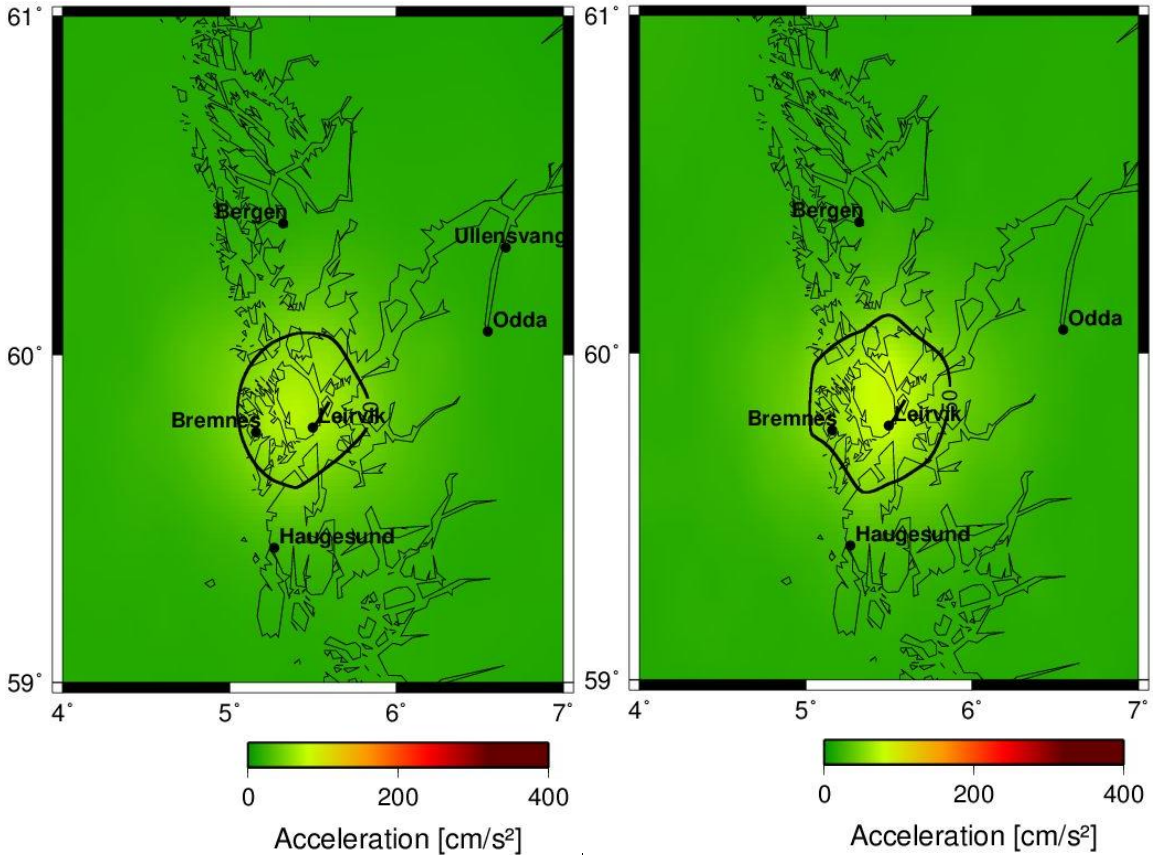

Figure 6.3-8 M_W 6.0 earthquake scenario for Northern Sunnhordland Fault simulated with 3 iterations (left) and 20 iterations (right).

6.3.3 Discussion of the results simulated with 20 iteration per site

The re-simulations of Nesna and Northern Sunnhordland Fault show that higher number of iterations smoothens the distribution of the PGA following the potential earthquake scenarios, making it more even around the center. The initial simulations using 3 iterations resulted in deviating values for both Nesna and Northern Sunnhordland Fault, and the maximum PGA varies between the different scenarios; it is highest for Northern Sunnhordland in the M_W 6.5 and M_W 6.0 scenarios, where the difference between the faults are 14.9 and 10.2 cm/s^2 respectively. In the M_W 7.2 earthquake scenarios, Nesna is higher by 11.6 cm/s^2, Table 6-2. For two faults with identical input-parameters are these differences notable.

Table 6-2 List of maximum ground acceleration for Nesna and Northern Sunnhordland Fault, simulated with 3 iterations (top) and 20 iterations (bottom).

Initial results of the simulation with 3 iterations							
Fault	**Max Mag**	**Fault type**	**Fault length**	**Dip**	**M 7.2**	**M 6.5**	**M6.0**
Nesna	M 7.2	Normal	60.0 km	60	239.5000	179.4000	117.7000
Northern Sunnhordland	M 7.2	Normal	60.0 km	60	217.3000	180.0000	91.1100
Results of the re-simulations with 20 iterations and random hypocenter location							
Nesna	M 7.2	Normal	60.0 km	60	224.8000	158.8000	93.3000
Northern Sunnhordland	M 7.2	Normal	60.0 km	60	213.2000	173.7000	103.5000

These results may occur because the higher number of iterations places the PGA values, including the maximum PGA, in different sites in each iteration due to the random hypocenter location setting. Therefore, when there are 20 iterations instead of 3, the final maximum PGA, which is the average value of all the iterations, will be lower because the maximum PGA has been placed in 20 different sites, instead of only 3, throughout the simulation.

Because the simulations with 20 iterations also resulted in quite large differences in maximum PGA between the two faults, I tested to see if simulating the earthquakes using a fixed hypocenter location instead of random hypocenter could result in smoother PGA distribution and less difference in maximum PGA in the earthquake scenarios.

6.4 LOCATION OF EPICENTER

In addition to the re-simulations with 20 iteration, the earthquake scenarios for Nesna and Northern Sunnhordland Fault were re-simulated again, this time using a fixed hypocenter location or epicenter in the earthquake and 20 iteration per site, instead of random hypocenter location, which is used for all my earthquake scenarios.

Simulating earthquake scenarios using random hypocenter location means that the rupture may start in any of the subfaults on the fault plane, and the location of the hypocenter may change between the iterations for each site. Each iteration simulates a possible outcome of the earthquake in question, and the final PGA value for each site is the average value of these possible outcomes. For instance, the rupture could start on opposite ends of two identical faults and spread from there, causing the distribution of PGA to be different in the scenarios. If this is the case, the reason for the difference could be explained by the directivity effect. The directivity effect occurs because the seismic energy spreads in all directions during an earthquake while the rupture propagation only moves in one direction. The amount of seismic energy is the same for all directions, but the energy traveling in the same direction as the rupture will arrive over a shorter time period than for the energy traveling on the opposite direction, and thus causing the ground acceleration to be more severe in this area (Stein and Wysession, 2012).

When the simulations using fixed hypocenter location are run, the start of the rupture is set to one of the subfaults on the fault plane, and it remains in the same subfault in all iterations. This causes the PGA to be lower because each iteration simulates the same outcome 20 times and uses the mean value to describe the expected PGA at each site.

The previous chapter discussed the effect of more iterations per site, and whether 20 iterations would result in less difference in the results in the earthquake scenarios on Nesna and Northern Sunnhordland Fault. In this chapter, I will discuss the results when the earthquake scenarios are re-simulated with 20 iteration per site and fixed hypocenter location compared to the results of the simulations with 20 iterations per site and random hypocenter location. I have chosen the first subfault on the fault length and the first subfault of the fault width as the location of the hypocenter. Table 6-3 at the end of this subchapter shows that the maximum PGA becomes more similar when the simulations are run with fixed hypocenter location.

6.4.1 Nesna Fault

Figure 6.4-1 shows the earthquake scenarios for a M_W 7.2 event on Nesna Fault simulated with 20 iterations per site and random hypocenter location (left) and fixed hypocenter location (right). The scenario with fixed hypocenter location has smoother contour lines and the area affected by the PGA is roughly the same size, approximately 16 000 km^2. The maximum PGA is reduced from 224.8 cm/s^2 in the random scenario to 203.2 cm/s^2 in the fixed scenario, a difference of 21.6 cm/s^2. The effect of the directivity is evident in the plot with fixed hypocenter location (right in Figure 6.4-1): the tale near Mo i Rana is formed in the direction opposite of the rupture propagation, because the PGA arrives over a longer time period than for the other end of the fault. This indicates that the rupture in this scenario started in the west-northwestern end of the fault and propagates due east-southeast, causing the PGA to be less severe in the northwestern end.

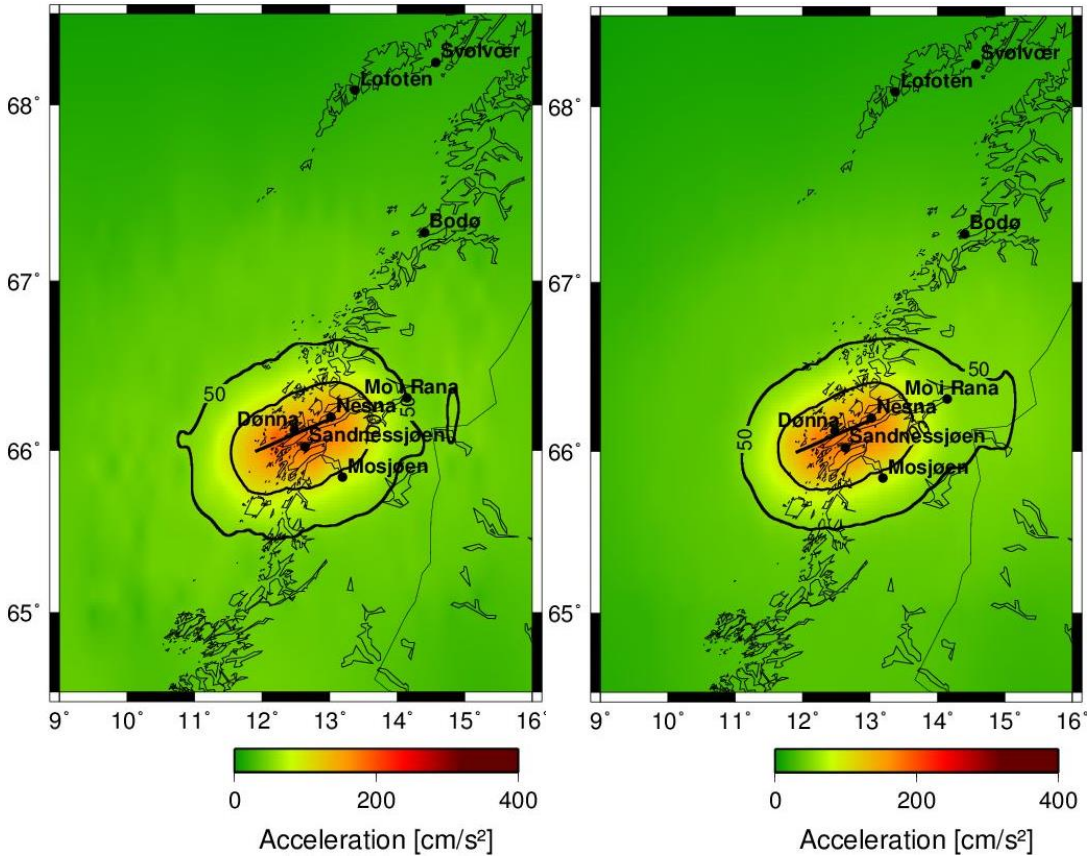

Figure 6.4-1 Earthquake scenarios for a M_w 7.2 event on Nesna Fault, simulated with random hypocenter location (left) and fixed hypocenter location (right)

Figure 6.4-2 shows the earthquake scenarios for a M_W 6.5 event on Nesna Fault simulated with 20 iterations per site and random hypocenter location (left) and fixed hypocenter location (right). Both contour lines in the scenario with fixed hypocenter location are smoother, and it looks like the affected area is a bit smaller in this plot. The maximum PGA is decreased by 19.7 cm/s^2 in the scenario with fixed hypocenter location (right plot in Figure 6.4-2); 139.1 cm/s^2 compared to 158.8 cm/s^2 for the scenario with random hypocenter location (left plot in Figure 6.4-2).

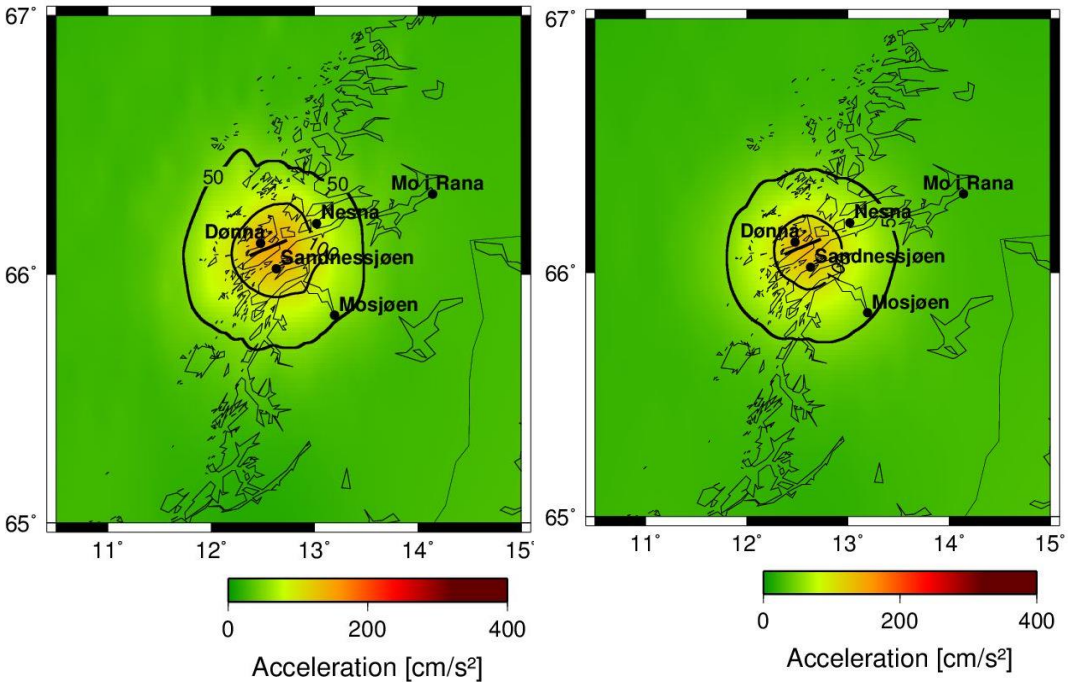

Figure 6.4-2 Earthquake scenarios for a M_W 6.5 event on Nesna Fault, simulated with random hypocenter location (right) and fixed hypocenter location (left)

Figure 6.4-3 shows the earthquake scenarios for a M_W 6.0 event on Nesna Fault, simulated with 20 iterations per site and random hypocenter location (left) and fixed hypocenter location (right). The maximum PGA is reduced for this scenario as well; it was 93.3 cm/s² in the scenario with random hypocenter location compared with 85.0 cm/s² in the scenario with fixed hypocenter location, which is a reduction of 8.3 cm/s². In addition, it appears in Figure 6.4-3 that the area affected by ground acceleration is slightly smaller for the fixed scenario than for the random scenario.

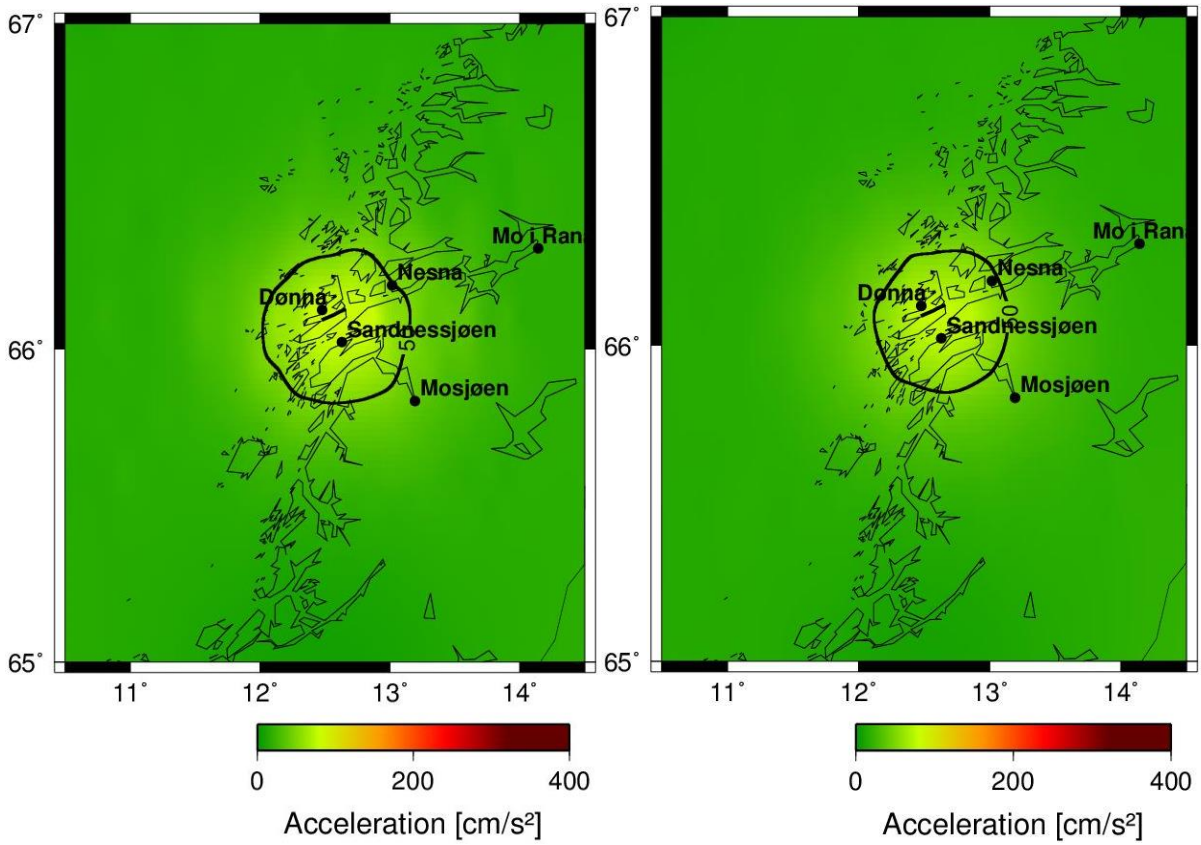

Figure 6.4-3 Earthquake scenarios for a M_W 6.0 event on Nesna Fault, simulated with random hypocenter location (right) and fixed hypocenter location (left).

6.4.2 Northern Sunnhordland Fault

Figure 6.4-4 shows the earthquake scenarios for a M_W 7.2 event on Northern Sunnhordland Fault, simulated with 20 iterations per site and random hypocenter location (left) and fixed hypocenter location (right). The area affected by the ground motion is approximately the same size in both plots, but the shape of the contour lines is narrower and a little longer for the fixed scenario (right plot in Figure 6.4-4), and in addition is the PGA caused by the earthquake smoother distributed for the fixed scenario. This may be caused by the fixed hypocenter location; when the hypocenter is fixed to a given subfault, the rupture will start and propagate from the same point in every iteration, causing the directivity effect to work in the same direction for each iteration on the sites. In this case, the rupture is set to start in the southwestern end of the fault and propagate due northeast, thus focusing the energy in this direction. The maximum PGA is reduced by 11.4 cm/s^2; it was 213.2 cm/s^2 in the scenario with random hypocenter location, while it is reduced to 201.8 cm/s^2 in the scenario with fixed hypocenter location.

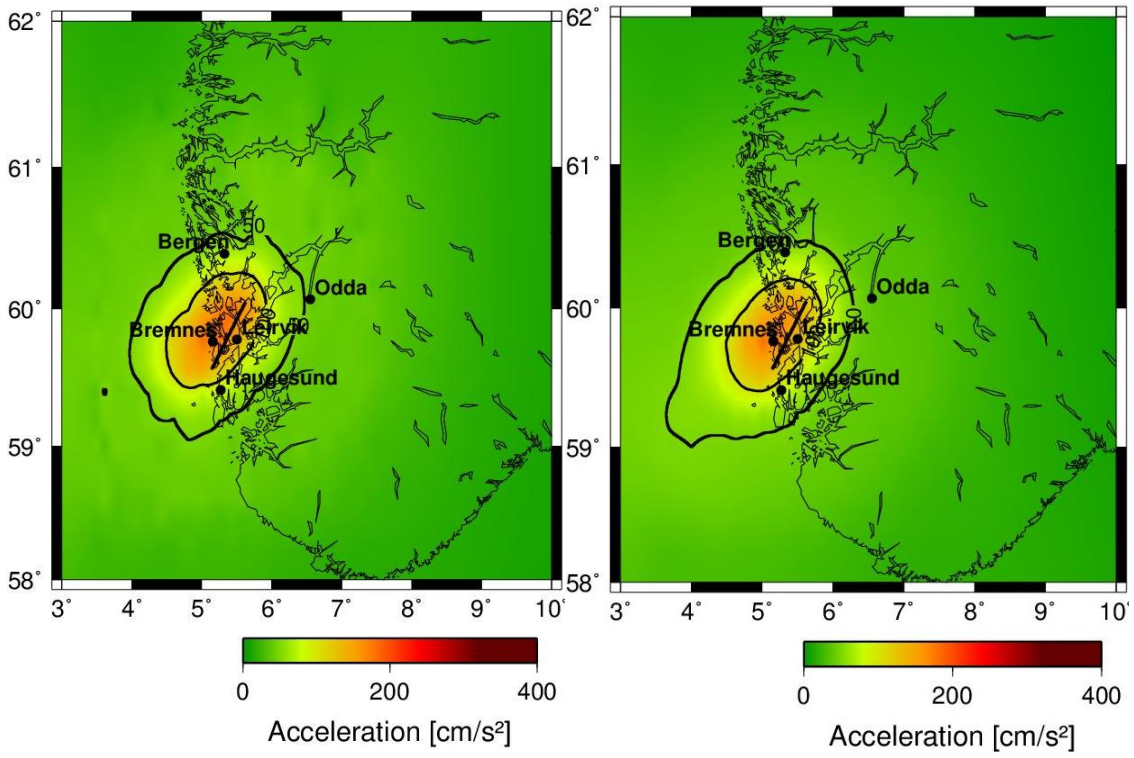

Figure 6.4-4 Earthquake scenarios for a M_W 6.0 event on Northern Sunnhordland Fault, simulated with random hypocenter location (right) and fixed hypocenter location (left).

Figure 6.4-5 shows the earthquake scenarios for a M_W 6.5 event on Northern Sunnhordland Fault, simulated with 20 iterations per site and random hypocenter location (left) and fixed hypo location (right). This scenario has the largest reduction, 39.1 cm/s^2, in maximum PGA: 173.7 cm7s^2 in the random hypocenter location scenario and 134.6 cm/s^2 in the fixed hypo location scenario. It is also clear that the area affected by PGA over 50 cm/s^2 is smaller for the scenario with fixed hypocenter location. The area within the 50 cm/s^2 is approximately 6100 km^2 in the scenario with random hypocenter location (left plot in Figure 6.4-5), while it is approximately 4000 km^2 in the scenario with fixed hypocenter location (right plot in Figure 6.4-5).

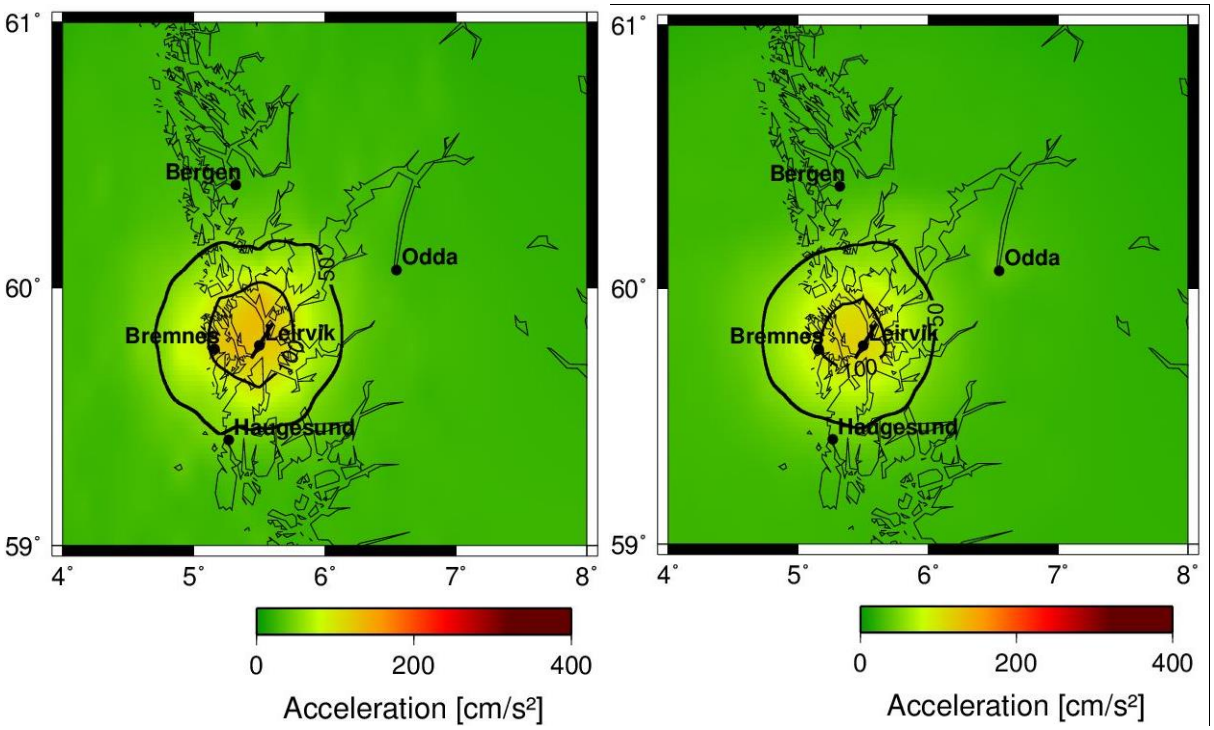

Figure 6.4-5 Earthquake scenarios for a M_W 6.5 event on Northern Sunnhordland Fault, simulated with random hypocenter location (right) and fixed hypocenter location (left).

Figure 6.4-6 shows the earthquake scenarios for a M_W 6.0 event on Northern Sunnhordland Fault, simulated with 20 iterations per site and random hypocenter location (left) and fixed hypocenter location (right). The reduction in maximum PGA is also evident for this scenario. The maximum PGA is 103.5 cm/s² in the scenario with random hypocenter location and only 83.18 cm/s² in the scenario simulated with fixed hypocenter location, a decrease of 20.3 cm/s². The affected area is also smaller for the scenario with fixed hypocenter location than for the one with random hypocenter location.

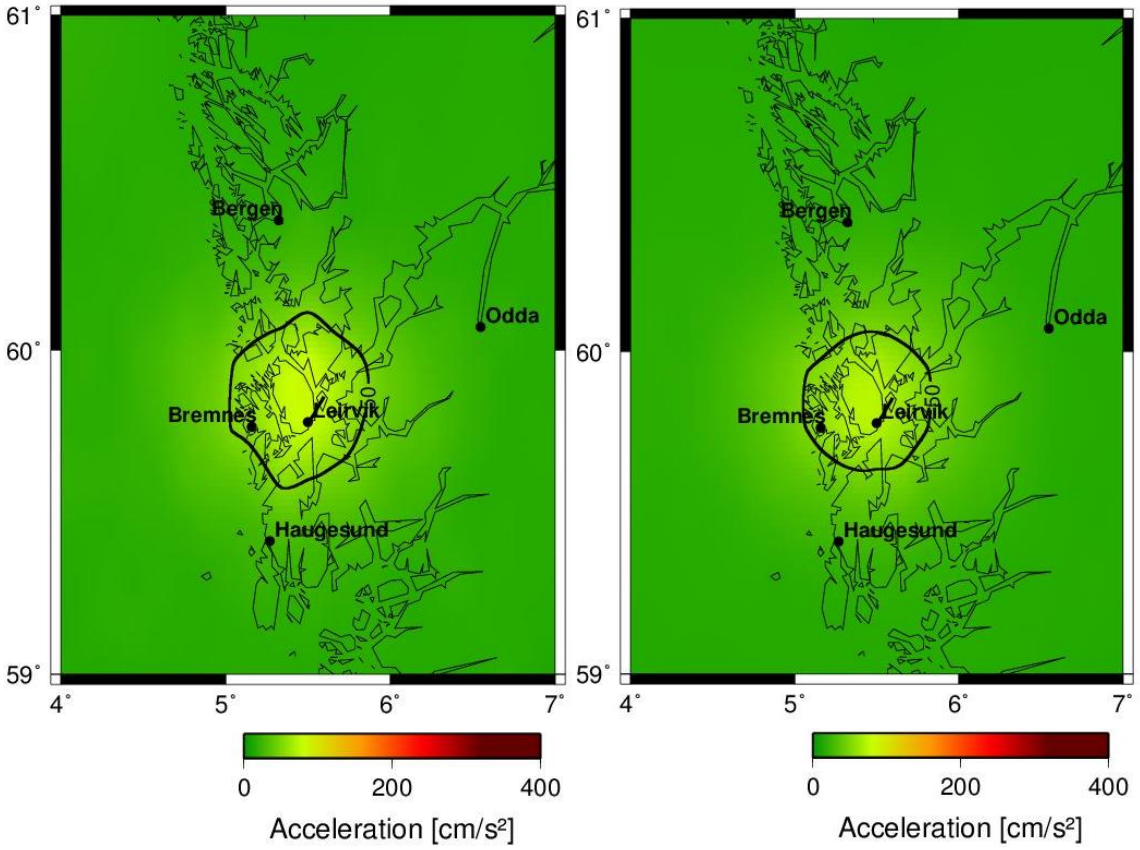

Figure 6.4-6 Earthquake scenario for a M_W 6.0 event on Northern Sunnhordland Fault, simulated with random hypocenter location (right) and fixed hypocenter location (left).

6.4.3 Discussion of the results simulated with fixed hypocenter location

Table 6-3 shows that the maximum PGA for the earthquake scenarios on Nesna and Northern Sunnhordland Fault became very similar after the simulations with fixed hypocenter location. In addition, the affected area became somewhat smaller and the contour lines in the plots became smoother. These observations are based on the comparison with the results if the simulations with random hypocenter locations, simulated with 20 iterations per site.

The difference in maximum PGA between the two faults was reduced even further; the difference is 1.4 cm/s^2 for the M_W 7.2 scenario, 4.5 cm/s^2 for the M_W 6.5 scenario, and 1.8 cm/s^2 for the M_W 6.0 scenario.

Table 6-3 Lists of the maximum peak ground acceleration for the earthquake scenarios on Nesna and Northern Sunnhordland Fault. The first two are the same as Table 6-2 and the last lists the maximum acceleration from the simulations with fixed hypocenter location.

Initial results of the simulation with 3 iterations							
Fault	**Max Mag**	**Fault type**	**Fault length**	**Dip**	**M 7.2**	**M 6.5**	**M6.0**
Nesna	M 7.2	Normal	60.0 km	60	239.5000	179.4000	117.7000
Northern Sunnhordland	M 7.2	Normal	60.0 km	60	217.3000	180.0000	91.1100
Results of the re-simulations with 20 iterations and random hypocenter location							
Nesna	M 7.2	Normal	60.0 km	60	224.8000	158.8000	93.3000
Northern Sunnhordland	M 7.2	Normal	60.0 km	60	213.2000	173.7000	103.5000
Results of the re-simulations with 20 iterations and fixed hypocenter location							
Nesna	M 7.2	Normal	60.0 km	60	203.2000	139.1000	85.0000
Northern Sunnhordland	M 7.2	Normal	60.0 km	60	201.8000	134.6000	83.18000

The main difference in simulating with random versus fixed hypocenter location is that in the scenarios with random hypocenter location, the rupture can start in any of the subfault, while the start of the rupture is set for a given subfault, in this case the first subfault on the fault length and width, in the scenarios with fixed hypocenter location. This means that for the fixed hypocenter location, the simulations are run with 20 iteration and the rupture starts at the same subfault for all iterations for each site and then the average PGA value for that site is calculated. Contrary for the order of random hypocenter location, where the rupture can start at any of the subfaults and the start of rupture varies for each site and iteration.

The rupture propagation will therefore be smoother distributed for the earthquake scenarios with fixed hypocenter location, making the PGA values a bit lower than for the scenarios with random hypocenter location.

6.5 EARTHQUAKE RECURRENCE IN NORWAY

Being located well within a lithospheric plate, Norway is not prone to very large earthquakes. In the past, however, there has been some earthquakes with magnitude 4.5 or larger. Oslo Rift Zone had a M_S 5.4 earthquake in Oslofjorden in 1904 (Bungum et al., 2009) and Lurøy in Nordland had a M_S 5.8 earthquake in 1819 (Bungum and Olesen, 2005). One of the largest know earthquakes in Hordaland is the M_L 4.25 event in Etne in 1989 (Karpuz et al., 1991). These earthquakes are deviations from most of the events that occur in Norway, which are of magnitude 3.5 or lower. Another example of intraplate earthquake activity can be found on Svalbard, where a M_W 6.0 earthquake occurred in 2008 (Pirli et al., 2010). This earthquake occurred off the coast of Spitsbergen, and it is not a part of the earthquakes in mainland Norway, but the stress generating mechanisms are the same for this event and the earthquakes in mainland Norway. The return time for large earthquakes, M_W 5 or larger, is very long for Norway; it can be thousands of years. We cannot know whether it is thousands or ten thousands of years between such large earthquakes on a fault, because the time of study on the faults is too short. The seismicity in Norway is characterized as intermediate to low, dependent on where in the county you are.

The seismic activity is controlled by the forces that promotes stress accumulation in the crust, which in Norway are dominated by ridge-push from the Mid-Atlantic Ridge, post-glacial rebound and sedimentary loading and unloading (Fjeldskaar et al., 2000). Bungum et al. (2010) performed a study where they discussed the driving forces behind earthquakes in Norway. There is little doubt that the stresses in the Norwegian crust are affected by the tectonic stresses caused by push from the Mid-Atlantic Ridge, and the principal stresses show NW-SE direction for the maximum horizontal principal stress, which supports this theory. As for the post-glacial rebound, the discussion deals with how much of the stresses uplift cause today. It is known that the abrupt and sudden rebound that followed the deglaciation of the continent resulted in many large earthquakes over relatively short time. This driving force is not as prominent today as it was shortly after the melting, but it is still considered one of the driving forces behind earthquakes in Norway and Fennoscandia. Loading of sediments is also accepted as a driving force, but it not clear how it works with the other driving forces. Regardless of which of these forces dominate the stress accumulation, scientists agree that even if they

all worked together, the force would still not be large enough to cause new rupture in the hard rock crust in Norway. The occurrence of earthquakes is therefore restricted to weakness zones or zones with high pore pressure causing the strength of the rocks to decrease (Bungum et al., 2010).

By using this reasoning, it is quite safe to assume that earthquake scenarios like the M_W 7.7 event on Hamar Fault, the M_W 7.4 event on Oslofjorden Fault, the M_W 7.0 on Rustefjorden Fault or even the smaller scenarios of M_W 6.5 and M_W 6.0 are highly unlikely. However, the probability does increase with decreasing magnitude. Moreover, the probability of an earthquake occurring with magnitude up to 6.0 should not be excluded, given that there has been earthquakes of magnitude 5.0 – 5.8 earlier. After all, Bungum et al. (2005) have calculated that the seismic activity in Norway may be equivalent to an earthquake of magnitude 5 rupturing every 10 years, and a magnitude 7 event every 1100 years, on average. As the last large earthquake (magnitude 5-6) occurred over 100 years ago, the M_W 6.0 event on Svalbard not included, and if these calculations are true, Norway may be prone to an occurrence of a new large earthquake.

6.6 Comparison of my results with the results from Tveit (2013) and Probabilistic Seismic Hazard Assessments

Tveit (2013) performed a seismic hazard study in Bergen, using Øygarden Fault Zone as source and M_W 6.0 as the magnitude for the earthquake scenarios. She used EXSIM12 to simulate the peak ground acceleration following a potential earthquake in the fault zone. The goal of her study was to find the worst- and best-case earthquake scenarios for Bergen and in doing so; she performed a sensitivity study on the input-parameters used for Norway in EXSIM12. As mentioned in the Data chapter, I used this sensitivity study when deciding which values to use for the input-parameters.

The Øygarden Fault Zone is located approximately 47 km northwest of Bergen and the results from Tveit (2013) are therefore not completely comparable to my results as they are focused on the PGA in Bergen instead of the PGA closer to the source. In addition, Tveit (2013) ended up using different values for two of the parameters; the depth of the earthquake and the stress drop. Both of these parameters have a large effect on the PGA, and result in quite different distributions of the PGA. Another difference between this

study and my study is that Øygarden Fault Zone is located offshore, while all the faults in my study are located onshore, and thus closer to Norwegian cities and towns.

Figure 6.6-1 shows that Tveit (2013) found the worst-case scenario on Øygarden Fault Zone would be if the M_W 6.0 earthquake ruptures at 5.0 km depth and has a stress drop of 120 bar. This scenario would cause PGA exceeding 100 cm/s^2 at the center of the ground motion, which may indicate shaking of intensity VII on the Modified Mercalli Intensity Scale, Table 5.2-1. However, this intensity would only occur within the innermost contour line in the plot. The city of Bergen would experience maximum PGA of 7.45 cm/s^2 (Tveit, 2013), which could correspond to intensity I - III on the Modified Mercalli Intensity Scale.

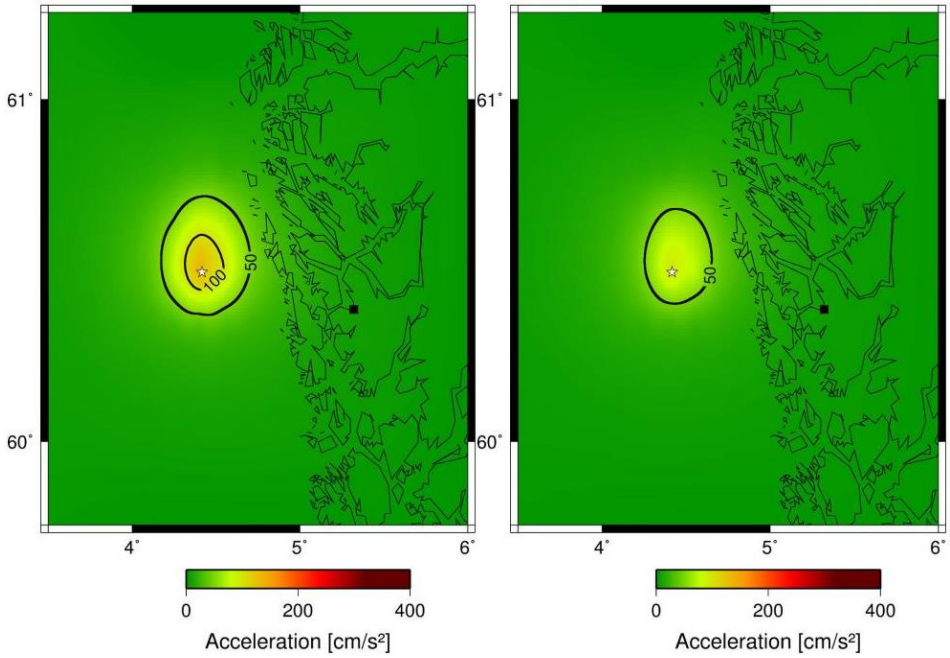

Figure 6.6-1 Peak ground motion distribution on two M_W 6.0 earthquake scenarios on Øygarden Fault Zone. The plot to the left is simulated using a depth of 5.0 km and a stress drop of 120 bar, while the right plot is simulated using the same depth and a stress drop of 80 bar (from (Tveit, 2013)).

Figure 6.6-2 shows that Tveit (2013) found that the best-case scenario on Øygarden Fault Zone would be if the M_W 6.0 earthquake ruptures at 20.0 km depth and has a stress drop of 80 bar. This scenario would cause PGA below 50 cm/s^2, as there are no contour lines in the plot. The maximum PGA in Bergen would be 5.55 cm/s^2 (Tveit, 2013), which could correspond to intensity I - III on the Modified Mercalli Intensity Scale. Intensity I – III means that the shaking may be felt indoors, but there is no damage caused by the tremors, Table 5.2-1.

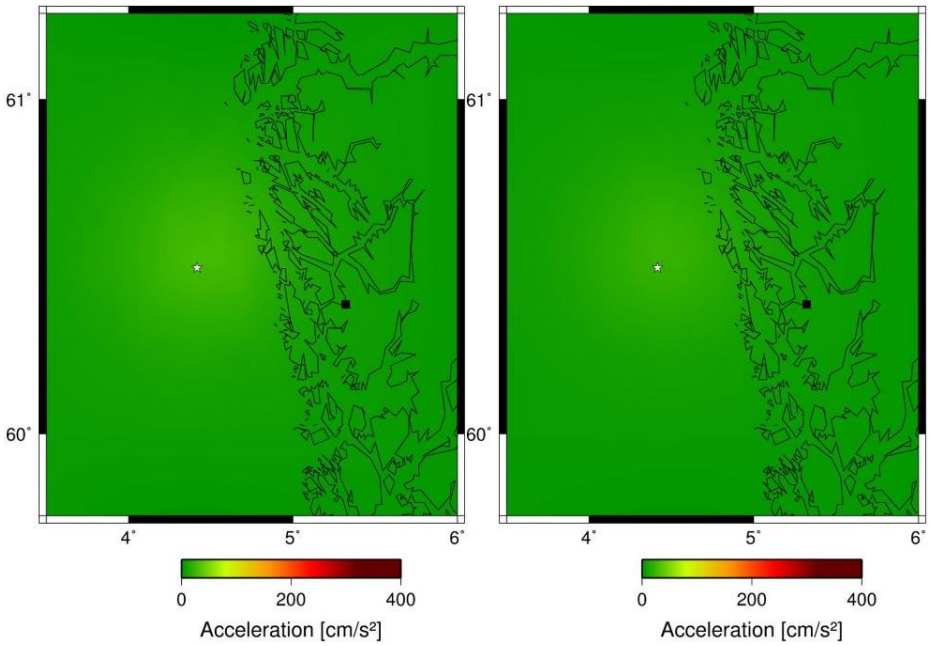

Figure 6.6-2 Peak ground motion distribution on two M_W 6.0 earthquake scenarios on Øygarden Fault Zone. The plot to the left is simulated using a depth of 20.0 km and a stress drop of 120 bar, while the right plot is simulated using the same depth and a stress drop of 80 bar (from (Tveit, 2013)).

Figure 6.6-3 shows the distribution of PGA for the M_W 6.0 earthquake scenarios rupturing on Hjeltefjorden Fault (left plot) and Totland Fault (right plot). Both scenario are simulated using 15.0 km as depth of rupture and a stress drop of 80 bar. The maximum PGA for the scenario on Hjeltefjorden Fault is 115.7 cm/s^2 and 132.8 cm/s^2 for Totland Fault. These results fall in between the results of Tveit (2013), but are closest to the scenario simulated at 5.0 km depth and a stress drop of 80 bar. However, the difference in depth of these results makes the comparison difficult.

Tveit (2013) calculated that the seismic hazard in Bergen is between maximum PGA values of 7.45 and 5.55 cm/s^2 for a potential earthquake on Øygarden Fault Zone; whereas the simulations I have performed show that the potential seismic hazard is much higher, between 115.7 and 132.0 cm/s^2 at the most for a M_W 6.0 earthquake. The

reason for this difference is the location of the faults. Øygarden Fault Zone is located 47 km due northwest from Bergen, while Hjeltefjorden Fault and Totland Fault, where my simulations are performed, are located only 12 km west and 9 km south from Bergen, respectively. Bergen is thus much closer to the source of the event if Hjeltefjorden or Totland Fault were to rupture, compared to Øygarden Fault Zone.

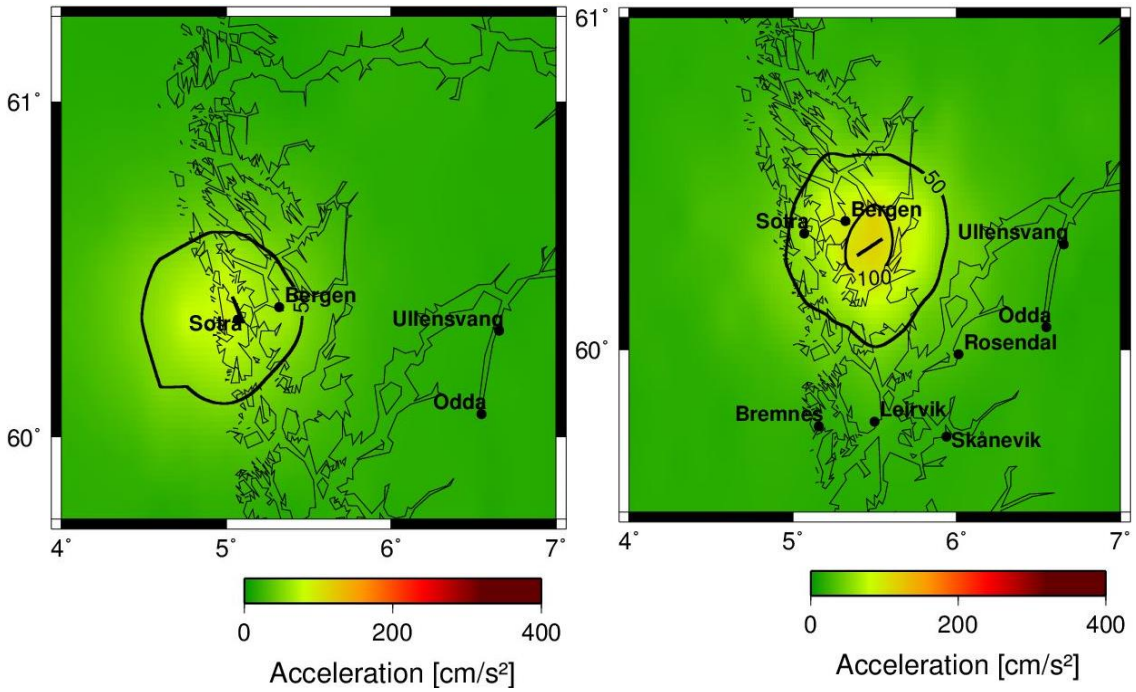

Figure 6.6-3 Distribution of peak ground acceleration for M_W 6.0 earthquake scenarios on Hjeltefjorden Fault (left) and Totland Fault (right), simulated using 15.0 km as depth of rupture and a stress drop of 80 bar.

Another method for simulating the seismic hazard in an area is using a Probabilistic Seismic Hazard Assessment. This method uses the known seismic activity in an area to predict the future ground motion. Reiter (1991) explains the approach for a probabilistic seismic hazard assessment in four basic steps. The first step is to define the source area for the study. The second step is to define the earthquake recurrence in the source area or the distribution of the earthquake probability. The earthquakes occurring in the source area are usually considered as single events when calculating a probabilistic hazard assessment, in other words, one earthquake occurring does not affect the probability of another earthquake occurrence. The third step is to estimate the effect caused by the earthquake. This is usually given as peak ground acceleration or peak ground velocity. The fourth and last step is to calculate the seismic hazard by summing the effects of all earthquakes of different sizes, locations and probabilities. The

result of such an assessment is a curve or a model that shows the probability of exceeding different levels of ground motions within a given time period.

Wahlström and Grünthal (2001) performed a Probabilistic Seismic Hazard Assessment in Fennoscandia. They found that the probability of not exceeding PGA of 500 - 600 cm/s^2 in Hordaland, 250 – 350 cm/s^2 in Oslo Rift Zone, and 350 – 500 cm/s^2 in Nordland is 90 % in 50 years, Figure 6.6-4. These values are higher than for the rest of Norway, which is between 150 – 300 cm/s^2. This probability corresponds to a mean return period of 475 years, in other words, earthquakes releasing these amounts of energy occur on average every 475 year.

Bungum et al. (2000) also performed a Probabilistic Seismic Hazard Assessment, but their study was focused on seismic hazard in Norway, England and the North Sea. Figure 6.6-5 is a contour plot showing that there is 0.0021 probability of expected PGA exceedance per year. The expected PGA values varies and are given as 400 – 800 cm/s^2 in Hordaland, Western Norway; 400 cm/s^2 in Oslo rift Zone; and 600 – 400 cm/s^2 in Nordland. These values corresponds well with the study of Wahlström and Grünthal (2001), shown in Figure 6.6-4.

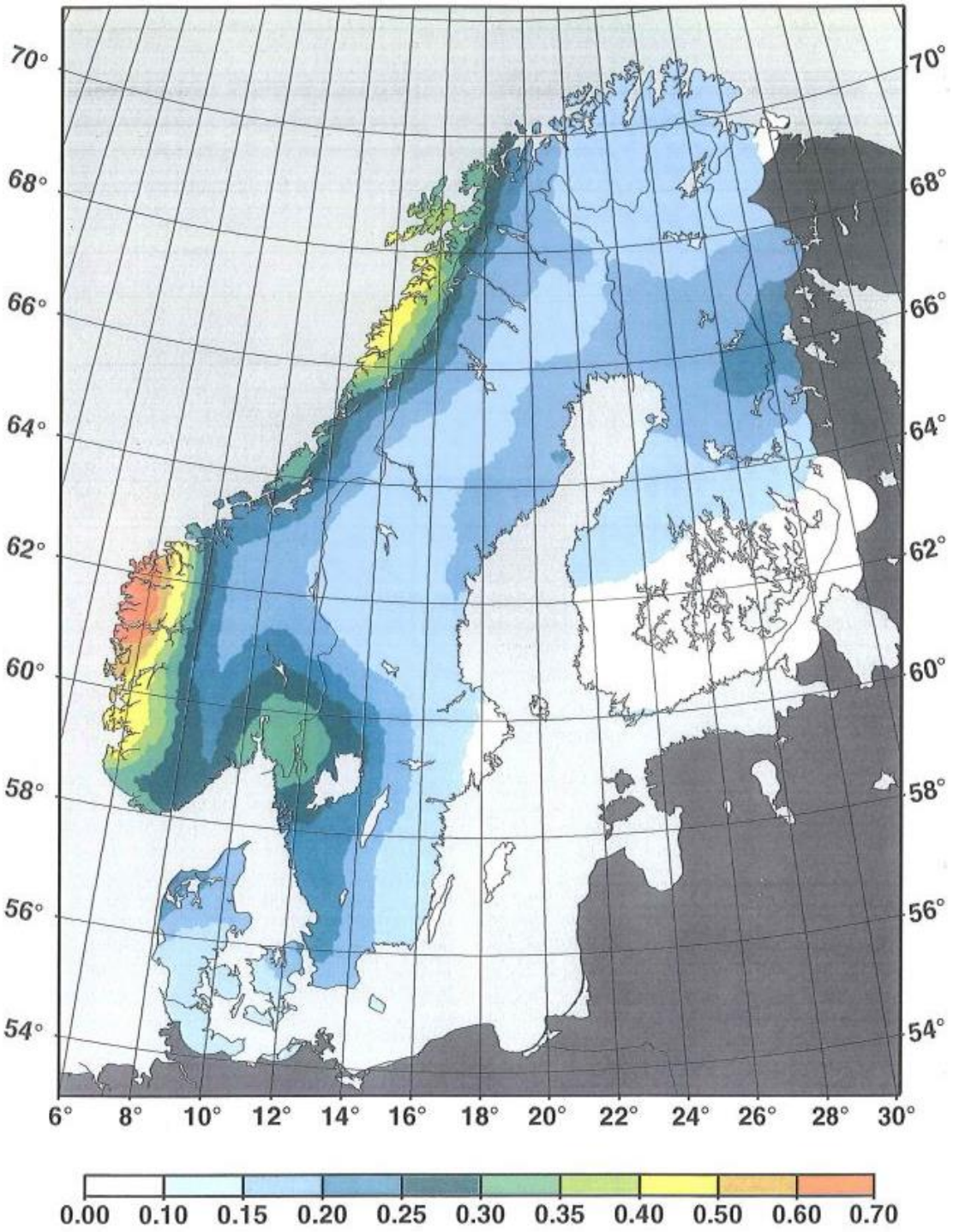

Figure 6.6-4 Hazard Map for Fennoscandia with 90 % probability of PGA not exceeding the values in the bar above (given in m/s²) in 50 years. This coincides with a mean return period of 475 years. (From (Wahlström and Grünthal, 2001)).

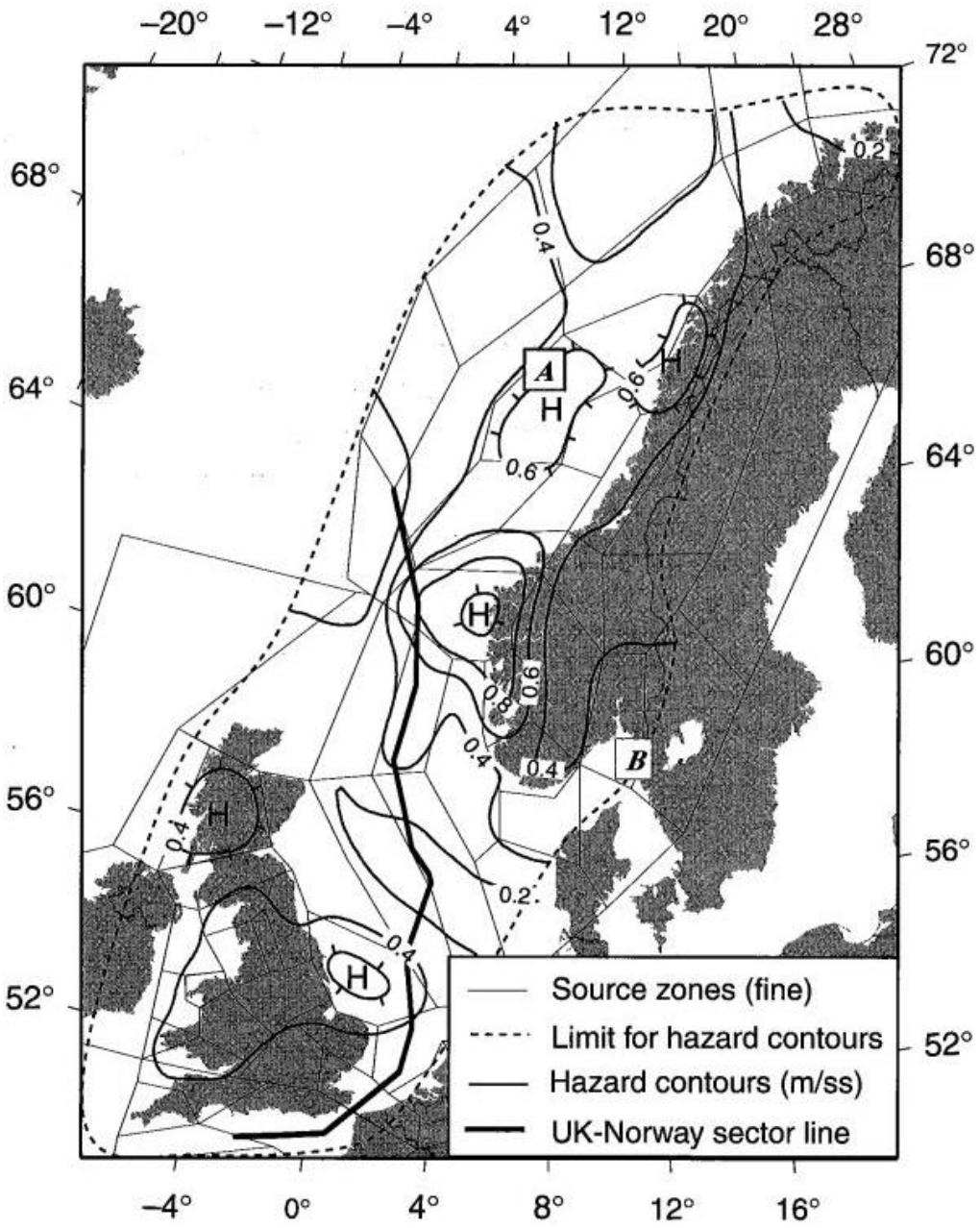

Figure 6.6-5 Contour plot of Norway and England, showing that the probability of exceeding PGA values is 0.0021 per year. This corresponds to a mean return period of 475 years. (From (Bungum et al., 2000)).

An additional hazard map is taken from the European Facility for Earthquake Hazard and Risk (EFEHR). The EFEHR has performed a Probabilistic Seismic Assessment for Europe that can be accessed on their web page (EFEHR, 2015). Figure 6.6-6 shows the hazard map for Norway: according to EFEHR there is a 10 % probability of PGA exceeding 50 – 100 cm/s^2 in 50 years in Western Norway, while the expected PGA is 0 – 50 cm/s^2 for the rest of Norway in the same time period. The mean return period is 475 years in this assessment as well.

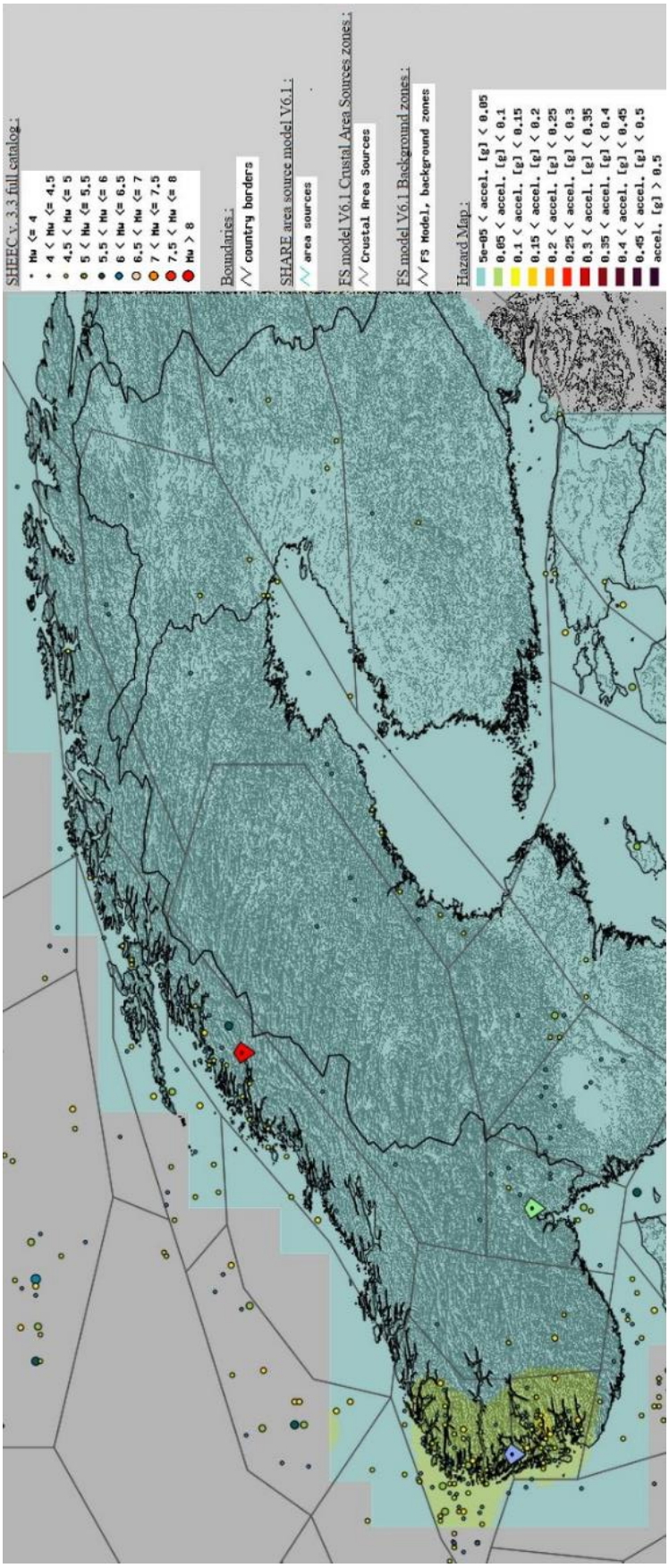

Figure 6.6-6 Hazard map from EFEHR, showing that there is 10 % probability of exceeding PGA of 50 cm/s² in 50 year, corresponding in mean return time of 475 years. (From (EFEHR, 2015)).

The expected PGA is notably lower for the assessment performed by EFEHR than for Wahlström and Grünthal (2001) and Bungum et al. (2000): 50 – 100 cm/s^2 and 600 – 800 cm/s^2 respectively. This difference may occur because the focus of the studies are different, Wahlström and Grünthal (2001) and Bungum et al. (2000) focus on Norway, while EFEHR (2015) focus on Europe as a whole. The hazard calculated using the Probabilistic Seismic Hazard Assessment are dependent on the choice of input parameters and division into zones, and different choices may have large impact on the hazard result. In addition, the results of the hazard assessment performed by Wahlström and Grünthal (2001) and Bungum et al. (2000) agrees the most with the results of my hazard study. I have found that there is potential for M_W 7.7 – M_W 7.0 earthquake scenarios on all but one of the faults in my study, and the possible PGA following these scenarios are between 206.5 cm/s^2 and 308.4 cm/s^2. These values are somewhat lower than for the other hazard assessments, but are simulated using a rupture depth of 15.0 km and stress drop of 80 bar. Decreasing the rupture depth and increasing the stress drop would lead to higher potential PGA, which could result in more corresponding values. My simulations does not have a parameter that calculates the probability of the earthquake scenarios actually occurring, they only state what the maximum potential PGA of that earthquake is. It is therefore not possible to compare the probability in the hazard assessment by Wahlström and Grünthal (2001), Bungum et al. (2000) and EFEHR (2015) to the results from my simulations. However, it is possible to compare the expected PGA values and both studies are plausible given the length of the faults in Norway, and an earthquake rupturing on a shallower depth, for instance 5.0 km, would cause higher PGA than the results in my simulations.

In addition, to the hazard maps, EFEHR (2015) has hazard curves describing the probability of exceeding given PGA values during the next 50 years. Figure 6.6-7 and Figure 6.6-8 shows the hazard curves for Oslo and Bergen respectively, and the probability of exceeding given PGA values during the next 50 years. The probability of exceeding is somewhat higher for Bergen, which agrees with the studies performed by Wahlström and Grünthal (2001) and Bungum et al. (2000).

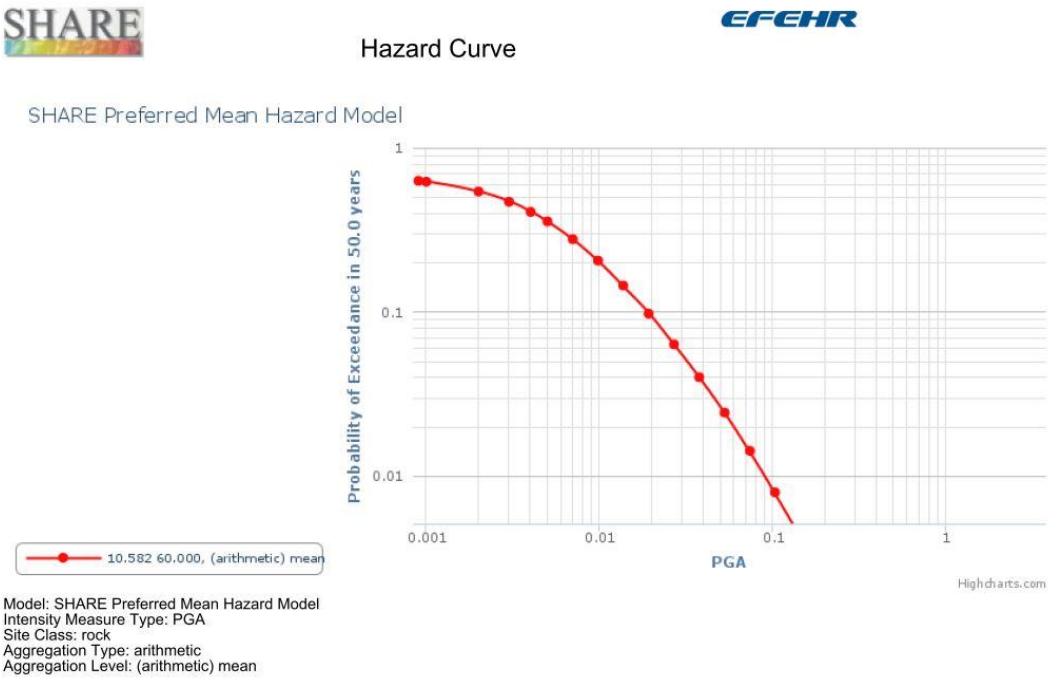

Figure 6.6-7 Hazard curve for Oslo, showing the probability of exceeding certain PGA values during the next 50 years. (From EFEHR (2015))

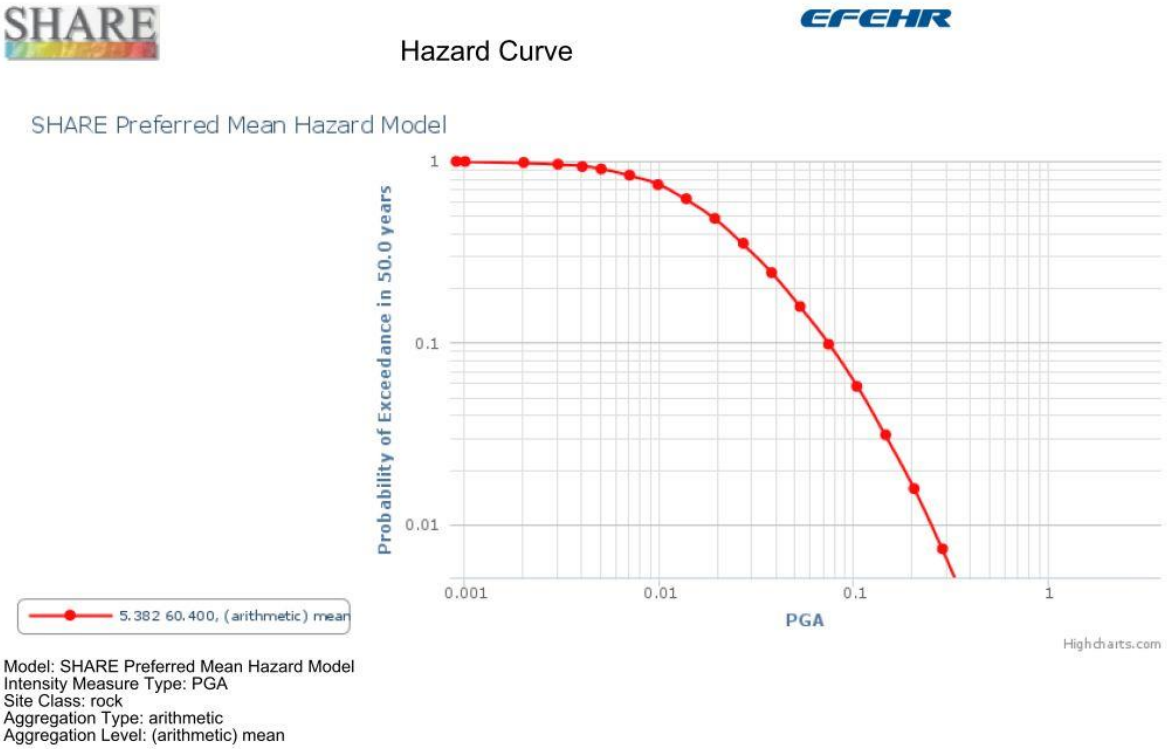

Figure 6.6-8 Hazard curve for Bergen, showing the probability of exceeding certain PGA values during the next 50 years. (From EFEHR (2015))

The seismograms, Figure 5.3.1-1 and Figure 5.3.1-2, Figure 5.3.2-1 and Figure 5.3.2-2 shown in the results are from Oslo and Bergen as well, and they represent a possible seismogram for a M_W 7.4 and a M_W 6.0 (Figure 5.2.1-1 and Figure 11.1.1-2) earthquake scenario in Oslo, and a M_W 7.2 and a M_W 6.0 (Figure 11.1.2-1 and Figure 5.2.2-2) earthquake scenario in Bergen. There are several faults close enough to cause severe shaking in both cities, for example Oslofjorden and Drammen Fault near Oslo, and Hjeltefjorden and Totland Fault near Bergen. However, these curves show that the probability of exceeding PGA of 100 cm/s^2 during the next 50 years is below 0.01 in Oslo and approximately 0.06 in Bergen. PGA of 100 cm/s^2 would approximately correspond to a M_W 6.0 earthquake on one of the faults in Norway.

7 CONCLUSION

The results of the earthquake simulations show that all of the potential magnitudes simulated in this study would affect the area around the fault by shaking that could correspond to intensities between V and VIII on the Modified Mercalli Intensity Scale. Intensity V could correspond to PGA values of 30 – 40 cm/s^2, which would be the shaking occurring outside the 50 cm/s^2 contour line in the plots. The PGA closer to the faults varies between 154.5 and 308.4 cm/s^2 for the scenarios with the highest possible magnitude for that fault length, M_W 7.0 and M_W 6.5. These PGA values may indicate shaking of intensity VII –VIII on the Modified Mercalli Intensity Scale, which include very strong to severe shaking and moderate to heavy damage. The PGA caused by the M_W 6.0 scenarios varies between 91.11 and 139.6 cm/s^2, which may indicate intensity VI - VII on the Modified Mercalli Intensity Scale, corresponding to strong to very strong shaking and light to moderate damage. This means that even the areas outside the contour lines could be exposed to moderate shaking that everyone most likely would feel and that could possibly result in light damage. The faults that I have used in the earthquake simulations are located near several larger cities; especially in Oslo Rift Zone and Hordaland, and the damage could be severe if one of the scenarios in these areas were to occur. Many towns and villages are situated in the areas around the faults, in addition are the two largest cities in Norway, Oslo and Bergen, and their surrounding vicinity, located near several of the faults.

The maximum PGA is affected by the fault length and width. This was evident in the M_W 7.5 scenarios on Vestfjorden and Mosjøen Fault, where the maximum PGA difference for the two earthquakes is 38.2 cm/s^2. Switching the fault length and width proved that it was indeed the difference of 2 km in fault length and 0.4 km in fault width that was the cause behind this. This is also evident in the faults of different type (Båsmoen and Totland Fault), which have different fault length and width than the other faults of similar magnitude, especially the M_W 6.0 scenario where both Båsmoen and Totland Fault are shorter and have significantly higher maximum PGA values compared to the normal faults. The M_W 7.5 scenarios on Oslofjorden Fault, however, did not support this theory, but the results can be considered inconclusive based on the random hypocenter location and low number of iterations in the simulations.

All of the simulations are performed using three iterations per site and random hypocenter location, and the resulting PGA is the mean value of these iterations. Because of the difference in maximum PGA for scenarios of the same magnitude, the scenarios for two identical faults, Nesna and Northern Sunnhordland Fault, were re-simulated using 20 iterations per site. The results showed that the contour lines in the plot became smoother and that the difference in maximum PGA became smaller. There was still some difference between the values, and the scenarios for these two faults were therefore re-simulated again, this time using 20 iterations and fixed hypocenter location for the rupture. The results of the simulations with fixed hypocenter location showed that the distribution of PGA became smoother, formed close to perfect circles and the maximum PGA became very similar between the earthquake scenarios on the two faults; only a couple of cm/s^2 separated them. In addition, the area affected by PGA following the earthquake with fixed hypocenter location became smaller as the rupture started in the first subfault on the fault length and first subfault on the fault width for all iterations per site, causing the PGA to propagate from the same subfault in each iteration.

The largest earthquake scenario is the M_W 7.7 scenario on Hamar Fault, which would result in maximum PGA of 308.4 cm/s^2 affecting approximately 60 300 km^2 by PGA over 50 cm/s^2. However, given the stress generating mechanisms in Norway and the fact that the largest earthquake in Norway is the M_S 5.8 event on Lurøy in Nordland in 1819, the probability of this event actually occurring is extremely low. The probability of occurrence increases as the magnitude of the event decreases. The lowest magnitude in my simulations are the M_W 6.0 scenarios. The M_W 6.0 earthquake scenarios result in PGA between 91.11 and 129.4 cm/s^2 for the normal faults. The maximum PGA is slightly higher for Båsmoen and Totland Fault because they are a reverse fault and a strike-slip fault respectively. The difference in PGA in scenarios of similar magnitude may be caused by the length and width of the fault or coincidences caused by the random hypocenter location and low number of iterations.

Compared to other methods for calculating earthquake hazard, the stochastic method is well suitable for estimating the potential ground motion, in this case PGA, which could follow a given scenario on a fault. However, as opposed to the probabilistic seismic hazard assessment, the stochastic method does not include the probability of one of these scenarios actually occurring. The simulations show possible scenarios after an

earthquake of M_W 7.7 – M_W 6.0 has ruptured in Norway, but does not take into account the fact that such events rarely occur and that there are very few large (M_W 5.5 or larger) events in Norway. It is therefore important to remember that the earthquake scenarios presented here only show the fault's potential without concern for the actual probability.

8 RECOMMENDATIONS FOR FUTURE STUDIES

Recommendations for future studies of the seismic hazard in Norway could be to perform earthquake simulations on more of the faults that are located in Norway, preferably faults that are nearby other cities, for example near Trondheim, Stavanger and Kristiansand. My study focused on the highest magnitude possible for the given fault lengths, in addition to M_W 7.0, M_W 6.5 and M_W 6.0. Future studies could focus on smaller magnitudes that will have higher probability of occurrence, for instance M_W 4.5, M_W 5.0 and M_W 5.5, as the probability of occurrence increases with decreasing magnitude. In addition, a future study could focus on the faults located offshore Norway and simulate the potential earthquake hazard they pose to mainland Norway or the various offshore production sites.

I would also recommend that future studies focus more on the effects caused by input parameters in EXSIM, especially the difference caused by number of iterations and random versus fixed hypocenter location. In addition, the stochastic finite-fault modeling could be improved by more knowledge of the crust and faults in Norway, for instance the input-parameters describing the stress drop, near-surface attenuation models and quality-factor, instead of basing this information on values from Eastern North America.

9 REFERENCES

ANDERSEN, T. B. & JANSEN, Ø. J. 1987. The Sunnhordland Batholith, W. Norway: regional setting and internal structure, with emphasis on the granitoid plutons. *Norsk geologisk tidsskrift,* 67**,** 159-183.

ATAKAN, K., LINDHOLM, C. D. & HAVSKOV, J. 1994. Earthquake swarm in Steigen, northern Norway: an unusual example of intraplate seismicity. *Terra Nova,* 6**,** 180-194.

ATKINSON, G. M., ASSATOURIANS, K., BOORE, D. M., CAMPBELL, K. & MOTAZEDIAN, D. 2009. A guide to differences between stochastic point-source and stochastic finite-fault simulations. *Bulletin of the Seismological Society of America,* 99**,** 3192-3201.

BERESNEV, I. A. & ATKINSON, G. M. 1997. Modeling finite-fault radiation from the ωn spectrum. *Bulletin of the Seismological Society of America,* 87**,** 67-84.

BERESNEV, I. A. & ATKINSON, G. M. 1998. FINSIM--a FORTRAN program for simulating stochastic acceleration time histories from finite faults. *Seismological Research Letters,* 69**,** 27-32.

BOLT, B. A. 1999. *Earthquakes,* San Fransisco.

BOORE, D. M. 1983. Stochastic simulation of high-frequency ground motions based on seismological models of the radiated spectra. *Bulletin of the Seismological Society of America,* 73**,** 1865-1894.

BOORE, D. M. 2003. Simulation of Ground Motion Using the Stochastic Method. *Pure and Applied Geophysics,* 160**,** 635-676.

BOORE, D. M. 2009. Comparing stochastic point-source and finite-source ground-motion simulations: SMSIM and EXSIM. *Bulletin of the Seismological Society of America,* 99**,** 3202-3216.

BUNGUM, H., HOKLAND, B., HUSEBYE, E. S. & RINGDAL, F. 1979. An exceptional intraplate earthquake sequence in Meløy, Northern Norway. *Nature,* 280**,** 32-35.

BUNGUM, H. & HUSEBYE, E. S. 1979. The Meleoy, northern Norway, earthquake sequence; a unique intraplate phenomenon. *Norsk geologisk tidsskrift,* 59**,** 189-193.

BUNGUM, H., LINDHOLM, C. & FALEIDE, J. 2005. Postglacial seismicity offshore mid-Norway with emphasis on spatio-temporal–magnitudal variations. *Marine and Petroleum Geology,* 22**,** 137-148.

BUNGUM, H. & OLESEN, O. 2005. The 31st of August 1819 Lurøy earthquake revisited. *Norwegian Journal of Geology,* 85**,** 245-252.

BUNGUM, H., OLESEN, O., PASCAL, C., GIBBONS, S., LINDHOLM, C. & VESTØL, O. 2010. To what extent is the present seismicity of Norway driven by post-glacial rebound? *Journal of the Geological Society,* 167**,** 373-384.

BUNGUM, H., PETTENATI, F., SCHWEITZER, J., SIROVICH, L. & FALEIDE, J. I. 2009. The 23 October 1904 MS 5.4 Oslofjord earthquake: Reanalysis based on macroseismic and instrumental data. *Bulletin of the Seismological Society of America,* 99**,** 2836-2854.

BUNGUM, H. H., LINDHOLM, C. D., DAHLE, A., WOO, G., NADIM, F., HOLME, J. K., GUDMESTAD, O. T., HAGBERG, T. & KARTHIGEYAN, K. 2000. New seismic zoning maps for Norway, the North Sea, and the United Kingdom. *Seismological research letters,* 71**,** 687-697.

CORTI, G. G. 2009. Continental rift evolution: From rift initiation to incipient break-up in the Main Ethiopian Rift, East Africa. *Earth-science reviews,* 96**,** 1-53.

DEPARTMENT OF EARTH SCIENCE, U. O. B. 2015. *Norwegian National Seismic Network* [Online]. Norway. Available: http://nnsn.geo.uib.no/link_2_02.shtml [Accessed 15.05 2015].

EBRAHIMIAN, B. 2013. *Simulation of Near-Field Strong GRound Motions Using Hybrid Method, Engineering Seismilogy, Geotechnical and Structural Earthquake Engineering*, InTech.

EFEHR. 2015. *European Facility for Earthquake Hazard and Risk* [Online]. Swiss Seismological Service, Zurich, Switzerland: EFEHR. Available: www.efehr.org [Accessed 22.05 2015].

FEJERSKOV, M. & LINDHOLM, C. 2000. Crustal stress in and around Norway: an evaluation of stress-generating mechanisms. *Geological Society, London, Special Publications,* 167**,** 451-467.

FJELDSKAAR, W., LINDHOLM, C., DEHLS, J. F. & FJELDSKAAR, I. 2000. Postglacial uplift, neotectonics and seismicity in Fennoscandia. *Quaternary Science Reviews,* 19**,** 1413-1422.

FOSSEN, H. 1998. Advances tn understanding the post-Caledonian structural evolution of the Bergen area, West Norway.

FOSSEN, H. 2000. Extensional tectonics in the Caledonides: Synorogenic or postorogenic? *Tectonics,* 19**,** 213-224.

FOSSEN, H. & HURICH, C. A. 2005. The Hardangerfjord Shear Zone in SW Norway and the North Sea: a large-scale low-angle shear zone in the Caledonian crust. *Journal of the Geological Society,* 162**,** 675-687.

HICKS, E. C., BUNGUM, H. & LINDHOLM, C. D. 2000. Seismic activity, inferred crustal stresses and seismotectonics in the Rana region, Northern Norway. *Quaternary Science Reviews,* 19**,** 1423-1436.

KARPUZ, M. R., GABRIELSEN, R. H., ENGELL-SØRENSEN, L. & ANUNDSEN, K. 1991. Seismotectonic significance of the 29 January 1989 Etne earthquake, SW Norway. *Terra Nova,* 3**,** 540-549.

LORENZ, H. H., LORENZA, D. D. & GEE, C. C. 2011. The Scandinavian Caledonides—Scientific Drilling at Mid-Crustal Level in a Palaeozoic Major Collisional Orogen. *Scientific drilling,* 11**,** 60-63.

MOTAZEDIAN, D. & ATKINSON, G. M. 2005. Stochastic finite-fault modeling based on a dynamic corner frequency. *Bulletin of the Seismological Society of America,* 95**,** 995-1010.

NEUMANN, E.-R., OLSEN, K., BALDRIDGE, W. & SUNDVOLL, B. 1992. The Oslo rift: A review. *Tectonophysics,* 208**,** 1-18.

OLESEN, O., BUNGUM, H., DEHLS, J., LINDHOLM, C., PASCAL, C. & ROBERTS, D. 2010. Neotectonics, seismicity and contemporary stress field in Norway–mechanisms and implications. *Roberts, D., Nordgulen, Ø. & Olsen, L.(eds.)*.

OLESEN, O., DEHLS, J., BUNGUM, H., RIIS, F., HICKS, E., LINDHOLM, C., BLIKRA, L. H., FJELDSKAAR, W., OLSEN, L. & LONGVA, O. 2000. Neotectonics in Norway, final report. *Geological Survey of Norway, Report*.

OLESEN, O., GJELLE, S., HENKEL, H., KARLSEN, T.A., OLSEN, L AND SKOGSETH, T. 1994. Neotectonic studies in the Ranafjorden area, northern Norway. *NGU Report 94.073.*

OLESEN, O., LUNDIN, E., NORDGULEN, Ø., OSMUNDSEN, P. T., SKILBREI, J. R., SMETHURST, M. A., SOLLI, A., BUGGE, T. & FICHLER, C. 2002. Bridging the gap between the onshore and offshore geology in Nordland, northern Norway. *Norsk geologisk tidsskrift,* 82**,** 243-262.

OROZOVA, I. M. & SUHADOLC, P. 1999. A deterministic-probabilistic approach for seismic hazard assessment. *Tectonophysics,* 312**,** 191 - 202.
PIRLI, M., SCHWEITZER, J., OTTERMÖLLER, L., RAEESI, M., MJELDE, R., ATAKAN, K., GUTERCH, A., GIBBONS, S. J., PAULSEN, B., DEBSKI, W., WIEJACZ, P. & KVÆRNA, T. 2010. Preliminary Analysis of the 21 February 2008 Svalbard (Norway) Seismic Sequenca. *Seismological Research Letters,* 81.
RAMBERG, I. B., BRYHNI, I., FORENING, N. G. & NØTTVEDT, A. 2013. *Landet blir til: Norges geologi*, Norsk geologisk forening.
REITER, L. 1991. *Earthquake Hazard Analysis: Issues and Insights,* New York, Columbia University Press.
RO, H. & FALEIDE, J. 1992. A stretching model for the Oslo Rift. *Tectonophysics,* 208**,** 19-36.
ROBERTS, D. 2003. The Scandinavian Caledonides: event chronology, palaeogeographic settings and likely modern analogues. *Tectonophysics,* 365**,** 283-299.
STEIN, S. & WYSESSION, M. 2012. *An introduction to seismology, earthquakes, and earth structures,* United Kingdom, Blackwell Publishing.
SUNDVOLL, B., NEUMANN, E.-R., LARSEN, B. & TUEN, E. 1990. Age relations among Oslo Rift magmatic rocks: implications for tectonic and magmatic modelling. *Tectonophysics,* 178**,** 67-87.
TVEIT, R. K. 2013. *Implications of a M=6.0 earthquake along the Øygarden Fault Zone for the city Bergen: Ground motion simulations and estimation of local site effects.* Master of Science, University of Bergen.
WAHLSTRÖM, R. R. & GRÜNTHAL, G. 2001. Probabilistic seismic hazard assessment (Horizontal PGA) for Fennoscandia using the logic tree approach for regionalization and nonregionalization models. *Seismological research letters,* 72**,** 33-45.
WELLS, D. L. & COPPERSMITH, K. J. 1994. New empirical relationships among magnitude, rupture length, rupture width, rupture area, and surface displacement. *Bulletin of the Seismological Society of America,* 84**,** 974-1002.
WESSEL, P., SMITH, W. H. F., SCHARROO, R., LUIS, J. & WOBBE, F. 2013. Generic Mapping Tools: Improved Version Released. *Earth & Space Science News,* 94**,** 409 - 410.

10 APPENDIX A

Below is an example of a file used to run EXSIM12. This example is from the M_W 7.1 earthquake scenario on Sunnhordland Fault.

```
!Input file for program EXSIM12
!Title
  EXSIM12 input for M7.1 80bars: 2 sites at Rjb 10, 50km
!Write acc, psa, husid files for each site?
 Y
!MW, Stress, flag (0=fmax; 1=kappa), fmax or kappa
  7.1 80.0  1  0.02
!lat and lon of upper edge of fault
  59.563333 5.179444
!strike,dip, depth of fault
  330.0 60 10.0
!fault type (S=strikeslip; R=reverse; N=normal;
U=undifferentiated)
! (Only used if Wells and Coppersmith is used to obtain FL and
FW).
  N
!fault length and width, dl, dw, stress_ref
!Note: Force program to use Wells and Coppersmith (WC) for FL
and/or FW if
! either entry = 0.0.
! dl and dw are the subsource length and width
! stress_ref is a reference to allow scaling of WC size as per
Atkinson&Boore(2006BSSA)
! If Wells and Coppersmith are used to obtain FL and/or FW,
the WC values are
! modified to account for the scaling implied by differences
in the stress
! specified above and a stress that is assumed to be valid for
the generic WC
! relations; this stress is stress_ref. The value of 70 bars
is an educated
! guess for stress_ref, but it is not based on a quantitative
analysis.
! The WC values of FL and/or FW are multiplied by the factor
! (stress_ref/stress)^(1/3).
! Note that four entries on the following line are needed as
placeholders,
! even if not used)
  50.0 18.0 5.0 5.0 70.0 !fault length and width, dl, dw,
stress_ref
!vrup/beta
  0.8
!hypo location in along fault and down dip distance from the
fault
```

```
!reference point (an upper corner)(-1.0, -1.0 for a random
location);
!number of iterations over hypocenter (need an entry, but only
used if
!either of the first two values are -1.0, indicating a random
location)
  -1.0 -1.0  1
!Enter type of risetime (1=original, 2=1/f0)
 1
!tpadl, tpadt, delta t (length of 0pads at front and back of
time series, timestep)
 50.0 20.0 0.002
!beta , rho
  3.7 2.8
!Geometric spreading: this example is for bilinear with
transition at 40km
! r_ref, nseg (hinged line segments), (rlow(i), slope)
! (Usually set r_ref = 1.0 km)
    1.0
    3
      1.0 -1.3
     70.0 0.2
    140.0 -0.5
!Quality factor: Qmin, Q0, and eta, Q=max(Qmin, Q0*F**eta)
   1000  893  0.32
!path duration: example has duration increasing as 0.05R
!(ndur_hinges,(rdur(i), dur(i), i = 1, ndur_hinges), durslope)
    3
    1.0 0.16
   70.0 -0.03
  130.0 0.04
  0.05
!Type of window: 1 for Saragoni-Hart taper windows, 0 for
tapered boxcar
!window, epsilon, and eta values of Saragoni-Hart window
  1    0.2    0.2
!low-cut filter corner (Hz), nslope (0 ==> no filter)
 0.05 8
! %damping of response spectra
 5.0
!# of f and Min and Max F for response spectra
  100 0.1   50.
!no. of frequencies for summary output (10 max):
 4
!frequency (-1.0, 99.0 for pgv, pga):
 -1.0 99.0 0.5 5.0
!Output file names stem:
  Sunnhordland_M71_GRID01_3
!Name of crustal amplification file:
  crustal_amps.txt
!Name of site amplification file:
```

```
  site_amps.txt
!Name of empirical filter file:
  empirical_amps.txt
!DynamicFlag (0=no; use 1 for dynamic corner freq),
PulsingPercent (typical 50.)
  1   50.0
!iflagscalefactor (1=vel^2; 2=acc^2; 3=asymptotic acc^2 (dmb);
typical=2)
  2
!iflagfas_avg (1=arithmetic; 2=geometric, 3=rms: USE 3!)
  3
!iflagpsa_avg (1=arithmetic; 2=geometric: USE 2!, 3=rms)
  2
!deterministic flag,gama,nu,t0, impulse peak (see Motazedian
and Atkinson, 2005)
  0  2.0  1.571  4.0  100.
!iseed, # of trials
  309  3
!islipweight = -1  -> unity slip for all subfaults,
!islipweight =  0  -> specify slips read from text file,
!islipweight =  1  -> random weights
   1
! Text file containing matrix of slip weights (need a
placeholder
! even if do not assign the slip weights
  slip_weights.txt
!Number of Sites, site coord flag (1=lat,long; 2=R,Az; 3=N,E)
  288  1
!If "Y" below and strike = 0.0:
!  if site coord flag = 2, move origin of the radial line to
the midpoint of
!                          the top edge of the fault
!  if site coord flag = 3 and siteLocation(1) = 0, redefine
!                          siteLocation(1) = 0 to be the
midpoint of the
!                          top edge of the fault (so that the
sites will be
!                          along a line normal to the midpoint)
!  if site coord flag = 3 and siteLocation(2) = 0, redefine
!                          siteLocation(1) = 0 to be the far
end of the fault,
!                          so that the sites are along a line
along the
!                          strike of the fault
 N
!Coordinates of each site
```

11 APPENDIX B

11.1 GROUND MOTION SIMULATIONS – RESULTS

Here are the earthquake scenarios that were not included in the Results-chapter presented.

11.1.1 Oslo Rift Zone, Eastern Norway

11.1.1.1 Oslofjorden Fault M_W 7.0

Figure 11.1.1-1 shows the PGA distribution that would follow a M_W 7.0 earthquake on Oslofjorden Fault. The maximum PGA is estimated to be 235.4 cm/s² for this event. The area affected by ground acceleration 50 – 235.4 cm/s² is approximately 9600 km², and located within this area are Hønefoss and Lillestrøm. Drammen, Oslo, Moss and Horten are situated within the 100 cm/s², where the PGA would cause shaking that could correspond to intensity VII – VIII on the Modified Mercalli Intensity Scale, Table 5.2-1.

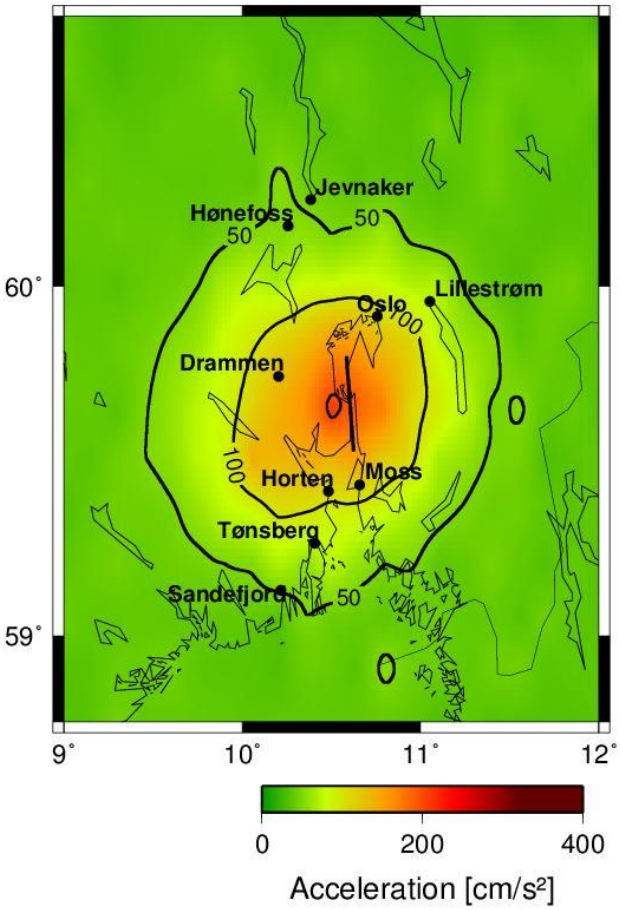

Figure 11.1.1-1 Distribution of PGA for a M_W 7.0 earthquake scenario on Oslofjorden Fault.

11.1.1.2 Oslofjorden Fault M_W 6.0

Figure 11.1.1-2 shows the PGA that would occur if Oslofjorden Fault ruptures in a M_W 6.0 earthquake. The maximum PGA for this scenario is estimated to be 106.3 cm/s^2, and the area exposed to ground acceleration between 50 and 106.3 cm/s^2 is approximately 2000 km^2 with the city of Oslo located outside the 50 cm/s^2 contour line. The head of Oslofjorden, along with Drammen, Horten and Moss would be subjected to shaking that could correspond to intensity VI – VII on the Modified Mercalli Intensity Scale, Table 5.2-1, if this earthquake was to occur.

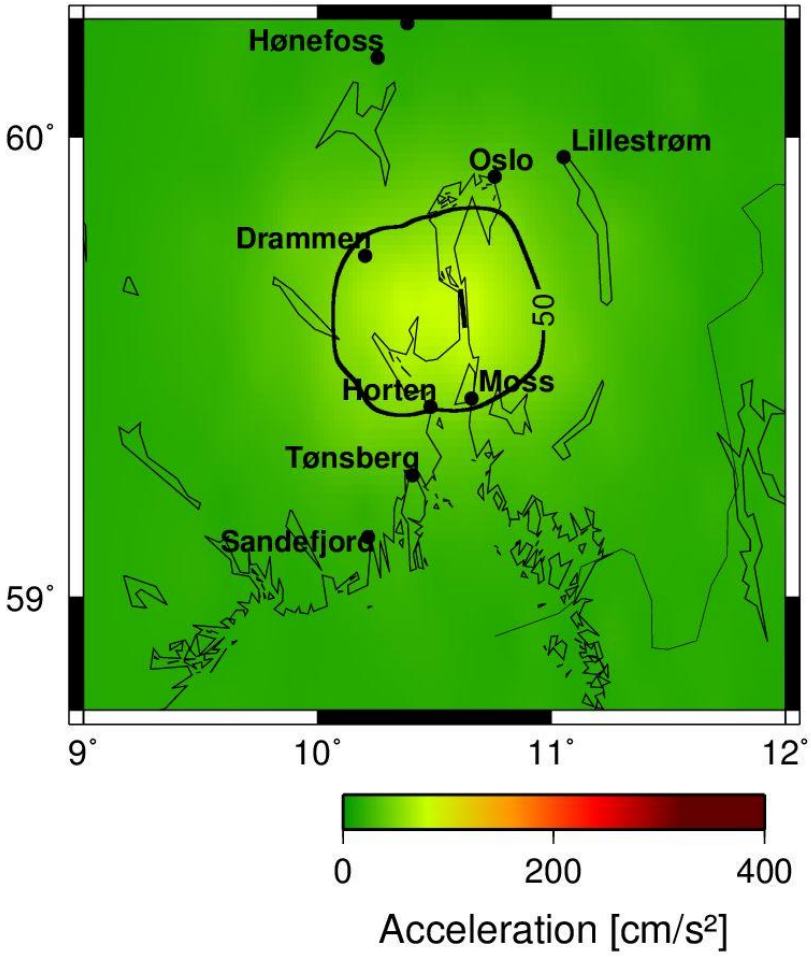

Figure 11.1.1-2 Distribution of PGA for a M_W 6.0 earthquake scenario on Oslofjorden Fault.

11.1.1.3 Drammen Fault M_W 6.5

Figure 11.1.1-3 shows the PGA that would occur if Drammen Fault ruptures in a M_W 6.5 earthquake. PGA between 50 and 164.6 cm/s^2 would affect approximately 5600 km^2, which may indicate shaking of intensity VI –VII on the Modified Mercalli Intensity Scale, Table 5.2-1. Jevnaker and Hønefoss are located within the 50 cm/s^2 contour line, while Drammen is located within the area where the PGA would exceed 100 cm/s^2.

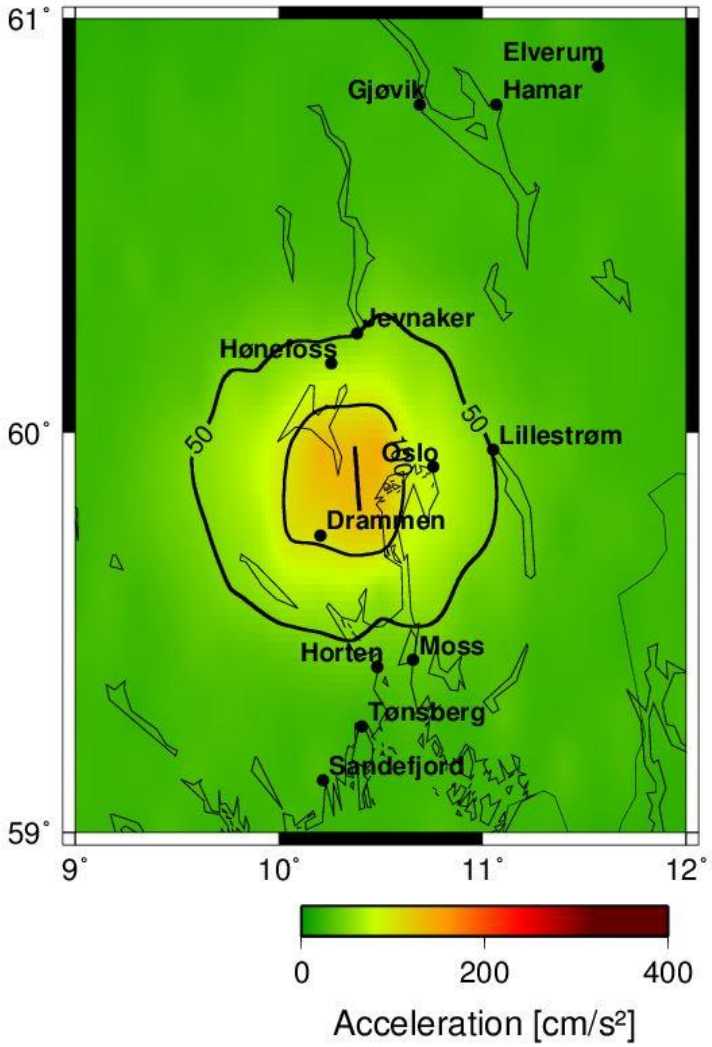

Figure 11.1.1-3 Distribution of PGA for a M_W 6.5 earthquake scenario on Drammen Fault.

11.1.1.4 Drammen Fault M_W 6.0

The maximum PGA for a M_W 6.0 earthquake on Drammen Fault is estimated to be 91.44 cm/s^2. Approximately 2000 km^2 are exposed to PGA between 50 and 91.44 cm/s^2. Figure 11.1.1-4 shows the distribution of the PGA following the earthquake. The cities that are located within the 2000 km^2, Oslo and Drammen, and the cities that are located just outside the 50 cm/s^2 contour line, Hønefoss and Jevnaker, would be exposed to ground shaking that could correspond to intensity VI – VII on the Modified Mercalli Intensity Scale, Table 5.2-1.

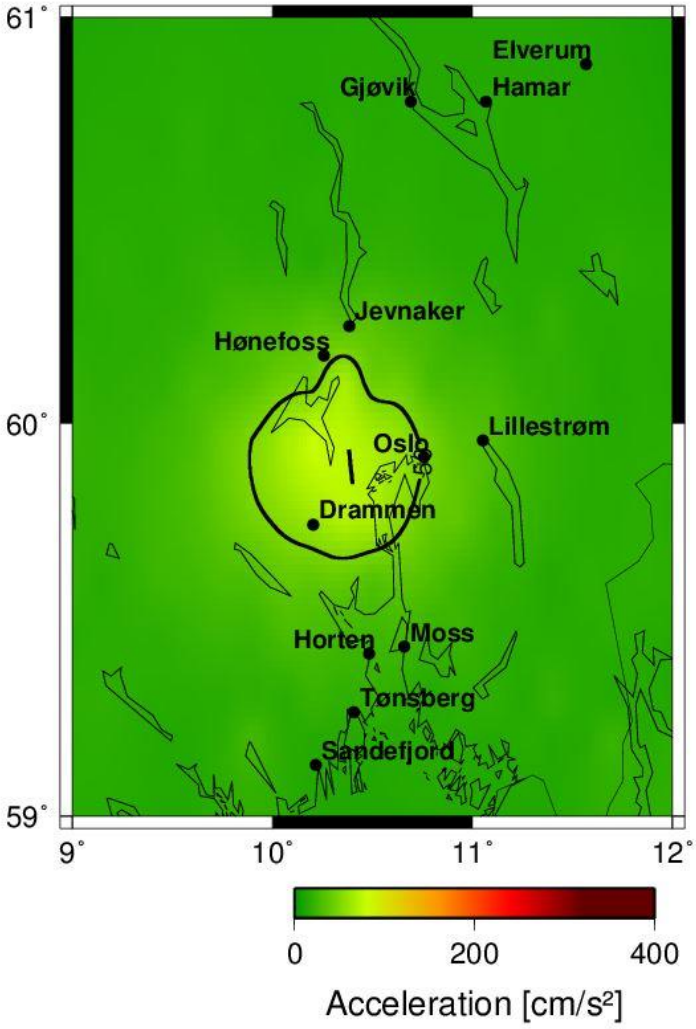

Figure 11.1.1-4 Distribution of PGA for a M_W 6.0 earthquake scenario on Drammen Fault.

11.1.2 Hordaland, Western Norway

11.1.2.1 Hjeltefjorden Fault M_W = 7.2

Figure 11.1.2-1 shows the PGA that would follow a M_W 7.2 earthquake on Hjeltefjorden Fault. The maximum PGA is estimated to be 267.0 cm/s² for this scenario. The area affected by PGA between 50 and 267.0 cm/s² is approximately 16 700 km². Bergen is located just within the 100 cm/s² contour line. The area that would be affected by PGA between 100 and 267.0 cm/s² is approximately 5400 km², and it is located at the coast near Bergen. These areas would be exposed to shaking that could correspond to intensity VII on the Modified Mercalli Intensity Scale, Table 5.2-1.

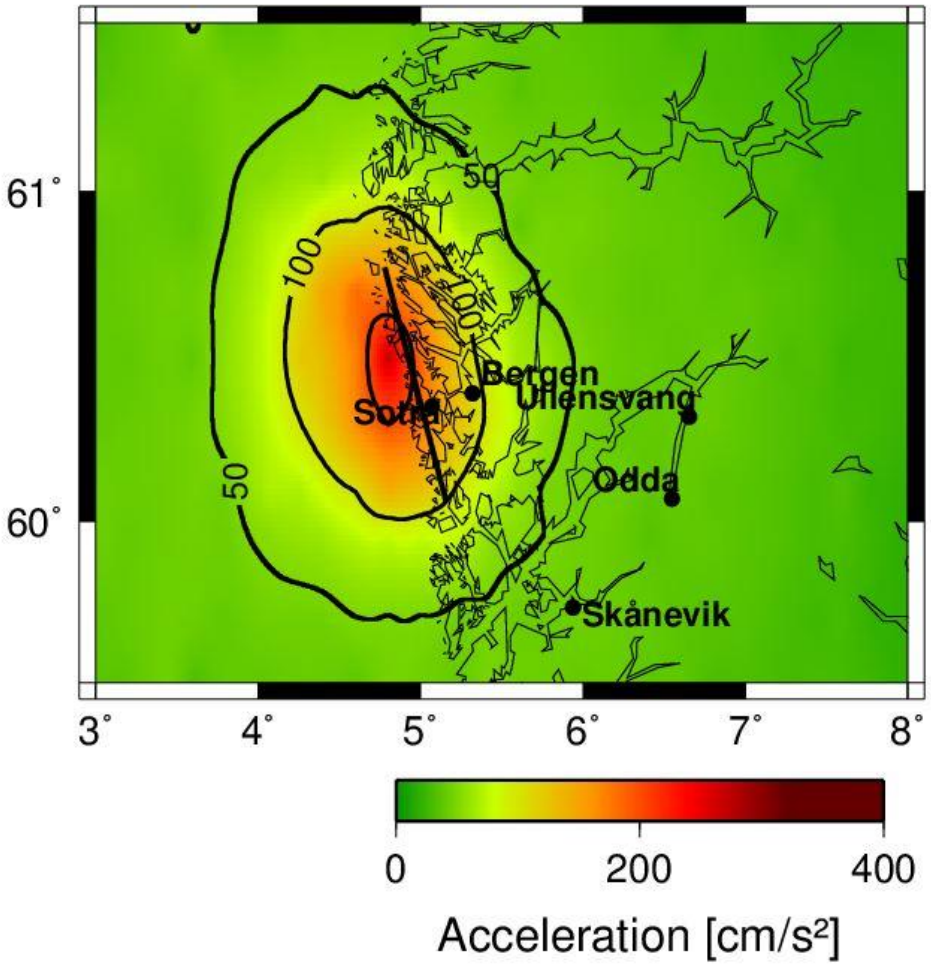

Figure 11.1.2-1 Distribution of PGA for a M_W 7.2 earthquake scenario on Hjeltefjorden Fault.

11.1.2.2 Rustefjorden Fault M_W = 6.5

Figure 11.1.2-2 shows the PGA distribution following a M_W 6.5 earthquake on Rustefjorden Fault. The maximum PGA in this scenario is estimated to be 188.9 cm/s^2. PGA between 50 and 188.9 cm/s^2 would approximately affect 5600 km^2. This may indicate shaking of intensity VI – VII on the Modified Mercalli Intensity Scale, Table 5.2-1. Bergen is located outside the 100 cm/s^2 contour line and Sotra within this line and would be exposed to somewhat higher PGA values than Bergen.

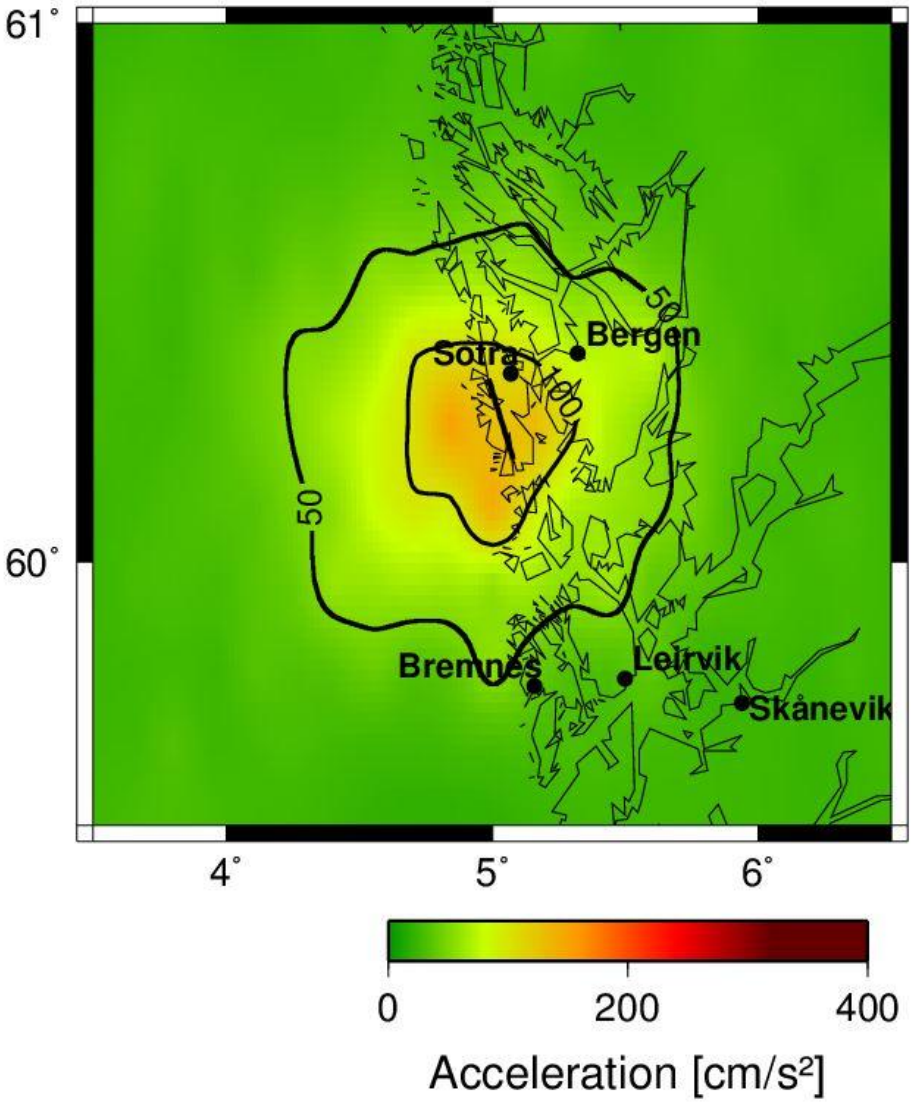

Figure 11.1.2-2 Distribution of PGA for a M_W 6.5 earthquake scenario on Rustefjorden Fault.

11.1.2.3 Rustefjorden Fault M_W = 6.0

Figure 11.1.2-3 shows the distribution of the PGA that would occur if Rustefjorden Fault ruptures in a M_W 6.0 earthquake. The maximum PGA for this scenario is estimated to be 96.12 cm/s^2. The area affected by PGA between 50 and 96.12 cm/s^2 is approximately 2000 km^2 and it includes Bergen and populated areas. These areas would experience ground shaking that could correspond to intensity VI – VII on the Modified Mercalli Intensity Scale, Table 5.2-1.

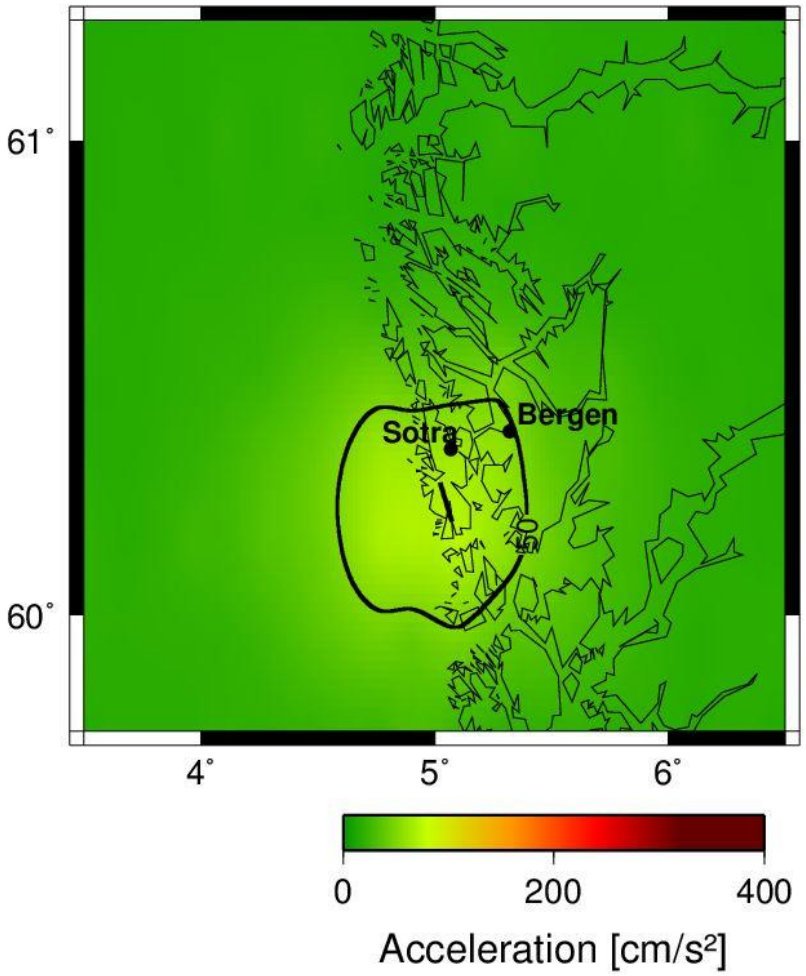

Figure 11.1.2-3 Distribution of PGA for a M_W 6.0 earthquake scenario on Rustefjorden Fault.

11.1.2.4 Totland Fault M_W = 6.0

Figure 11.1.2-4 shows the PGA that would occur if Totland Fault ruptures in a M_W 6.0 earthquake. The estimated maximum PGA is 132.0 cm/s^2. The area affected by PGA between 50 and 132.0 cm/s^2 is approximately 2000 km^2. This area would thus be exposed to ground shaking that could correspond to of intensity VI – VII on the Modified Mercalli Intensity Scale, Table 5.2-1. Bergen and surrounding vicinity are located within this affected area. Totland Fault is the only strike slip fault in the ground motion simulations.

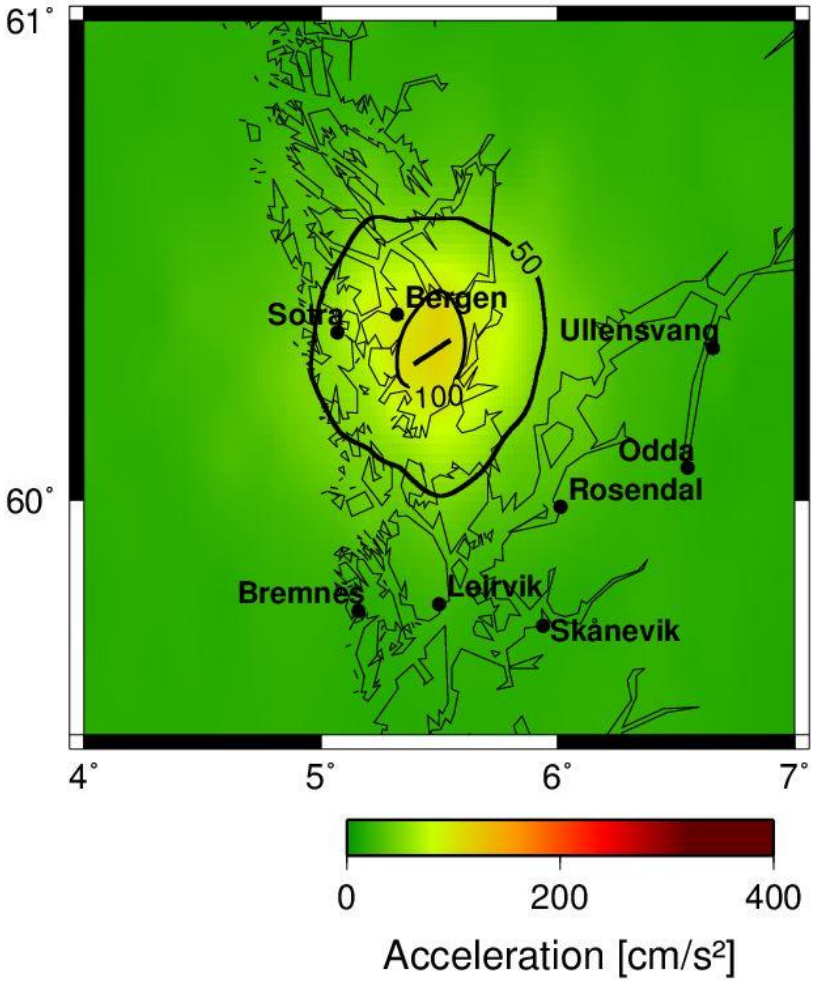

Figure 11.1.2-4 Distribution of PGA for a M_W 6.0 earthquake scenario on Totland Fault.

11.1.2.5 Northern Sunnhordland M_W 7.2

Figure 11.1.2-5 shows the PGA that would follow a M_W 7.2 earthquake on Northern Sunnhordland Fault. The estimated maximum PGA is 267.0 cm/s² for this scenario. Approximately 16 500 km² would be exposed to PGA between 50 and 267.0 cm/s², and the area exposed to PGA between 100 and 267.0 cm/s² is approximately 4300 km². Bergen and Haugesund are located within the 50 cm/s² contour line, and would be prone to shaking that could correspond to intensity VI, while Leirvik and Bremnes are situated within the 100 cm/s² and could be exposed to shaking that may indicate intensity VIII (Modified Mercalli Intensity Scale, Table 5.2-1).

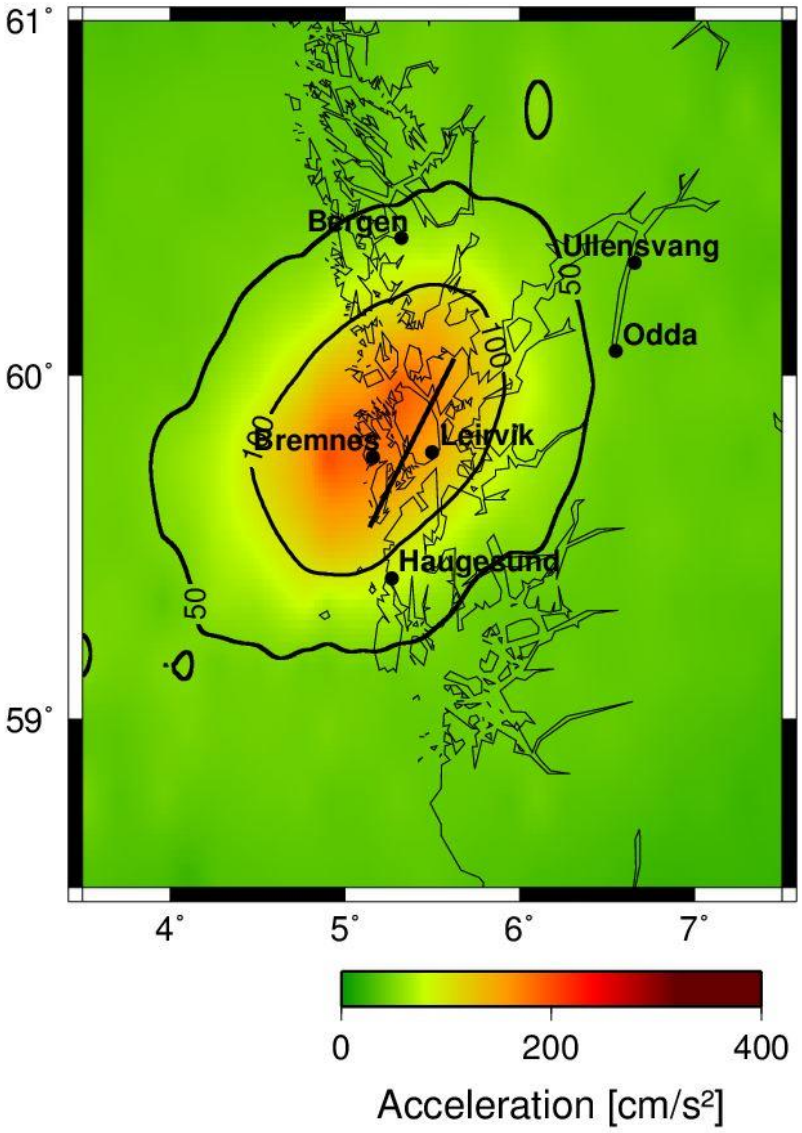

Figure 11.1.2-5 Distribution of PGA for a M_W 7.2 earthquake scenario on Northern Sunnhordland Fault.

11.1.2.6 Northern Sunnhordland M_W 6.5

Figure 11.1.2-6 shows the distribution of the PGA that would occur if Northern Sunnhordland Fault ruptures in a M_W 6.5 earthquake. The maximum PGA is estimated to be 180.0 cm/s^2 for this scenario. Approximately 6100 km^2 would be affected by PGA acceleration between 50 and 180.0 cm/s^2 if this scenario were to happen. Leirvik and Bremnes would be exposed to shaking that could correspond to intensity VI – VII on the Modified Mercalli Intensity Scale, Table 5.2-1.

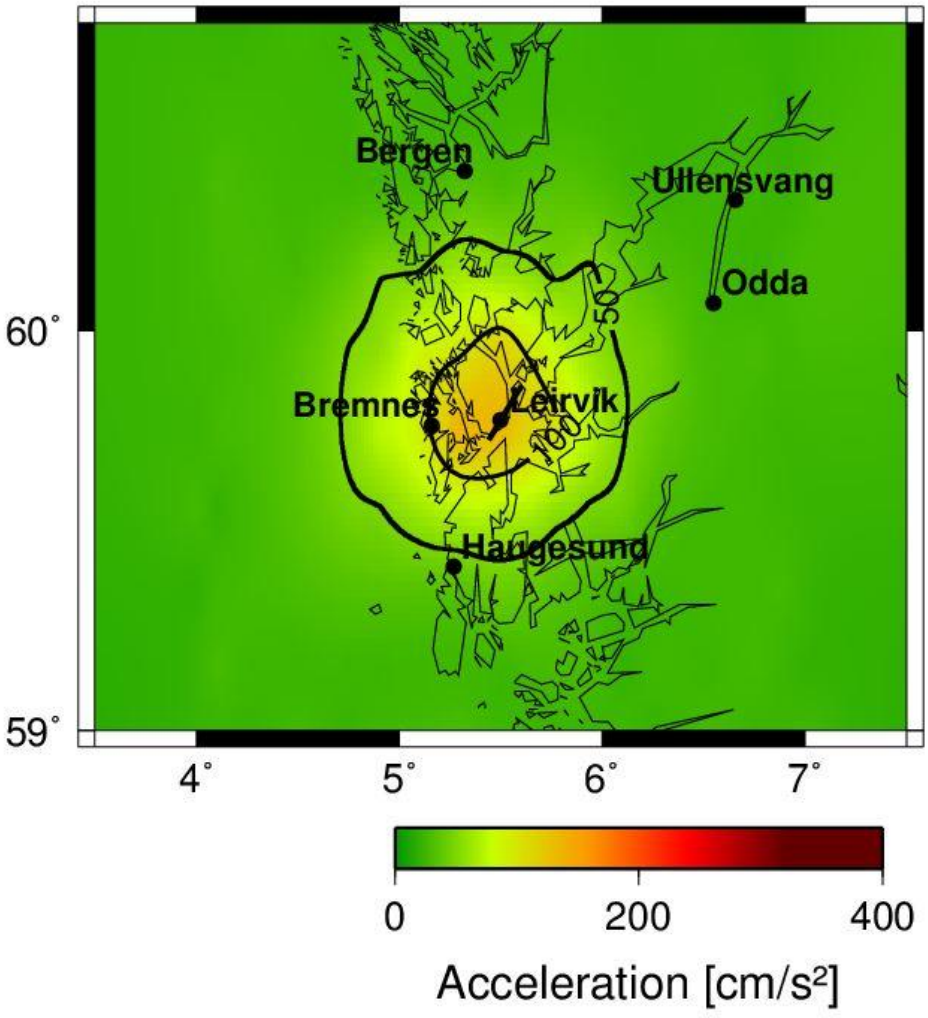

Figure 11.1.2-6 Distribution of PGA for a M_W 6.5 earthquake scenario on Northern Sunnhordland Fault.

11.1.2.7 Sauda Fault M_W = 6.5

The maximum PGA is estimated to be 177.7 cm/s² for a M_W 6.5 earthquake on Sauda Fault. The area affected by PGA between 50 and 177.7 cm/s² is approximately 5300 km², and it would be exposed to shaking that could correspond to intensity VI – VII on the Modified Mercalli Intensity Scale, Table 5.2-1. The cities of Odda and Sauda is situated within the 50 cm/s² contour line, while places like Ullensvang, Rosendal and Leirvik are located outside this line and would experience PGA below 50 cm/s². Figure 11.1.2-7 shows the distribution of the ground acceleration following the earthquake.

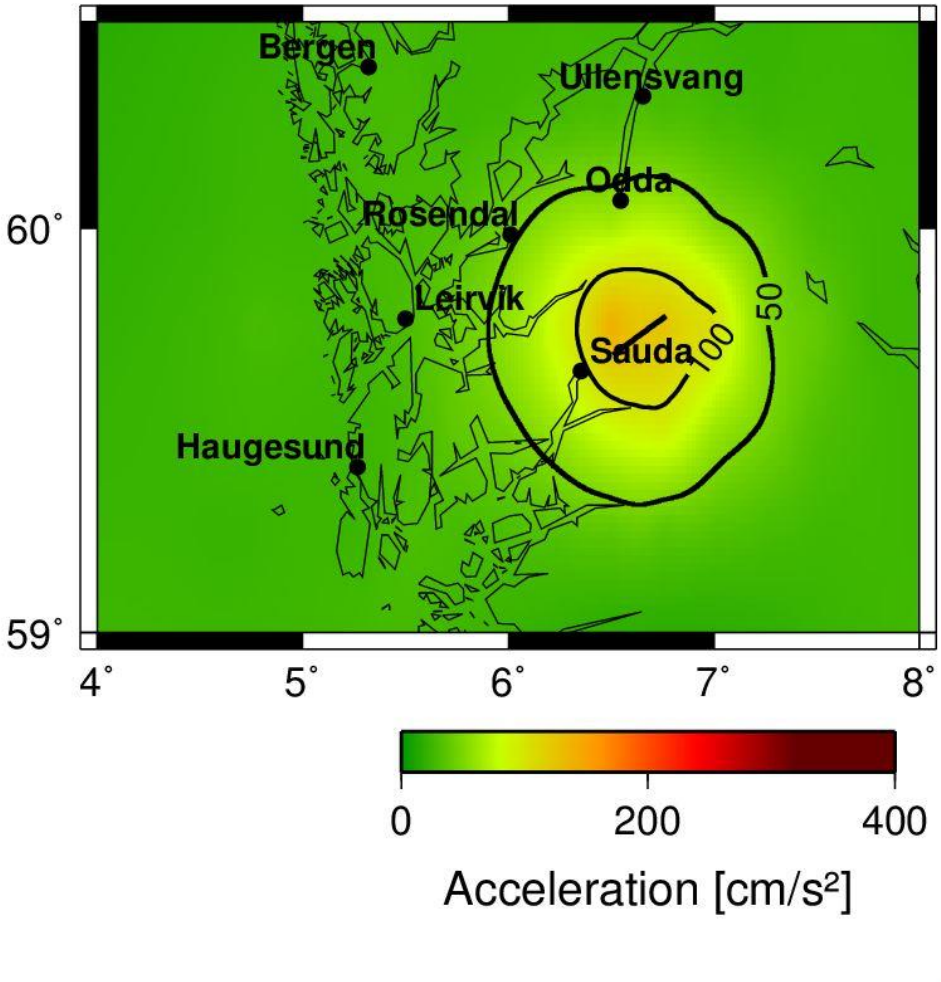

Figure 11.1.2-7 Distribution of PGA for a M_W 6.5 earthquake scenario on Sauda Fault.

11.1.2.8 Sauda Fault M_W = 6.0

Figure 11.1.2-8 shows the PGA distribution that would occur if Sauda Fault ruptures in a M_W 6.0 earthquake. The maximum PGA is estimated to be 96.13 cm/s^2 for this event. Approximately 1700 km^2 would be exposed to ground shaking of that could correspond to intensity VI – VII (Modified Mercalli Intensity Scale, Table 5.2-1) within the 50 cm/s^2 contour line. This area include the town of Sauda, which is situated near the center of the ground motion.

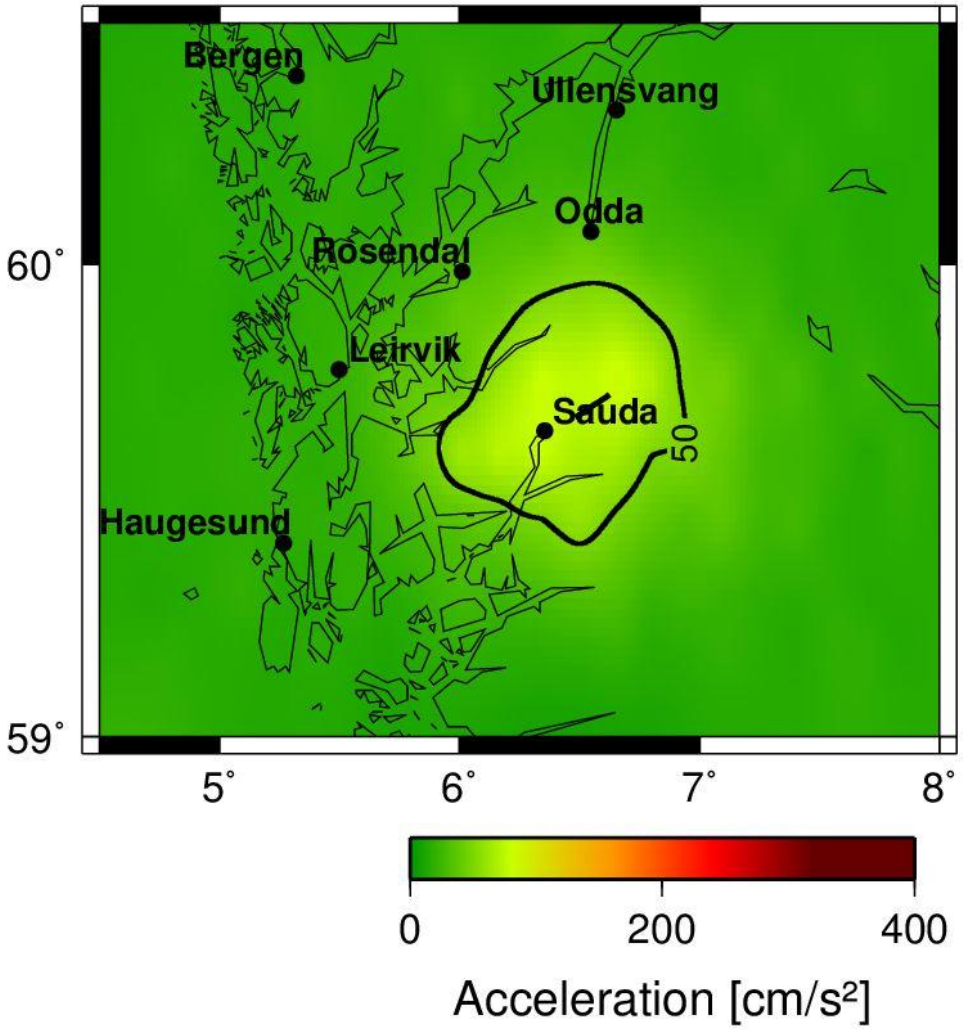

Figure 11.1.2-8 Distribution of PGA for a M_W 6.0 earthquake scenario on Sauda Fault.

11.1.3 Nordland, Northern Norway

11.1.3.1 Båsmoen Fault M_W = 6.5

Figure 11.1.3-1 shows the PGA that would follow a M_W 6.5 earthquake on Båsmoen Fault. The maximum PGA for this scenario is estimated to be 157.6 cm/s^2. The PGA between 50 and 157.6 cm/s^2 covers approximately 5700 km^2, and the strongest shaking occurs in an area that is approximately 990 km^2. Mo i Rana, the second largest city in Nordland, is situated within this area, and it would be exposed to shaking the could correspond to intensity VII (Modified Mercalli Intensity Scale, Table 5.2-1).

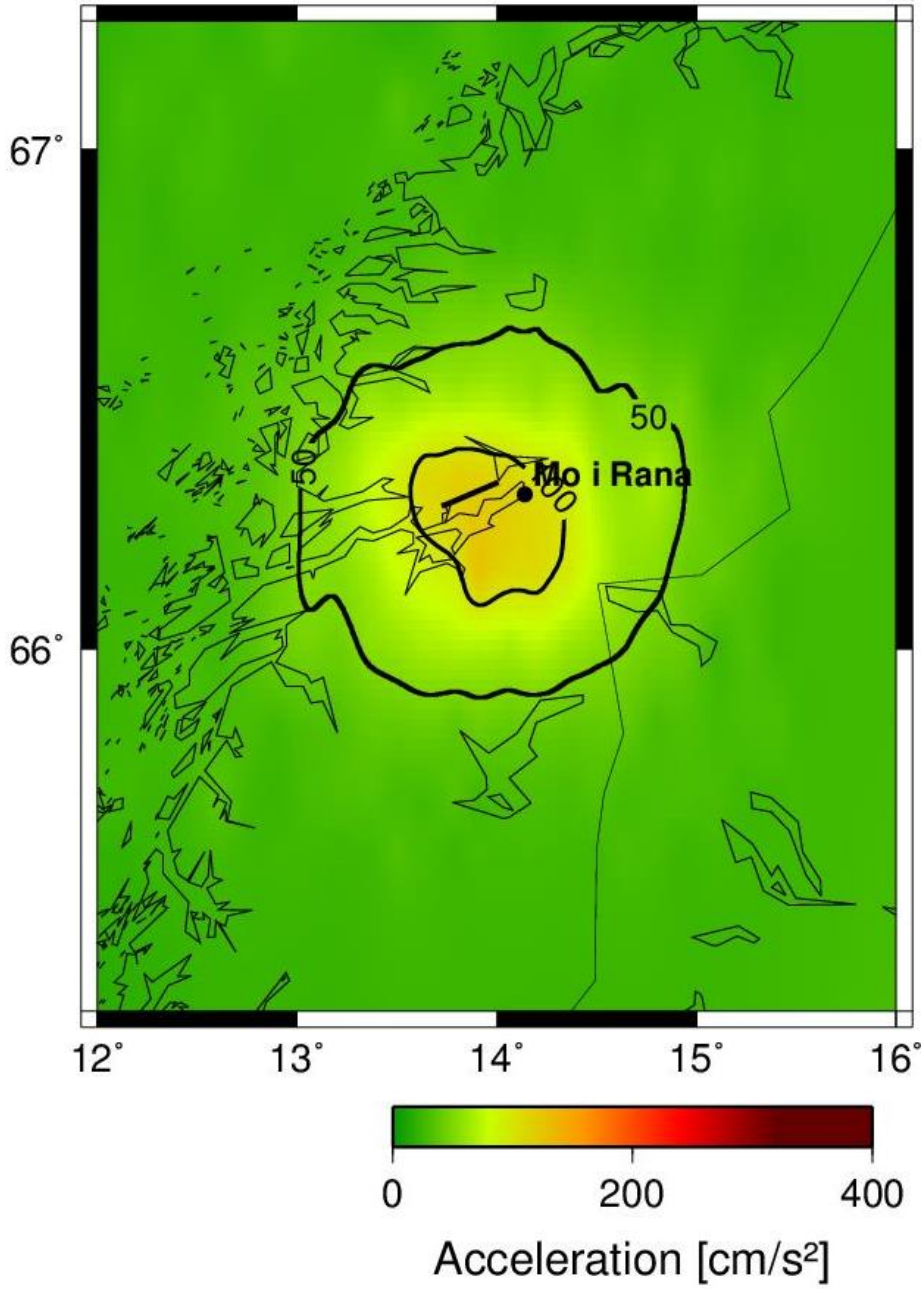

Figure 11.1.3-1 Distribution of PGA for a M_W 6.5 earthquake scenario on Båsmoen Fault.

11.1.3.2 Nesna Fault M_W = 7.2

Figure 11.1.3-2 shows the PGA that would occur if Nesna Fault ruptures in a M_W 7.2 earthquake. The maximum PGA is estimated to be 239.5 cm/s^2 for this scenario. Approximately 16 000 km^2 would be affected by PGA between 50 and 239.5 cm/s^2 if this earthquake were to occur. Approximately 4300 km^2 is within the area that would be exposed to PGA between 100 and 239.5 cm/s^2, which may indicate shaking of intensity VII – VIII on the Modified Mercalli Intensity Scale, Table 5.2-1. Towns like Sandnessjøen, Dønna and Nesna are located within this area, while Mosjøen and Mo i Rana are situated between the 50 and 100 cm/s^2 contour lines, and are prone to shaking that could correspond to intensity V –VI (Table 5.2-1).

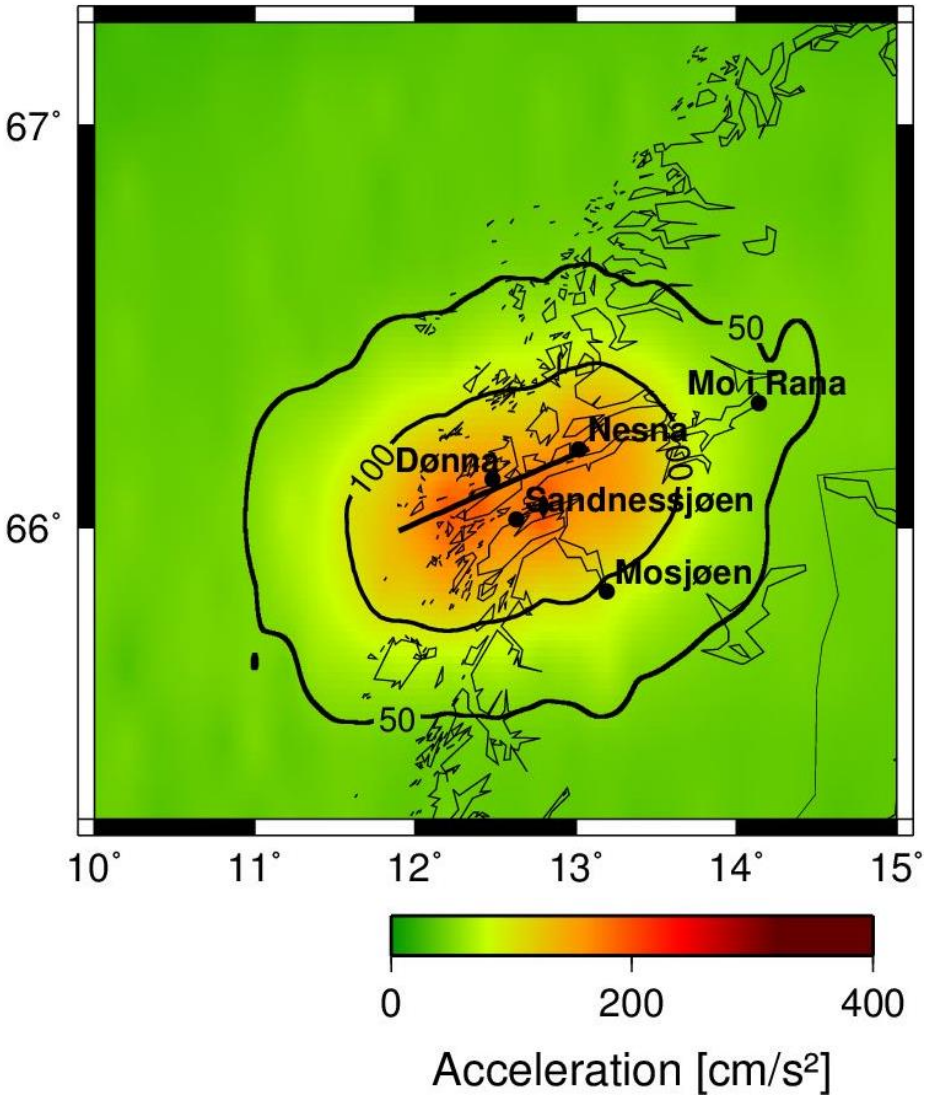

Figure 11.1.3-2 Distribution of PGA for a M_W 7.2 earthquake scenario on Nesna Fault.

11.1.3.3 Nesna Fault M_W = 6.5

Figure 11.1.3-3 shows the PGA following a M_W 6.5 earthquake on Nesna Fault. The maximum PGA is estimated to be 179.0 cm/s^2 for this scenario. The area affected by PGA between 50 and 179.0 cm/s^2 is approximately 6000 km^2. The center of this area includes several towns, like Nesna, Dønna, Sandnessjøen and Mosjøen, and they would be exposed to shaking that could correspond to intensity VII on the Modified Mercalli Intensity Scale (Table 5.2-1) if this earthquake was to occur.

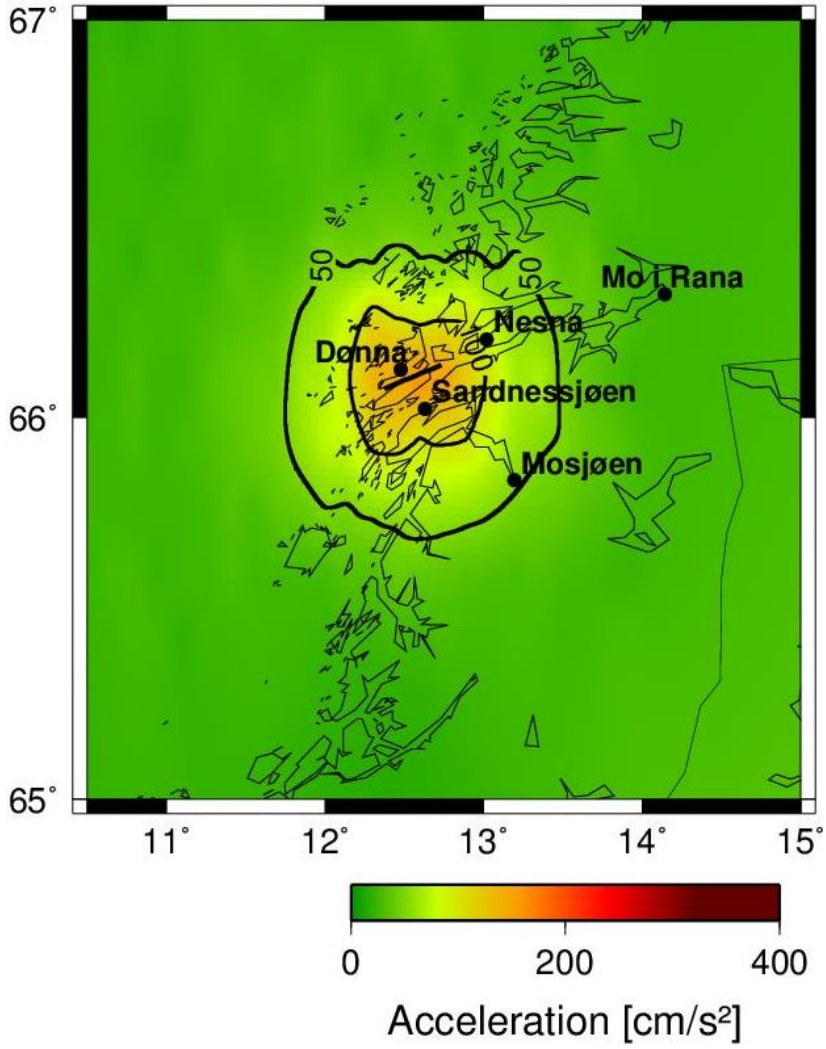

Figure 11.1.3-3 Distribution of PGA for a M_W 6.5 earthquake scenario on Nesna Fault.

11.1.3.4 Mosjøen Fault M_W = 7.0

Figure 11.1.3-4 shows the PGA following a M_W 7.0 earthquake on Mosjøen Fault. The maximum PGA for this scenario is estimated to be 319.4 cm/s^2. Approximately 13 000 km^2 would be affected by PGA between 50 and 319.4 cm/s^2, and approximately 3300 km^2 would be affected by shaking between 100 and 319.4 cm/s^2. These values could correspond to shaking of intensity VII – VIII on the Modified Mercalli Intensity Scale, Table 5.2-1. Mosjøen is situated just within the 100 cm/s^2 contour line and Brønnøysund is located just within the 50 cm/s^2 contour line where the intensity may indicate VIII and VI respectively.

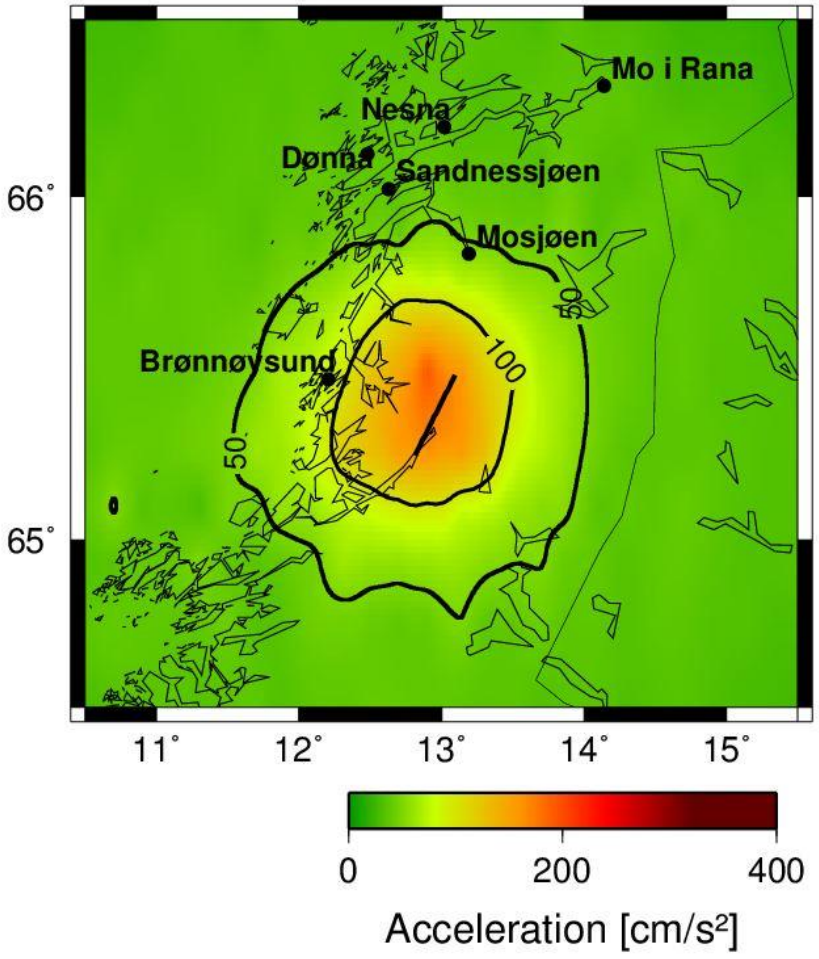

Figure 11.1.3-4 Distribution of PGA for a M_W 7.0 earthquake scenario on Mosjøen Fault.

11.1.3.5 Mosjøen Fault M_W = 6.0

Figure 11.1.3-5 shows the PGA that would occur if Mosjøen Fault ruptures in a M_W 6.0 earthquake. The maximum PGA is estimated to be 111.5 cm/s^2 for this scenario. PGA between 50 and 111.6 cm/s^2 would approximately affect 1800 km^2,which may indicate shaking of intensity VI on the Modified Mercalli Intensity Scale, Table 5.2-1. Mosjøen and Brønnøysund are both situated outside the 50 cm/s^2 contour line.

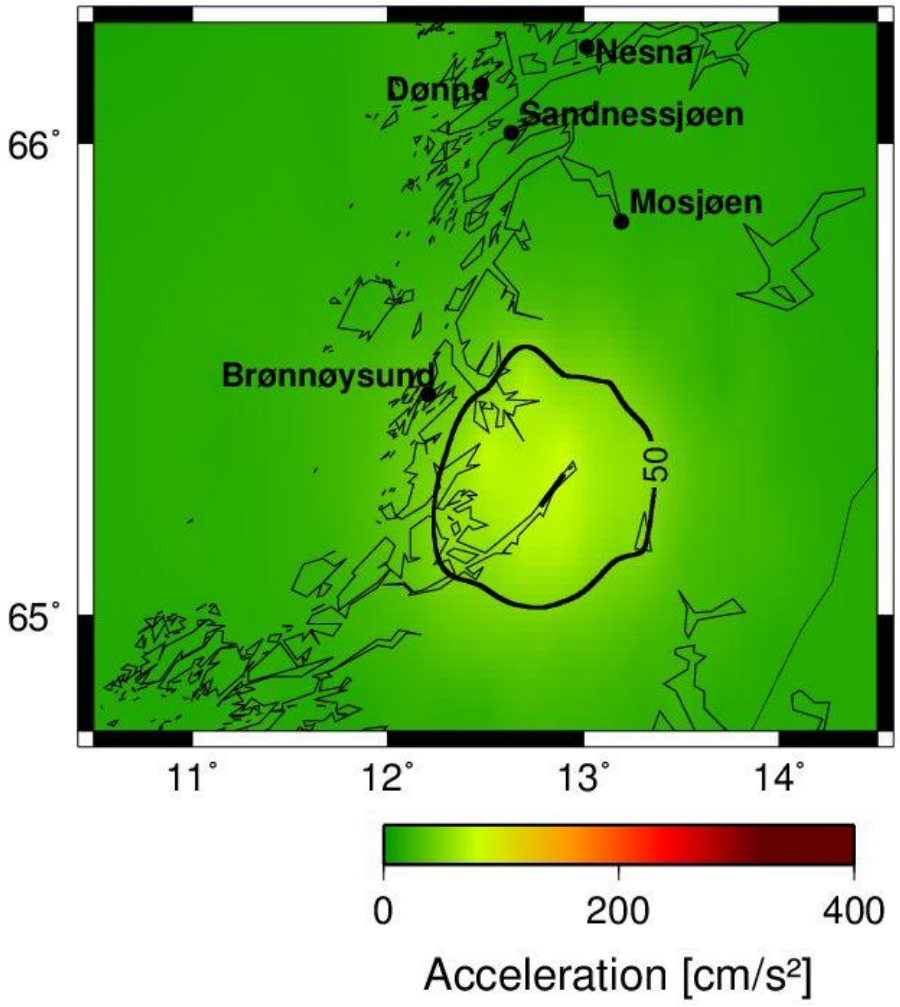

Figure 11.1.3-5 Distribution of PGA for a M_W 6.0 earthquake scenario on Mosjøen Fault.